Fate and Transformation of Oils and Trace Metals in Alabama and Louisiana Coastal Marsh Sediments Associated with the British Petroleum Gulf Oil Spill

by

Michael Gilbert Natter

A thesis submitted to the Graduate Faculty of
Auburn University
in partial fulfillment of the
requirements for the Degree of
Master of Science

Auburn, Alabama
May 7, 2012

Copyright 2012 by Michael Gilbert Natter

Approved by

Dr. Ming-Kuo Lee, Chair, Professor, Department of Geology and Geography
Dr. James Saunders, Professor, Department of Geology and Geography
Dr. Charles Savrda, Professor, Department of Geology and Geography

Abstract

The effects of the 2010 BP Macondo-1 well oil spill on the geochemistry of sediments and water columns at ten Gulf salt-marsh sites were investigated, months after the spill ceased. The ten sampling sites include four heavily contaminated sites in Louisiana (Bay Jimmy North, Bay Jimmy South, Bayou Dulac, and Bay Batiste), three intermediately contaminated sites in Alabama (Walker Island), Mississippi (Point Aux Chenes Bay), and Louisiana (Rigolets), and three pristine sites in Alabama (Weeks Bay, Longs Bayou) and Mississippi (Bayou Heron). Five of the ten sites are discussed at length in this thesis; they include Bay Jimmy South, Rigolets, Walker Island, Longs Bayou, and Weeks Bay.

Results indicate immediate and potentially long-term impacts of MC-252 Macondo-1 spilled oil on sediments and pore-waters of coastal wetlands. High levels of total organic carbon (TOC) contents of oiled wetland sediments range from 10-28%, whereas pristine sites are generally < 3%. Furthermore, dissolved organic carbon (DOC) levels in pore-waters at oiled locations, which reach hundreds of mg/kg, are one to two orders of magnitude higher than those at pristine locations. GC-MS analysis of oil extracts clearly correlate source MC-252 crude to oil extracted from sediments down to 15 cm. GC-MS analysis also shows significant degradation of lighter compounds while heavier oils still persist in sediments.

Most probable number analysis of bacteria suggests that the oil and organic carbon that washed into the coastal wetlands have accelerated the growth and colonization of sulfate- and iron-reducing bacteria. Oiled sediments are characterized by very high sulfide concentrations (up to 80-100 mg/kg) and an abundance of sulfate-reducing bacteria. The influx of oil and its

biodegradation creates strong reducing conditions along with the increased microbial activity, which in turn facilitate the biological and chemical transformation of toxic trace metals. Highly elevated concentrations of certain trace metals and elements (Cu, Pb, Zn, Fe, Hg, As, V, Ni, and S) are found in heavily oiled sediments, likely resulting from MC-252 oil and its associated chemical constituents. Additionally, oiled wetlands are dominated by fine-grained mud and organic matter, which have a high capacity to adsorb metals. Interestingly, despite high levels of trace metals in bulk sediments, concentrations of trace metals dissolved in pore waters are generally low. Petrographic, SEM EDAX, and Laser Ablation-ICP/MS analyses indicate that many toxic metals (As, Hg, Pb, Zn, Cu, etc.) have been sequestered in biogenically produced metal sulfides at heavily oiled sites.

Results indicate that the increase of organic carbon (i.e., oil) at heavily contaminated sites causes an acceleration of sulfate- and iron-reducing bacteria colonization that promotes strongly reducing conditions. Under strongly reducing conditions, dissolved trace metals are sequestered by sulfate reducers through the formation of sulfide solids. Although heavier components of crude continue to exist in sediments, the biodegradation over the long term and possible oxidation of biogenically produced metal sulfides and the resultant re-mobilization of trace metals remains unclear. Continued evaluation of ecologically sensitive estuarine environments is needed to fully understand the long-term effects of the oil spill.

Acknowledgments

This research was made possible through the financial support of the U.S. National Science Foundation, British Petroleum-Marine Environmental Science Consortium, Gulf Coast Association of Geological Societies, and the Alabama Geological Society. I would like to thank my thesis advisor Dr. Ming-Kuo Lee, whose tireless guidance and patience has been instrumental in the completion of this research and my studies. I would also like to thank my thesis committee members Drs. James Saunders and Charles Savrda in addition to the rest of the faculty at the Geology and Geography Department for their guidance and financial support.

I would like to express my sincere gratitude to all collaborating professors that have provided invaluable assistance in my research efforts. This includes Drs. Ahjeong Son, Benedict Okeke, Yang Wang, Alison Keimowitz, Munir Humayun, Just Cebrian, Yucheng Feng, Charlotte Brunner, Randall Clark, Yonnie Wu, and Michael Meadows. Special thanks go out to Robin Governo, Mike Shelton, and graduate students Joel Abrahams and Eric Sparks who aided in sample collection and analysis. I am forever indebted to my research partner and collaborator Jeffrey Keevan for his arduous hours spent with me in the field and laboratory.

Finally, I thank my family and friends for their encouragement, patience, and prayers, especially my parents Mike and Susan. Most importantly, I owe a debt of gratitude and forever will remember the encouragement and patience of my wife Heather without whom I could not complete this task.

Table of Contents

List of Tables

List of Figures

INTRODUCTION

The devastating explosion and subsequent sinking of the oil platform Deepwater Horizon at the British Petroleum Macondo-1 well on April 20, 2010, released approximately 4.9 million barrels of crude oil into the Northern Gulf of Mexico (Flow Rate Technical Group, 2010; Crone and Tolstoy, 2010). This oil, which in itself can have adverse effects when introduced into the environment, also changes the geochemistry of sediments and water column with which it comes in contact. Most research on the oil release at the Macondo-1 well site has focused on the immediate and direct impacts of the 68,000 square mile slick on surrounding aquatic environments (Amos, 2010). Although these studies are of utmost importance, the alteration of sediment and pore-water geochemistry by influx of oil could have an equally profound effect on the aquatic and coastal ecosystems for years to come. Possible long-term detrimental effects include the enhanced biotransformation and mobilization of toxic metals (e.g., mercury and arsenic) due to increased concentrations of organic carbon in the system (King et al., 2002; Keimowitz et al., 2005; Hollibaugh et al., 2005; Lee et al., 2005, 2007, 2010; Planer-Friedrich et al., 2009). Although most light compounds of oil may be easily degraded by natural microbes on the short term, saturated heavy oil (e.g., asphaltenes, resins, polycyclic aromatics, etc.) and those adsorbed by sediments could persist in the environment for decades (Oudot and Chaillan, 2010).

Recent studies have shown that the enrichment of soluble arsenic takes place when minerals that have adsorbed arsenic (e.g., Fe and Mn oxides) are reduced in a strongly reducing environment by iron- and sulfate-reducing bacteria (Freeze and Cherry, 1979; Drever, 1997;

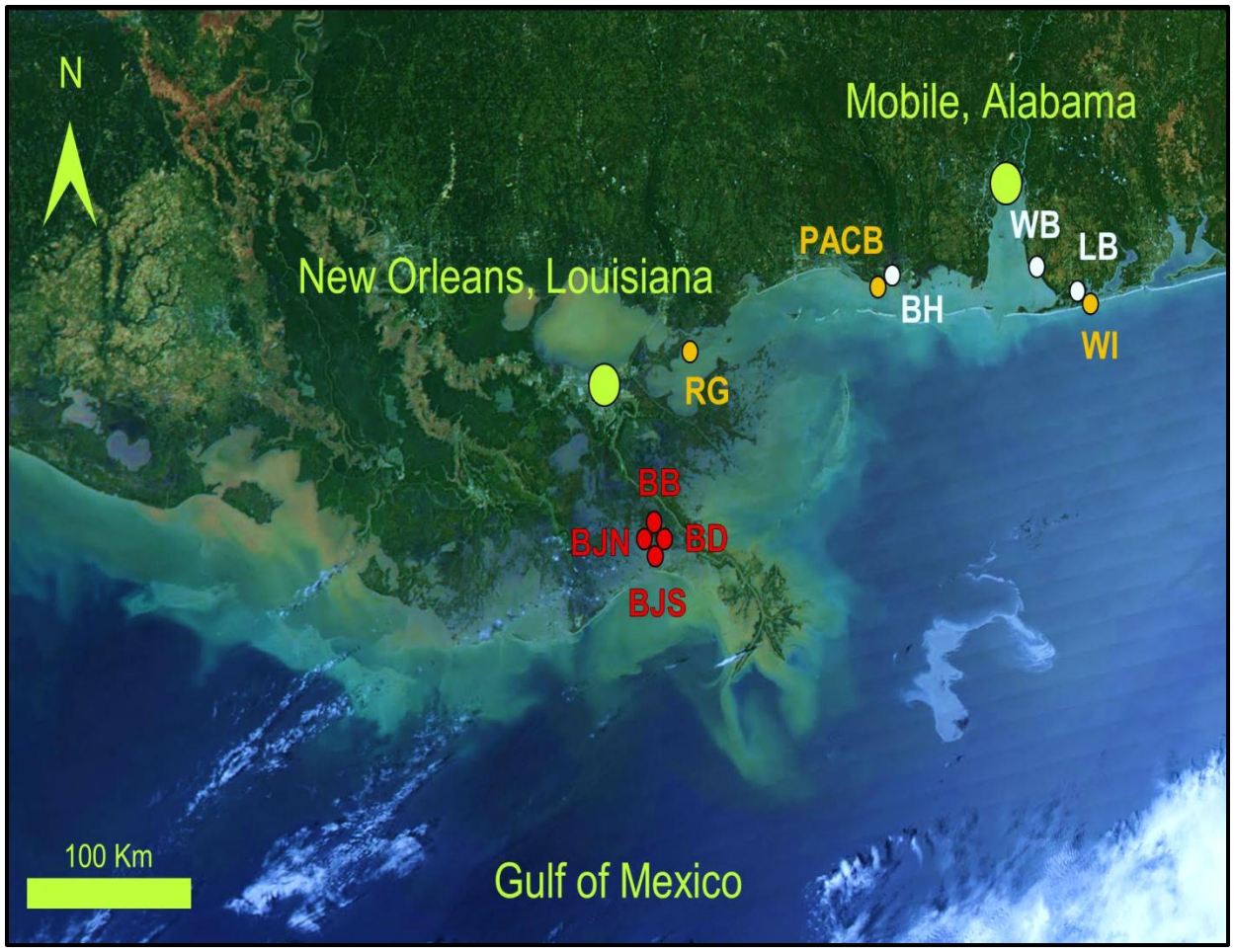

Figure 1. Location map of sediment samples collected from ten coastal wetland sites in Alabama, Mississippi, and Louisiana (white indicates no contamination, yellow indicates slightly contaminated, and red denotes heavily contaminated sites).

Lee et al., 2005; Saunders et al., 2008). The oil and organic carbon that washed into the coastal wetlands can greatly facilitate the growth and colonization of sulfate and iron-reducing bacteria. Consequent amplification of reducing conditions, along with microbial activity, has been shown to facilitate the mobilization, transportation, and speciation of arsenic (Keimowitz et al., 2005).

While atmospheric deposition and riverine inputs are the dominant sources of mercury over most areas (Mason et al., 1994; USGS Fact Sheet 146, 2000), the toxicity of mercury often is determined by its chemical form and route of exposure. Methylmercury (CH_3Hg) is the most toxic form (USGS Fact Sheet 146, 2000; Ullrich et al., 2001). Recent studies show that organic-rich, strongly reducing environments can facilitate mercury methylation (USGS Fact Sheet 146, 2000; Mason et al., 1994; Monrreal, 2007). This is a process in which inorganic mercury and carbon are joined to make monomethylmercury under strongly reducing environments by iron- and sulfate-reducing bacteria. Environmentally, this is of particular concern due to the fact that monomethylmercury is a bioenvironmental toxicant and can become a major source of contaminant in the aquatic food chain (Keimowitz et al., 2005; Ullrich et al., 2001). In many Gulf estuaries and coastal watersheds, Hg bioaccumulation from fish consumption already poses a health hazard. The methylation and bioaccumulation process can be enhanced by large amounts of organic carbon entering the aqueous environment (King et al., 2002). The main objective of this study is to assess the geochemical changes resulting from the interaction of oil with coastal wetland sediments in selected Gulf marsh locations (Figure 1). Sediment cores, surface bulk sediments, surface water, degraded oil, oiled dead marsh grass, and live marsh grass were collected from a total of ten different marsh locations in Louisiana, Mississippi, and Alabama (Figure 2). Five of these sites, including Bay Jimmy South (BJS), Rigolets (RG),

Walker Island (WI), Longs Bayou (LB), and Weeks Bay (WB) are considered in this study (Figure 1). Source Macondo-1 MC-252 crude oil was also obtained for comparison purposes.

Sampling sites varied from pristine, unaffected marshes (e.g., Weeks Bay and Wolf Bay of Alabama) to heavily oiled wetlands (e.g., Bay Jimmy of Louisiana). Sediment and pore-water samples were analyzed to test four key hypotheses: 1) influx of oil and organic matter promotes microbial growth and therefore causes release and biotransformation of some metals such as iron, arsenic, and mercury; 2) influx of oil in coastal wetlands elevates levels of certain trace metals, specifically Ni, Cu, V, and S, that are all compositional constituents of crude oil; 3) sulfate- and iron-reducing horizons are altered due to the additions of limiting substrates (i.e., carbon and metals) provided by spilled oil and 4) natural microbes digest lighter compounds of oil quickly (within months) while heavier oil fractions may persist much longer in wetland environments.

Geochemical alterations as a result of the oil spill were documented by comparing data obtained from oiled and pristine sites. These alterations can then be correlated with any changes in geochemistry (e.g., sediment and pore-water chemistry, organic carbon contents, reduced Fe and S, etc.) and biotransformation of trace metals, especially arsenic and mercury if present. Spilled oil present at sites and residing in sediments were also fingerprinted and correlated to source MC-252 crude using geochemical biomarkers and stable carbon-isotope signatures. This study documents significant geochemical changes that can be utilized at a later date in efforts to remediate and mitigate the damages caused by this and other oil spills worldwide.

SITE LOCATIONS AND BACKGROUND

Field sampling was conducted in affected Gulf coastal wetlands to investigate the spatial range and changes in the levels of oil, trace metals and their biogeochemical impacts. Ten sampling sites (Figure 1) include four heavily contaminated zones in Louisiana (Bay Jimmy North, Bay Jimmy South, Bay Batiste, Bayou Dulac) (Figure 2), three intermediate sites in Alabama (Walker Island), Mississippi (Point Aux Chenes Bay), and Louisiana (Rigolets), and three pristine sites in Alabama (Weeks Bay, Longs Bayou) and Mississippi (Bayou Heron). Five locations were chosen in Alabama and Louisiana's coastal wetlands for this particular study (Walker Island, Longs Bayou, Weeks Bay, Rigolets, and Bay Jimmy South). Five other wetland locations in Mississippi and Louisiana are studied by Keevan (2012). Each of these areas was chosen for their specific geographical location and varying degree of contamination. All ten sampling sites are included in results and analysis sections for comparison (Table 1 and Figure 1).

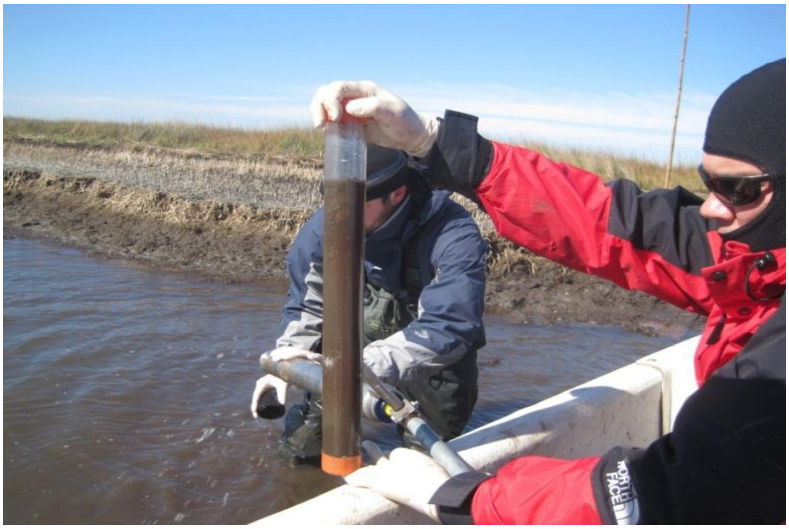

Figure 2. Sediment core recovered at the heavily oiled Bay Jimmy site, Louisiana.

Table 1. Salt-marsh sampling locations in the Gulf region.

Sampling Sites	Sample ID	Latitude (degrees)	Longitude (degrees)	Date Sampled	Water Temp °C
Weeks Bay	WB	30.413	87.831	10/19/10	22.8
Longs Bayou	LB	30.308	87.623	10/20/10	22.6
Walker Island	WI	30.288	87.541	10/20/10	23.0
Bayou Heron	BH	30.396	88.401	10/22/10	21.6
Point Aux Chenes Bay	PACB	30.335	88.451	10/22/10	23.1
Rigolets	RG	30.172	89.690	01/10/11	8.8
Bayou Dulac	BD	29.456	89.808	01/11/11	11.5
Bay Batiste	BB	29.472	89.831	01/11/11	10.4
Bay Jimmy North	BJN	29.454	89.885	01/13/11	6.6
Bay Jimmy South	BJS	29.445	89.891	01/13/11	7.2

Weeks Bay, Alabama- This core-sampling site was abbreviated WB for all labeling and identification purposes (Table 1). WB sampling took place in the northwestern portion of the bay (Lat. 30.413, Long. 87.831). Water depth at this site was 85 cm at the time of sampling (October 19, 2010). Weeks Bay is an estuary of Mobile Bay and has a watershed of 126,000 acres. Watersheds in the areas that feed Weeks Bay are surrounded by populated residential and urban areas that host large industrial and agricultural activities. These activities are potential point and non-point sources of metals pollution. Previous studies have demonstrated that bays or ocean estuaries are efficient traps for Hg and other metals in estuaries like Weeks Bay (Mason et al., 1994, 1999). Fish consumption advisories have been issued at Weeks Bay due to elevated Hg levels (ADEM, 1996; ADPH, 2008).

This sampling location (Figure 3) was chosen because it is in close proximity to the mixing area of Fish River's freshwater and the Gulf of Mexico's seawater, as identified by Monrreal (2007). Weeks Bay receives its freshwater and metal inputs from Fish River, the largest surface stream in Baldwin County. Several maps of surface-water quality (i.e., temperature, pH, electrical conductivity, dissolved oxygen, oxidation-reduction potential) were produced using data from a previous study by Monrreal (2007) (Figures 4-8). Water-quality data were gathered

from more than 30 locations at the surface and 1 meter water depths throughout Weeks Bay, Fish River, and four nearby USGS monitoring wells (Figure 3). The water-sample sets were analyzed in conjunction with the current study's results in order to construct maps and identify favorable environments for microbial activity. The water-quality maps show a distinct saltwater wedge produced by mixing freshwater with saltwater. Water collected from 1 m depth has higher pH and conductivity values with respect to those collected near the surface. This trend suggests that the seawater intrudes along the bottom portion of the water column in the bay before mixing with acidic freshwater from the Fish River. Seawater intrusion creates a front of salty water that penetrates below acidic, low-conductivity freshwater, forming a saline wedge, which is also indicated by steep contour gradients of conductivity, temperature, and pH in the upper bay. The neutral pH of waters in mixing zones favors precipitation of minerals (i.e., iron-oxyhydroxides), and perhaps adsorption of trace metals and other pollutants that were mobile in more acidic Fish River waters. The freshwater and seawater mixing zone also provides desired geochemical conditions (i.e., warm temperatures, low salinity, high levels of nutrients and biological activity) for biological transformation of heavy metals such as mercury. This specific coring location was also chosen because the silt and clay size sediments that dominate here provide high surface area for trace-metal adsorption and precipitation. Surface water near the mouth of Fish River where river water mixes with bay water has the lowest dissolved oxygen (DO) values (Figure 7). The reduced oxygen levels in the mixing zone may reflect enhanced microbial activity, which is an important factor in mercury methylation. Some bacteria, such as sulfate-reducing bacteria (SRB), prefer anaerobic waters with low DO or ORP that may contribute to the methylation of mercury (King et al., 2002). WB's location was not contaminated by the oil spill and, thus, was chosen as a control site for comparison with known oiled sites in the Gulf region.

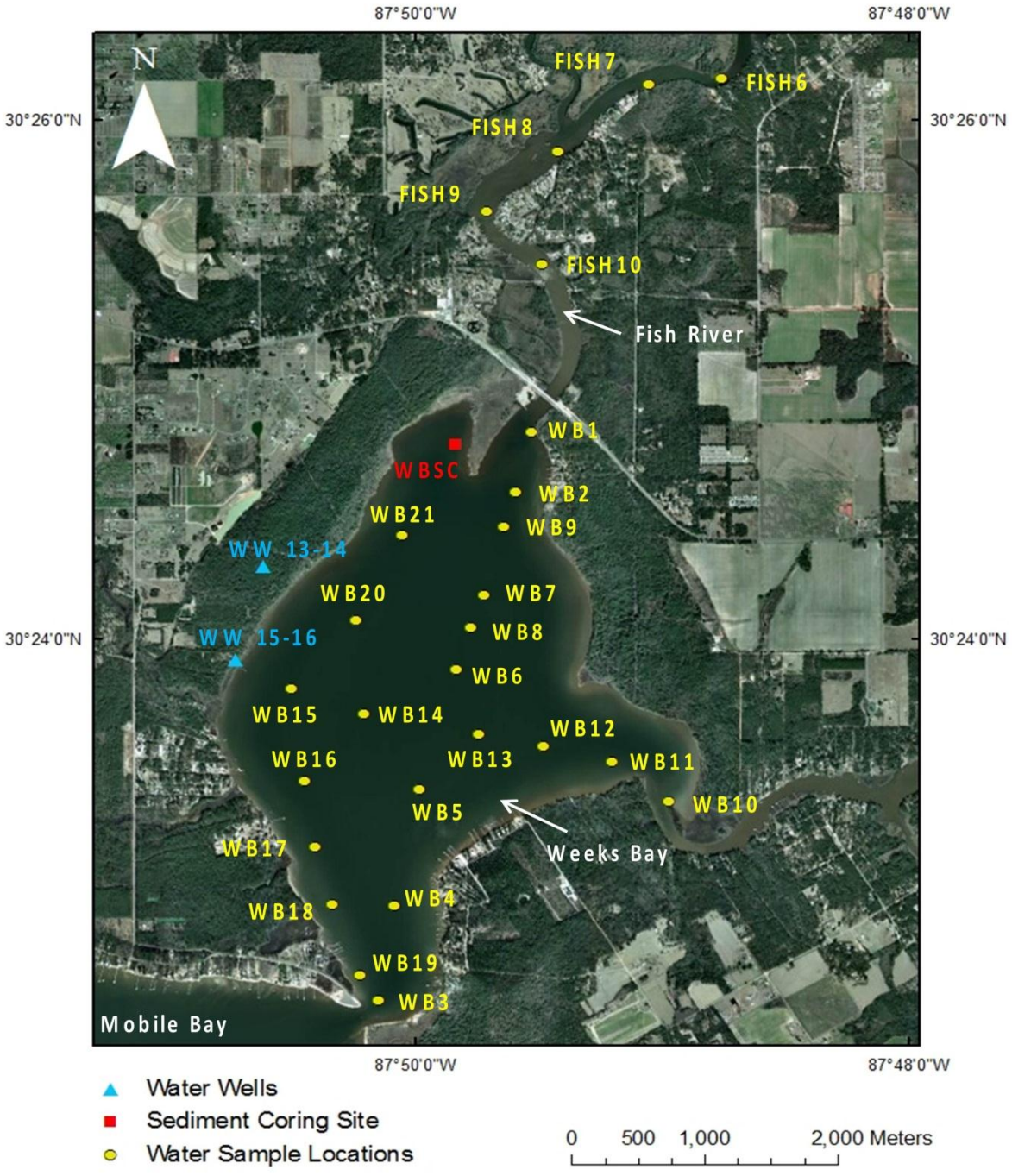

Figure 3. Map showing surface-water-sampling locations (yellow dots), USGS water wells (blue triangles), and sediment coring site (red square) in Weeks Bay, Alabama. Surface and water well data taken from Monrreal (2007).

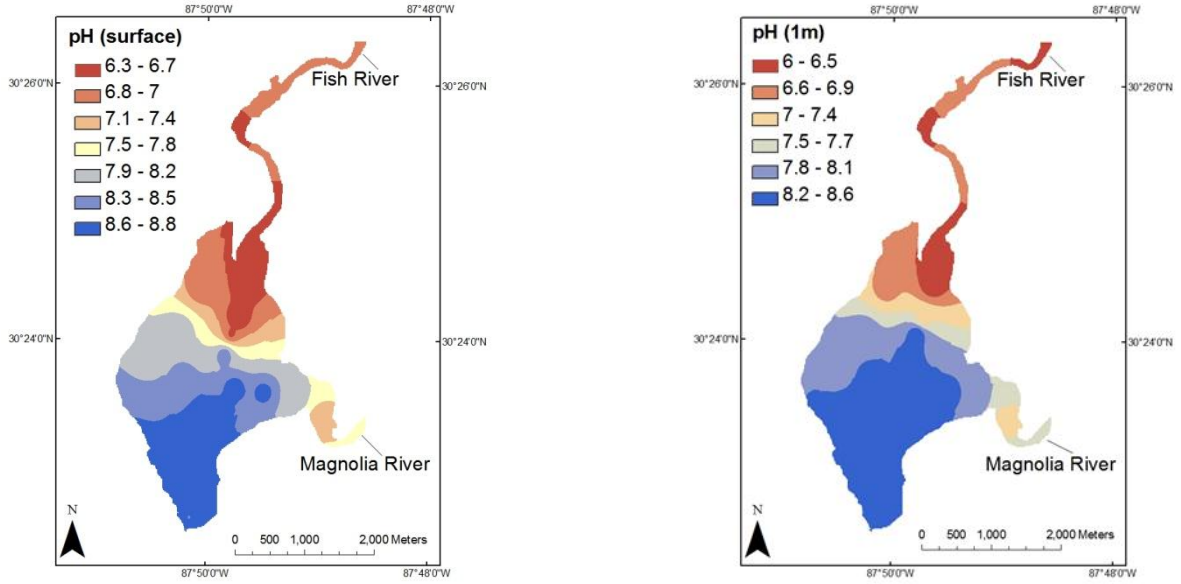

Figure 4. Maps showing variations in pH of bay water at surface (left) and 1-meter (right) levels in Weeks Bay and Fish River. Data used to construct maps taken from Monrreal (2007).

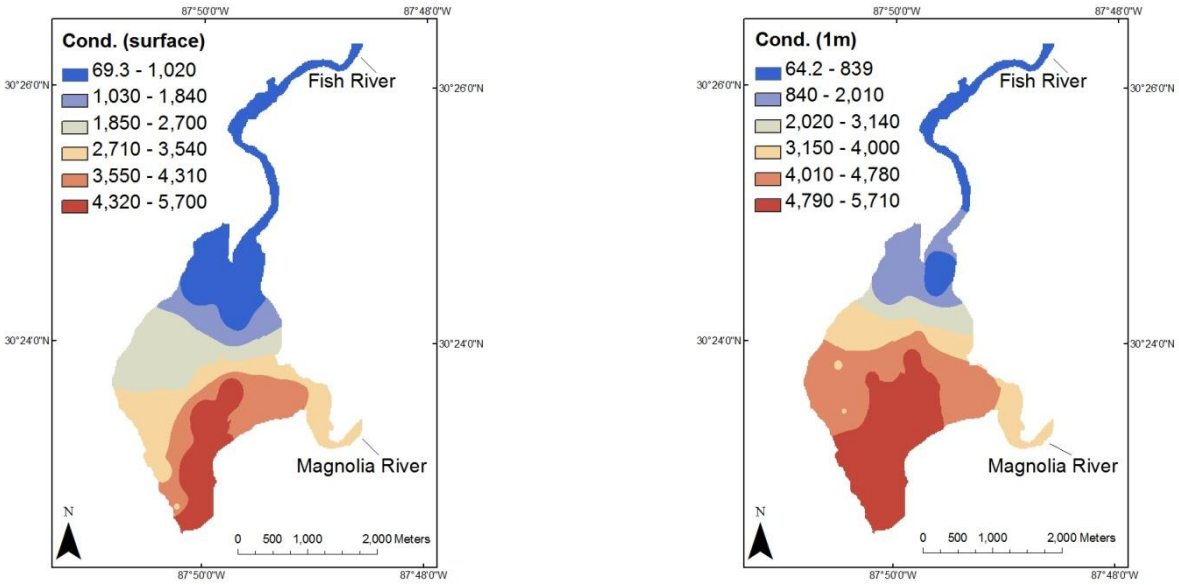

Figure 5. Maps showing variations in electrical conductivity (µs/cm) of bay water at surface (left) and 1-meter (right) levels in Weeks Bay and Fish River. Data used to construct maps taken from Monrreal (2007).

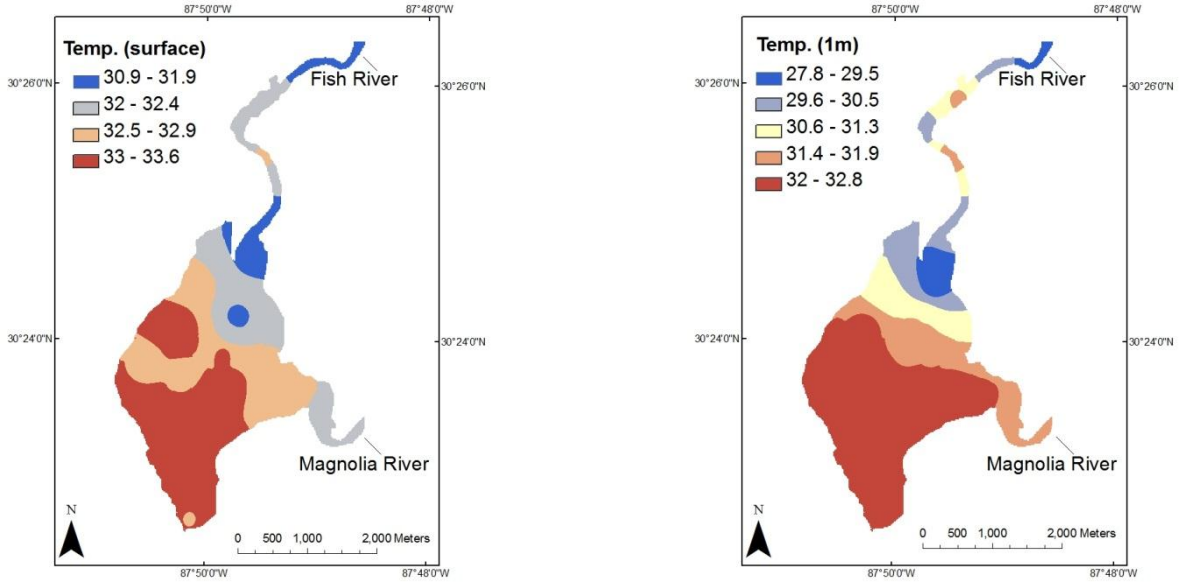

Figures 6. Maps showing variations in temperature (°C) of bay water at surface (left) and 1-meter (right) levels in Weeks Bay and Fish River. Data used to construct maps taken from Monrreal (2007).

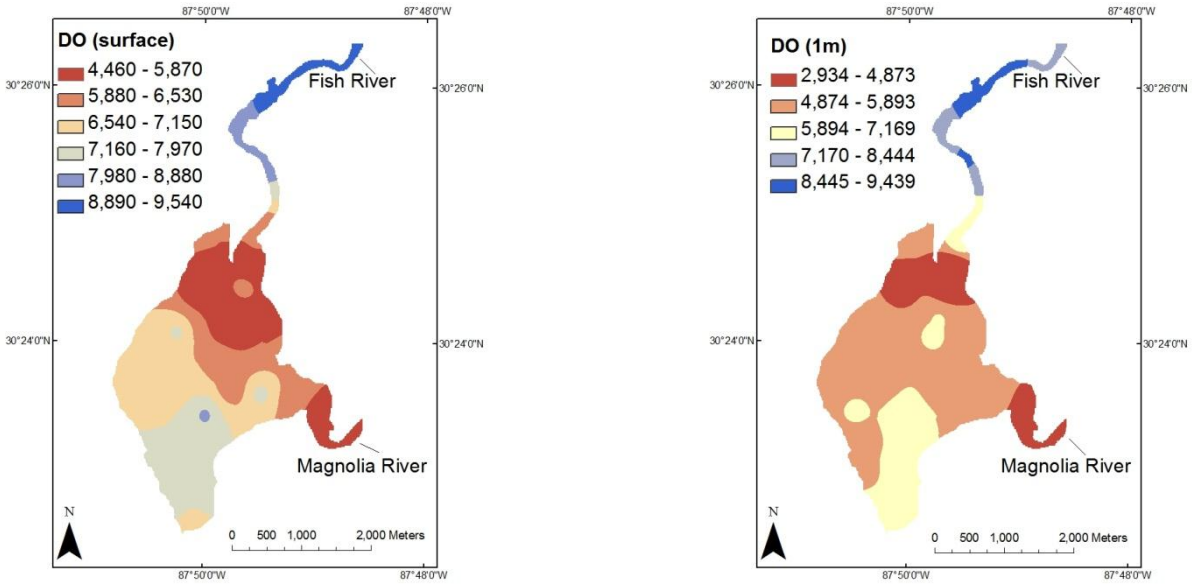

Figures 7. Maps showing variations in dissolved oxygen (μg/kg) of bay water at surface (left) and 1-meter (right) levels in Weeks Bay and Fish River. Data used to construct maps taken from Monrreal (2007).

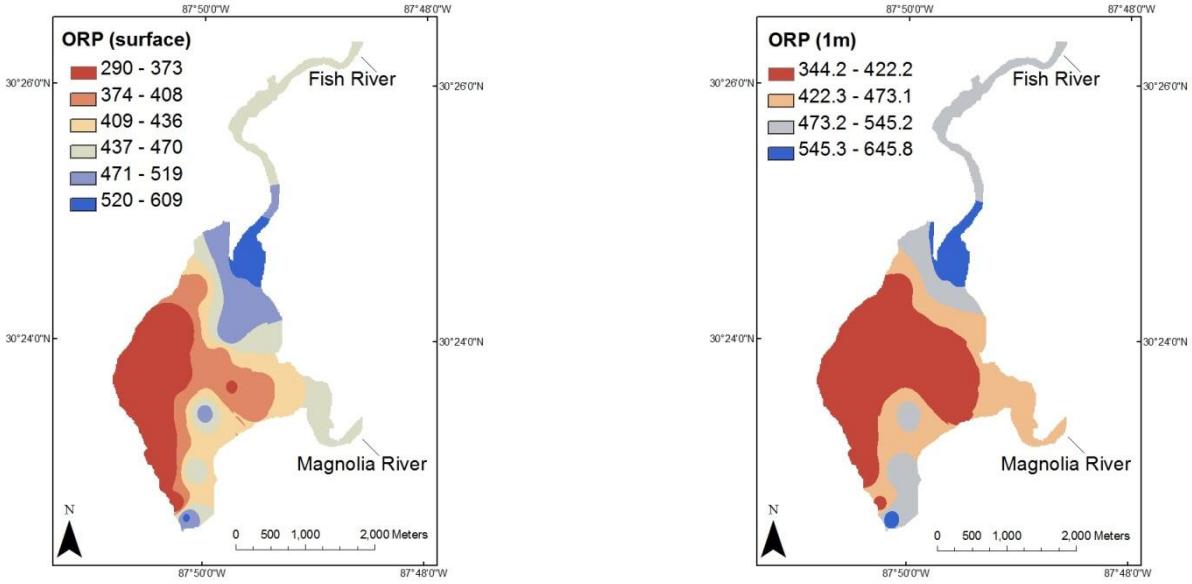

Figures 8. Maps showing variations in oxidation-reduction potential (mV) of bay water at surface (left) and 1-meter (right) levels in Weeks Bay and Fish River. Data used to construct maps taken from Monrreal (2007).

Longs Bayou, Alabama- This sampling site was abbreviated LB for all labeling and identification purposes (Table 1). LB samples were collected from a small inlet in the southwestern corner of Wolf Bay (Lat. 37.353, Long. 87.623) (Figure 2). Water depth at this site was 40 cm at the time of sampling (October 20, 2010). This location was chosen because of its protected location in Wolf Bay. Wolf Bay, an EPA Classified "Outstanding Alabama Water," is located on the Gulf of Mexico in southern Baldwin County between Perdido Bay to the east and Mobile Bay to the west. Wolf Bay is an estuary where freshwater and seawater mix and its environment hosts a diversity of aquatic, avian, and reptilian species. Streams that empty into Wolf Bay include Wolf Creek, Sandy Creek, Mifflin Creek, Graham Creek, Owens Bayou, Moccasin Bayou, and Hammock Creek. Wolf Bay also is connected to the Gulf Intercoastal Waterway, which carries commercial barge traffic and connects Perdido Bay to Mobile Bay. Several maps of surface-water quality were produced with data collected by Beasley (2010) (Figures 10-14). Water-quality measurements were determined by Beasley (2010) for more than 30 locations at the surface and 1 meter depths throughout Wolf Bay (Figure 9).

Beasley's (2010) data was used in conjunction with data derived in the current study in order to construct maps and help identify favorable environments for microbial activity. Parameters measured in Beasley's (2010) study included temperature, pH, specific conductance, dissolved oxygen (DO), and oxidation-reduction potential (ORP). Saltwater wedge, temperature and salinity stratifications in the Wolf Bay watershed are similar to those that exist in Weeks Bay, AL (see Figures 10-14). The data collected at depth show a higher pH and conductivity than those of surface waters. This trend suggests that the higher pH and denser seawater is intruding along the bottom of the water column and mixing with the more acidic and less saline waters from the creeks flowing into Wolf Bay. The electrical conductivity values in Wolf Bay (22,980

to 40,000 µS/cm) are much higher than those in Weeks Bay (70 to 5,700 µS/cm). High salinities imply less favorable conditions for Hg methylation (Compeau and Bartha, 1987; Ullrich et al., 2001; Celo et al., 2005; Kongchem et al., 2006). The pH values show slightly greater variations in Weeks Bay (6.3 to 8.8) than those in Wolf Bay (6.9 to 8.8), possibly reflecting stronger mixing and freshwater inputs in the Weeks Bay watershed.

Local news agencies reported that spilled oil penetrated the boom system in the narrow Perdido Pass that connects the Gulf of Mexico to Wolf Bay. Tidal currents bring seawater into Perdido Pass and help feed the bays and estuarine system. However, it is unlikely that this site was contaminated by the oil spill. Northwesterly littoral drift and winds that predominate in the Gulf of Mexico during the spring and summer months likely would have taken any contaminants in the opposite direction of LB. Hence, this protected site serves as an additional control site.

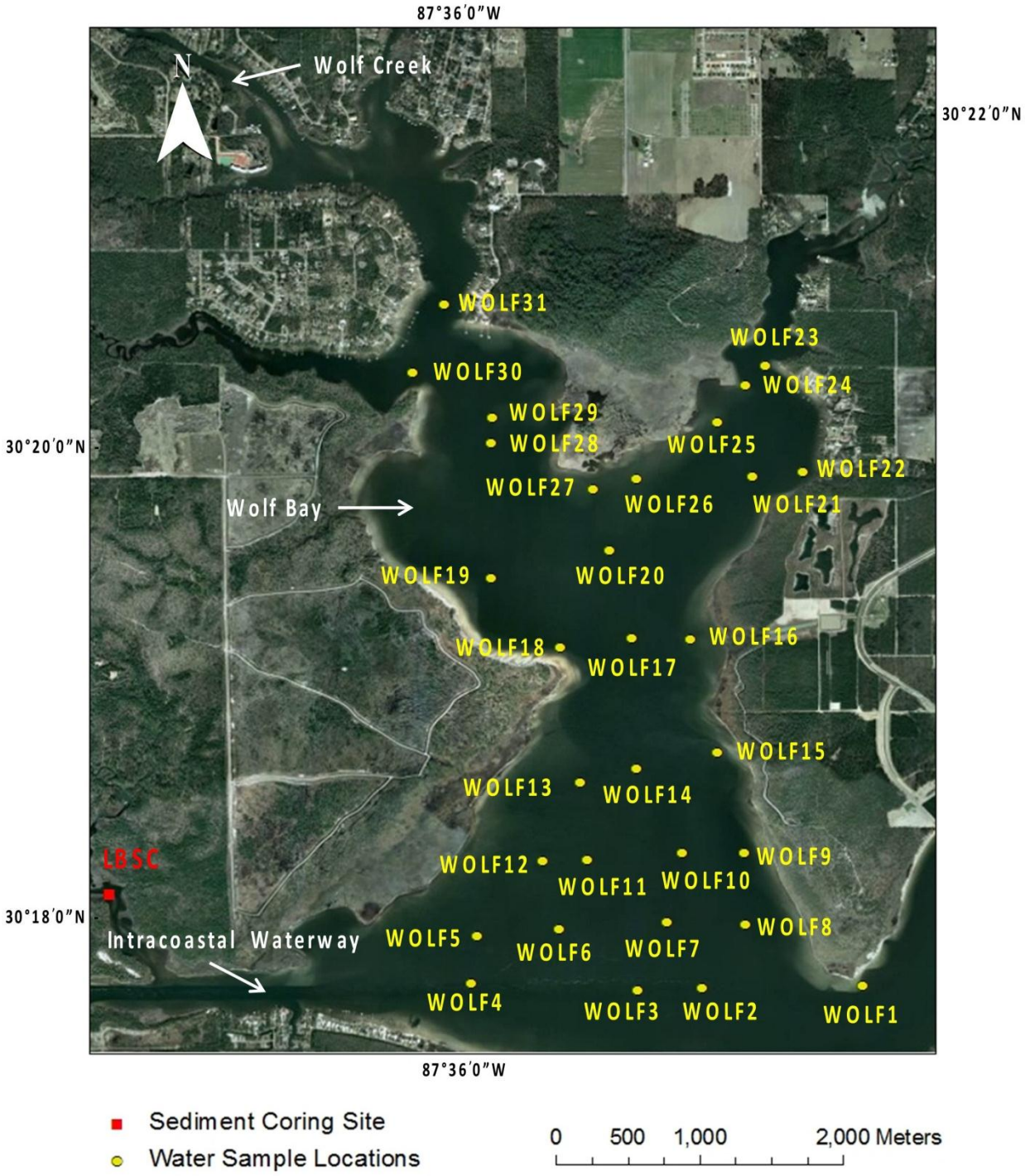

Figure 9. Map showing surface-water-sampling locations from Beasley (2010) (yellow dots) and sediment coring site (red square) for current study in Wolf Bay, AL.

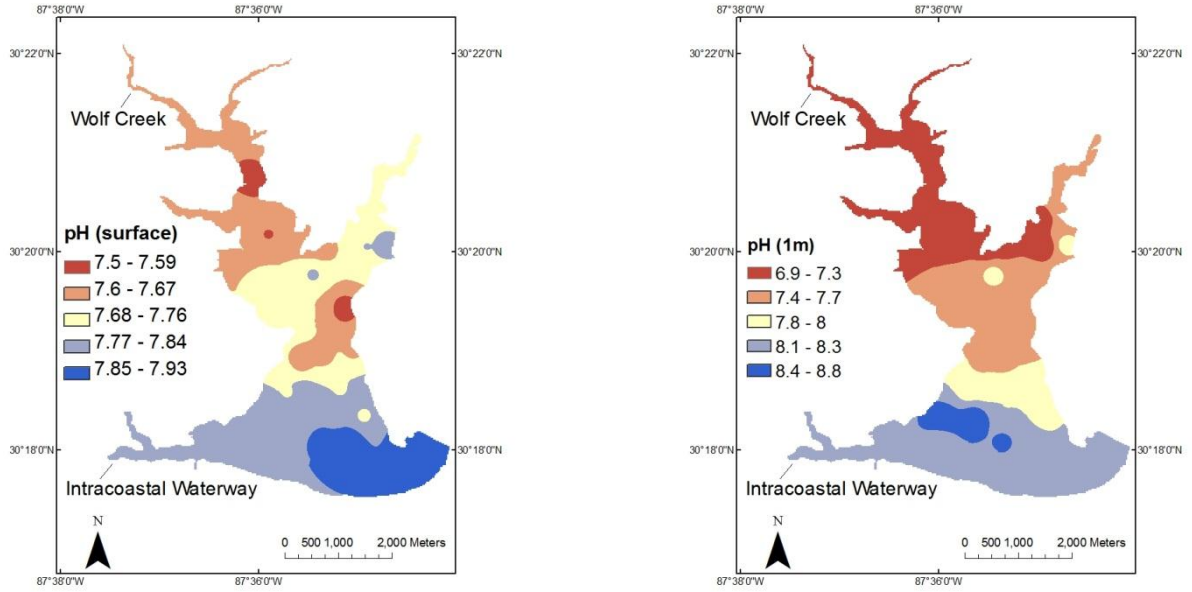

Figure 10. Maps showing variations in pH of bay water at surface (left) and 1-meter (right) levels in Wolf Bay, Alabama. Data used to construct maps taken from Beasley (2010).

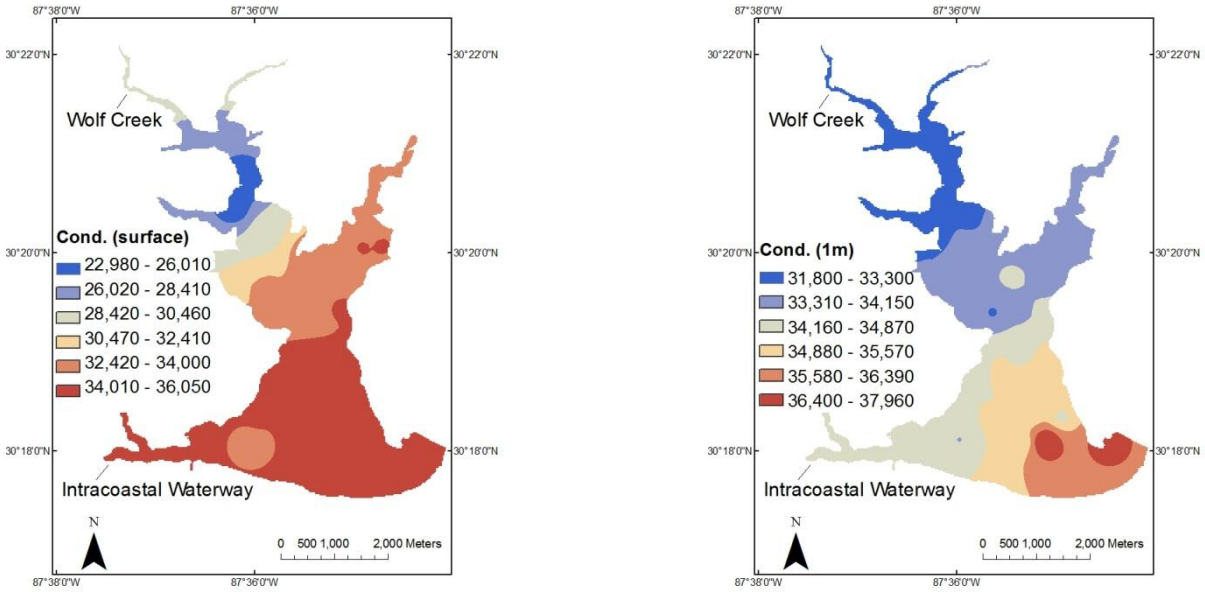

Figure 11. Maps showing variations in electrical conductivity (µs/cm) of bay water at surface (left) and 1-meter (right) levels in Wolf Bay, Alabama. Data used to construct maps taken from Beasley (2010).

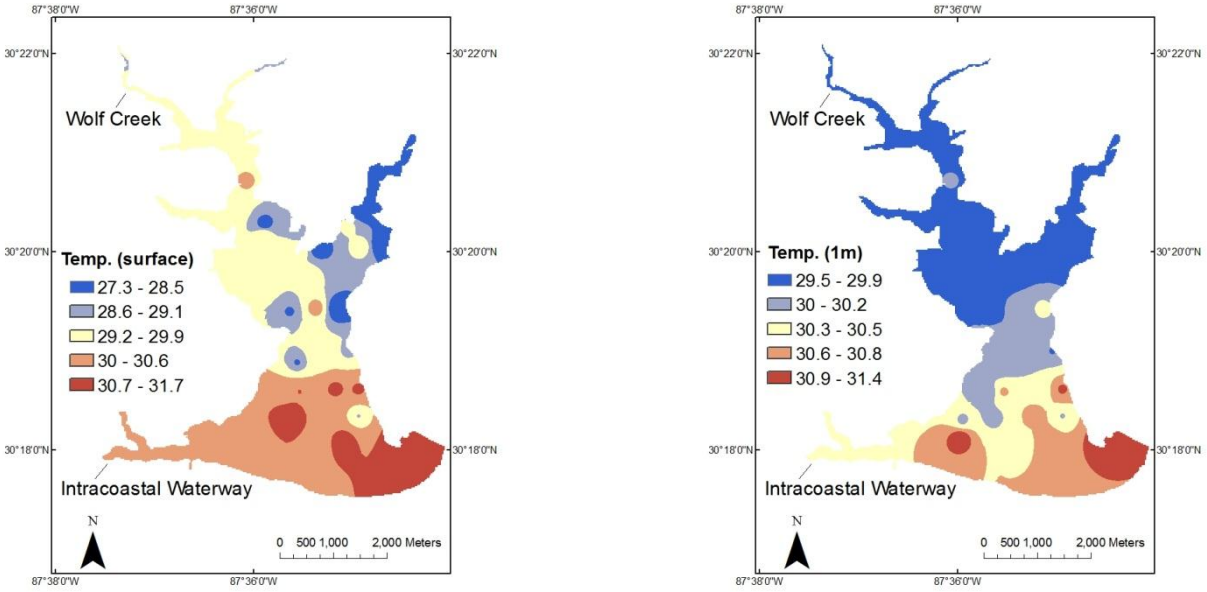

Figure 12. Maps showing variations in temperature (°C) of bay water at surface (left) and 1-meter (right) levels in Wolf Bay, Alabama. Data used to construct maps taken from Beasley (2010).

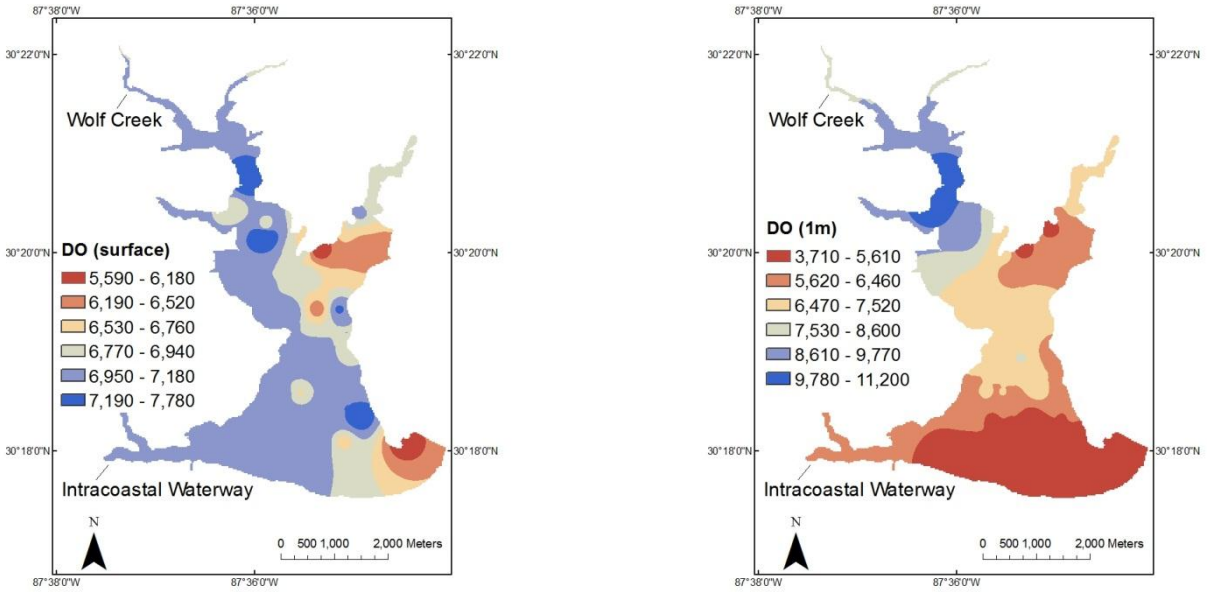

Figure 13. Maps showing variations in dissolved oxygen (μg/kg) of bay water at surface (left) and 1-meter (right) levels in Wolf Bay, Alabama. Data used to construct maps taken from Beasley (2010).

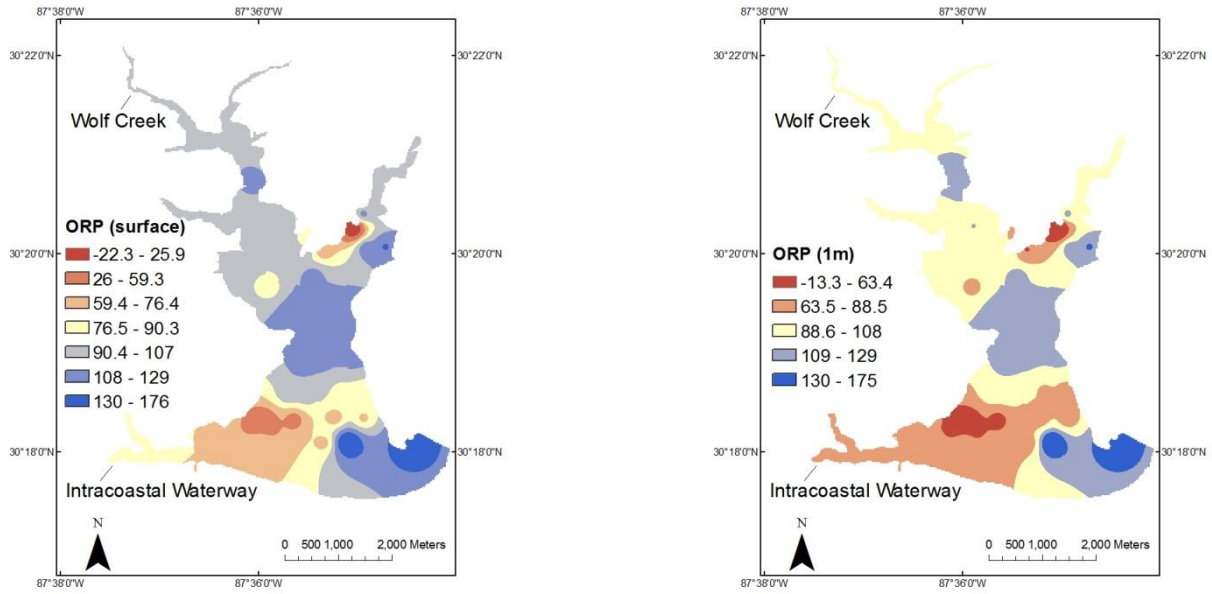

Figure 14. Maps showing variations in oxidation-reduction potential (mV) of bay water at surface (left) and 1-meter (right) levels in Wolf Bay, Alabama. Data used to construct maps taken from Beasley (2010).

Walker Island, Alabama- This sampling site was abbreviated WI for all labeling and identification purposes (Table 1). WI sediment samples were collected from a small inlet in the northeast corner of Walker Island (Lat. 30.288, Long. 87.541) (Figure 2). Water depth at this site was 40 cm at the time of sampling (October 20, 2010). This location was chosen because it is one of the most contaminated sites inside the Perdido Pass. Walker Island is one of three exposed flood tidal shoals that has become vegetated and a permanent exposed shoal just north of Perdido Pass (Figure 15). The Pass allows access from the Gulf of Mexico to Cotton Bayou and Bayou St. John. During the Deepwater Horizon oil spill, a pipe boom was installed at the Pass and access to the bays was closed during flood tidal activity. Multiple local news sources reported contamination to various degrees in Perdido Pass and surrounding bays (WKRG CBS News, 2010). The pipe booms had limited effect during peak phases of oil contamination allowing the influx of oil through Perdido Pass onto Walker Island. However, no visible oil was seen in the surface water during sampling, six months after the initiation of the oil spill.

Figure 15. Map showing sediment-coring and water-sampling site in Walker Island, AL.

Rigolets, Louisiana- This sampling site was abbreviated RG for all labeling and identification purposes (Table 1). RG samples were collected from Rigolets Pass (Lat. 30.172, Long. 89.690) (Figure 2), which is a deep water pass between Lake Ponchartrain, Louisiana and the Gulf of Mexico. Water depth at the edge of the pass were sampling was conducted was 20 cm (January 10, 2011). This location was chosen because it was only slightly contaminated and thus serves as a control site to heavily oiled sites in LA. Rigolets is a 12.7-km-long deep-water tidal pass that supplies saltwater to Lake Ponchartrain via the Gulf (Figure 16). After the Deepwater oil spill, pilings for boom systems were installed and barges strategically placed in the Pass in attempt to close off and protect the surrounding wetlands. However, according to local news sources, minor amounts of oil penetrated the system and entered Lake Ponchartrain via the Pass and through its defenses (The Times-Picayune News, 2010). However, no visible oil was seen in the surface water during sampling, nine months after the initiation of the oil spill.

Figure 16. Map showing sediment-coring and water-sampling site in Rigolets Pass, LA.

Bay Jimmy South, Louisiana- This sampling site was abbreviated BJS for all labeling and identification purposes (Table 1). BJS samples were collected from the southern portion of Bay Jimmy, Louisiana (Lat. 29.445, Long. 89.891) (Figure 2). Water depth at this site was 10 cm at the time of sampling (January 13, 2011). Bay Jimmy is a small body of water 64 km south of New Orleans, Louisiana. It was one of the most heavily contaminated coastal wetlands in Louisiana (Figure 17). This site was chosen because it was heavily contaminated occupies a unique ocean-front setting. Bay Jimmy is part of the Barataria Bay basin and is located along the shores of southeastern Louisiana as part of the Mississippi River delta (Figure 18). The Barataria Bay basin is a large estuary that holds a diversity of wildlife, including shrimp, crab, sea turtles, and a variety of avian and fish species. Degraded oils in oil-covered marsh grasses were present at this site during sampling. A chemical odor was detected, and a film of oil coated sediment coring devices. Erosion of the marsh shore was in progress at an accelerated rate due to the suppression and mortality of marsh grasses.

Figure 17. Photograph of suppressed oil covered marsh grass in Bay Jimmy, LA.

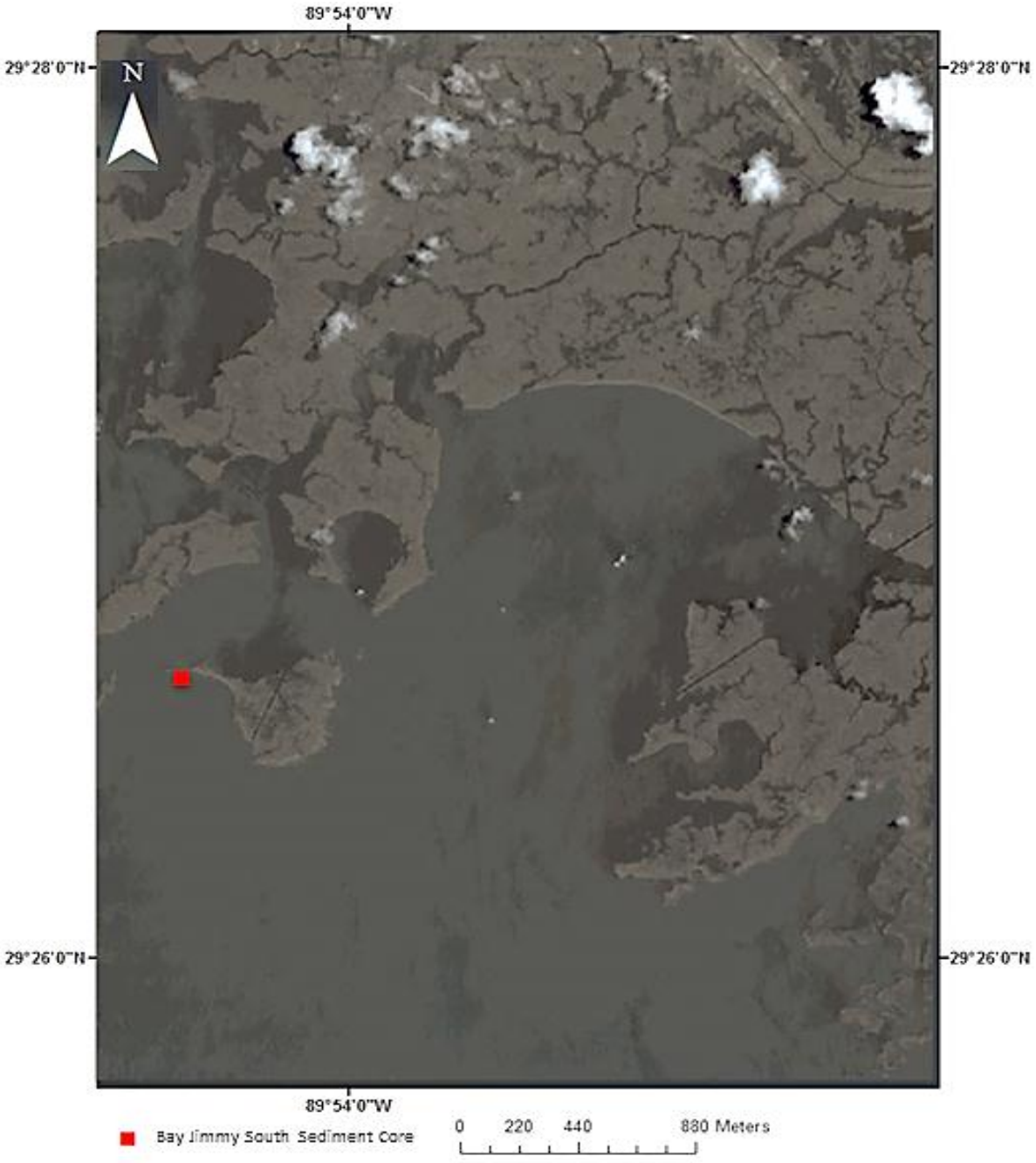

Figure 18. Map showing sediment-coring and water-sampling site in Bay Jimmy South, LA.

BACKGROUND

This research focuses on biogeochemical changes and mobilization and biotransformation of trace metals (e.g., arsenic and mercury) in coastal wetlands in response to increased levels of organic carbon resulting from the Gulf oil spill. Background information on site geology and on the fate and transformation of arsenic and mercury follows, with a brief explanation of the biogeochemical processes that could be attributed to the oil spill.

Geologic Setting

The five wetland sampling locations utilized in this study all reside in the Coastal Plain province of Alabama and southern Louisiana. Alabama Coastal Plain sediments in the area can be divided into three major groups. In ascending order, these are the Miocene undifferentiated series, Pleistocene Citronelle Formation, and Holocene alluvium (Chandler et al., 1996). All sediments analyzed for this study from Alabama and Louisiana are classified as Holocene alluvium and were located in delta-plain or coastal salt-marsh locals. The Louisiana sediments directly overlay Late Pleistocene continental shelf deposits, Late Pleistocene Citronelle and Willis formations, or Pleistocene terrace deposits.

Sediment samples collected from all Alabama and Louisiana sites consist of coastal deposits that include fine to medium quartz sand, silt, and clay. These delta-plain and salt marsh sampling sites all contain relatively high levels of organic content with various amounts of peat. While Alabama sampling sites reside in Weeks and Wolf Bay watersheds, the Louisiana sampling sites are areas of active or abandoned delta lobes of the Mississippi River.

Trace Metal Speciation, Mobilization, and Bioaccumulation

Heavy metals, more commonly known as trace metals (e.g., mercury, arsenic, lead, cadmium, copper, zinc, nickel, etc.), have been determined to be extremely toxic to wildlife and humans when elevated in the environment. Anthropogenic inputs of trace metals in coastal and estuarine environments have been identified as a major environmental concern due to the long residence time of metals in coastal wetlands (Cohen et al., 2001). Specifically, arsenic and mercury, which are concentrated by industrial activities, may be found at elevated levels in coastal bays and estuaries. Little is known about the biogeochemical and hydrological controls on the fate and transformation of trace metals in coastal watersheds, which often depends on aquatic chemical and redox conditions.

Arsenic and mercury are recognized as two of the most toxic inorganic contaminants in drinking water. Current EPA drinking-water standards for arsenic and mercury are 10 μg/L and 2 μg/L, respectively (EPA Fact Sheet, 2009). While these two highly toxic heavy metals are found in insignificant amounts in Earth's crust, they are often concentrated deliberately for industrial purposes and have been used for many commercial applications. Arsenic also is commonly found incorporated into solid phase Fe sulfides (e.g., pyrite) under sulfate-reducing conditions (Saunders et al., 2008). Arsenic can also be sorbed onto the surface of iron-oxide minerals under oxidizing conditions (Welch et al., 1988; Madigan et al., 1997). This adsorption process often takes place as geochemical or redox changes allow soluble arsenic to precipitate onto the surface of minerals (King et al., 2002). Mercury, while only having an average crustal abundance by mass of about 80 μg/kg, does not readily blend geochemically with minerals in the Earth's crust (EPA Fact Sheet 146, 2000). When found in terrestrial environments, it is typically sequestered and has limited mobility. The movement and transportation of these

pollutants often depend on chemical conditions present in the aqueous environment (Keimowitz et al., 2005).

Arsenic enrichment in natural waters occurs around the world as a result of various biogeochemical processes (Smedley and Kinniburgh, 2002). Recent studies have shown that enrichment of soluble arsenic takes place when minerals that have sorbed arsenic (e.g., Fe- and Mn-oxides) are reduced in Fe-reducing environments (Saunders et al., 2008). The arsenic becomes mobilized and goes into solution as iron-reducing bacteria reduce the minerals and use the freed electrons for energy during anaerobic respiration (Nickson et al., 1998, 2000; McArthur et al., 2004; Islam et al., 2004). In sulfate-reducing environments, dissolved arsenic may be removed by co-precipitation with sulfide solids, or remain in solution as it reacts with reduced sulfur to form thioarsenite aqueous complexes (Lee et al., 2005).

Increasing reducing conditions and microbial activities may facilitate the mobilization, transformation, and speciation of arsenic (Keimowitz et al., 2005). In the resulting redox reactions, arsenic is freed from its sediment or mineral hosts, goes into solution and can accumulate as aqueous species in elevated amounts. This mobilized arsenic can then form aqueous compounds and become bio-accumulated in nature. The bio-accumulation of arsenite (As(III), in the chemical form of $As(OH)_3$) as reduced neutral aqueous compounds is of particular concern due to its extremely high toxicity and mobility with respect to other As species (Saunders et al., 2008). Arsenates (As(V), in the chemical form of $HAsO_4^{2-}$ or AsO_4^{3-}) are negative-charged anions and are more strongly adsorbed by Fe- or Mn-oxyhydroxides with positive surface charges.

Mercury is a highly toxic element that is found both naturally and as an industrial contaminant in the environment. Metal processing, combustion of coal, medical waste and

mining of gold and mercury contribute to high concentrations in certain areas (USGS Fact Sheet 146, 2000). However, atmospheric release from burning fossil fuels in conjunction with mercury's volatilization is the dominant source of mercury over most areas (Mason et al., 1994; USGS Fact Sheet 146, 2000). Once in the atmosphere, mercury can be widely circulated and distributed by winds and weather patterns. The toxicity of mercury often is determined by its chemical form. Methylmercury (CH_3Hg) is widely accepted as its most toxic form (Madigan et al., 1997). Recent studies have shown that strongly reducing environments created by sulfate- and iron-reducing bacteria can facilitate mercury methylation (USGS Fact Sheet146, 2000; Mason et al., 2005; Monreal, 2007). In this process, inorganic mercury and carbon are joined to make monomethylmercury. Sulfate-reducing bacteria are particularly efficient mercury methylators (Chapelle, 1994). In many Gulf estuaries and coastal watersheds, mercury bioaccumulation from fish consumption already poses a health hazard. The methylation and bio-accumulation process can be enhanced by the introduction into aqueous environments of large amounts of organic carbon such as those delivered from the Gulf oil spill.

Carbon

Carbon is the fifteenth most abundant element in the Earth's crust and the fourth most abundant by mass in the universe. The carbon atom, also referred to as the building block of life, exists in nature as various allotropes and is stable in a number of oxidation states from -4 to +4. Energy is released during carbons oxidation and the series of redox reactions that alter its oxidation state is referred to what is known as the carbon cycle. The cycle places carbon into two forms, organic and inorganic. While inorganic forms contain carbon as an oxidized species (+4) typically as CO_2 in atmospheric gas or in water as a dissolved species, it also can be bound in aquatic environments by calcium-carbonate precipitating organisms. Organic carbon is a

reduced species of carbon (0) that has been reduced from CO_2 to carbohydrates by the process of photosynthesis. This organic carbon is often then re-oxidized by means of respiration from animals and microorganisms as part of the carbon cycle.

Organic carbon created by plants and organisms in both aquatic and terrestrial environments often becomes buried and broken down into simpler forms of carbohydrates or organic acids by fermentators and other bacterium (Chapelle, 1993). The oxidation of buried organic compounds leads to increased levels of CO_2, creating more reducing and anoxic environments where anaerobic bacteria utilize the remaining simplified organic compounds for energy (Rittmann et al., 2001). Increased amounts of organic carbon in sequestered environments such as wetlands lead to increased populations of microorganisms that utilize the carbon substrate for energy, in turn creating increasing amounts of biomass in the system (Berner, 1984). Furthermore, oil and organic carbon that wash into the coastal wetlands from oil spills can greatly facilitate the growth and colonization of sulfate- and iron-reducing bacteria, which may lead to intensification of reducing conditions. This, in turn, may facilitate the mobilization, transformation, and speciation of toxic trace metals (Keimowitz et al., 2005).

Carbon isotopic signatures of petroleum hydrocarbons are influenced by various factors, including the source of organic matter, biogeochemical reactions, and isotopic fractionation involved in the generation of the petroleum. Photosynthesis enriches biologically synthesized organic compounds in lighter ^{12}C. Fossil fuels such as petroleum and materials formed from the bacterial oxidation of organic compounds (products of photosynthesis) are typically depleted in ^{13}C (< -15‰, PDB) relative to inorganic carbon sources such as marine carbonate rocks (≈ 0 ‰) (Faure, 1997). Stable isotopic signatures do not change much during environmental alterations

and fluctuation. However, introducing new organic compounds that have different signatures will alter the ratios, thus providing a reliable way to correlate the spilled oil with the source.

The stable carbon isotopic composition of organic matter in marsh sediments is primarily controlled by the type of vegetation growing in the marsh. Coastal salt marshes dominated by C_4 plants (i.e., primarily *Spartina patens* and *Spartina alterniflora*) have $\delta^{13}C$ signatures of -14.4 to -17.7‰ (Chmura et al., 1987). Crude oils by contrast have more negative $d^{13}C$ values ranging from -23 to -32‰ depending on the source of the oil (Stahl, 1977; Macko and Parker, 1983; Jackson et al., 1996). The reported $\delta^{13}C$ values of crude oils from different reservoir rocks of the southern USA and the Gulf of Mexico are –26.6 to -33.0‰ (Stahl, 1977; Macko and Parker, 1983), which are very different from the $\delta^{13}C$ signatures of sedimentary carbon in salt marshes along the Louisiana coast (Chmura et al., 1987). Salt marshes dominated by C_3-type plant *Juncus*, which has more depleted $\delta^{13}C$ signatures (<-24 ‰) similar to those of crude oils. Large carbon isotopic difference between the C4-type marsh vegetation and the oil provides a unique opportunity to trace the source of the spilled oil in coastal marshes.

Crude oil

Crude oils and petroleum are naturally occurring flammable mixtures of hydrocarbons that exist in nature as gaseous, liquid, and solid states. Hydrocarbons are essentially organic materials chemically converted during deposition under various pressure, thermal, geological and microbial conditions. By definition hydrocarbons are molecular chains that only contain hydrogen and carbon and account for an infinite number of complexes. Petroleum hydrocarbons are dominated by saturates or alkanes, which are saturated hydrocarbons with single carbon to carbon sigma bonds. Crude oil also contains various amounts of alkenes, aromatic hydrocarbons, and polar compounds. While crude oil is mostly composed of petroleum

hydrocarbons, which include small volatile compounds to heavy non-volatile ones, it also contains minor amounts of sulfur, oxygen, nitrogen, and trace metals (e.g., vanadium, nickel, and others) (Morrison et al., 2006). Weathering and biodegradation of crude when it is exposed to oxygen can alter the structures of the lighter compounds as microbes preferentially attack and break down the single bonds in the lighter molecules. Although most light compounds of oil may be easily degraded by natural microbes on the short term, saturated heavy oil (e.g., asphaltenes, resins, polycyclic aromatics, etc.) and those adsorbed by sediments can persist in the environment for decades (Oudot and Chaillan, 2010).

Variations in source factors, microbial activity, and environments deposition lead to a unique chemical make-up for each crude oil (Wang et al., 1999). This distinct chemical make-up, also known as a fingerprint, can lead to analysis and correlation of oil to source, original organic matter, thermal maturity, migration, depositional environment, and source-rock ages (Peters et al., 1991, 1986; Morrison et al., 2006). Organic molecules present in the crude, such as terpanes, steranes, and acyclic isoprenoids and their isomers known as bio-markers, can be analyzed to construct a chemical signature or fingerprint. The selected bio-markers used for fingerprinting show little change in structure during prolonged weathering and oxidation when introduced to the environment (Peters et al., 2005; Morrison et al., 2006; Wang et al., 2007). The fingerprint constructed from resistant bio-markers can then be used in environmental forensics for correlation of spilled oil to source contamination.

MC-252 Crude oil

The crude oil released from the M-151 well in the Mississippi Canyon lease block 252 eventually created an oil slick in the Gulf that covered an estimated 68,000 square miles. An estimated 1.84 million gallons of Corexit dispersant was applied to both the surface slick and at the well site in an attempt to disperse and breakdown the leaked oil. MC-252 crude is classified as light mature oil with an American Institute gravity of 38.8. On September 24, 2010 the U.S. Coast Guard asked the USGS to perform fingerprinting identification of tar balls and degraded surface oil along the coast and affected wetlands of Texas, Louisiana, Mississippi, Alabama, and Florida (Rosenbauer et al., 2010). Rosenbauer et al. (2010) demonstrated that spilled oil present in sediments and tar balls positively correlated to MC-252 crude in various locations in this area. Rosenbauer et al. (2010) published several reference standards that can be used to correlate spilled oils to possible sources. In the current study, the ratio of several bio-markers present in MC-252 crude (see Rosenbauer et al., 2010) was used in conjunction with GC/MS-SIM analysis of sampled MC-252 crude for biomarker analysis.

Bacterial Processes

Aerobic and anaerobic bacteria contribute to or mediate many of the biogeochemical processes that take place in sediments and pore waters under various redox conditions. These processes, while complex in nature, account for various auspicious and detrimental organic and inorganic reactions. These thermodynamically spontaneous redox reactions are catalyzed by microorganisms in natural waters (Freeze and Cherry, 1979; Chapelle, 1993; Drever, 1997). Natural microbial species compete among one another for substrates, carbon sources (also function as electron donors), and availability of electron acceptors (e.g., O_2, NO^{-3}, Mn(IV),

Fe(III), SO_4^{-2}, etc.). The relationship between microorganisms becomes competitive in these instances as they vie for space, moisture, electron donors, and electron acceptors (Chapelle, 1993). This competitive relationship leads to distinct environmental zones in which selected species thrive. Zones create separation in populations that can fluctuate from location to location based on the resources present and levels of biomass. The typical zonation in Coastal Plain sediments follow a downward sequence of progressively more reducing conditions: O_2 oxidizers $\rightarrow$ NO^{-3} reducers $\rightarrow$ Mn(IV) reducers $\rightarrow$ Fe(III) reducers $\rightarrow$ SO_4^{-2} reducers $\rightarrow$ CO_2 reducers (Figure 19) (Froelich et al. 1979; Chapelle, 1993; Rittmann et al., 2001; Griffin. 2005).

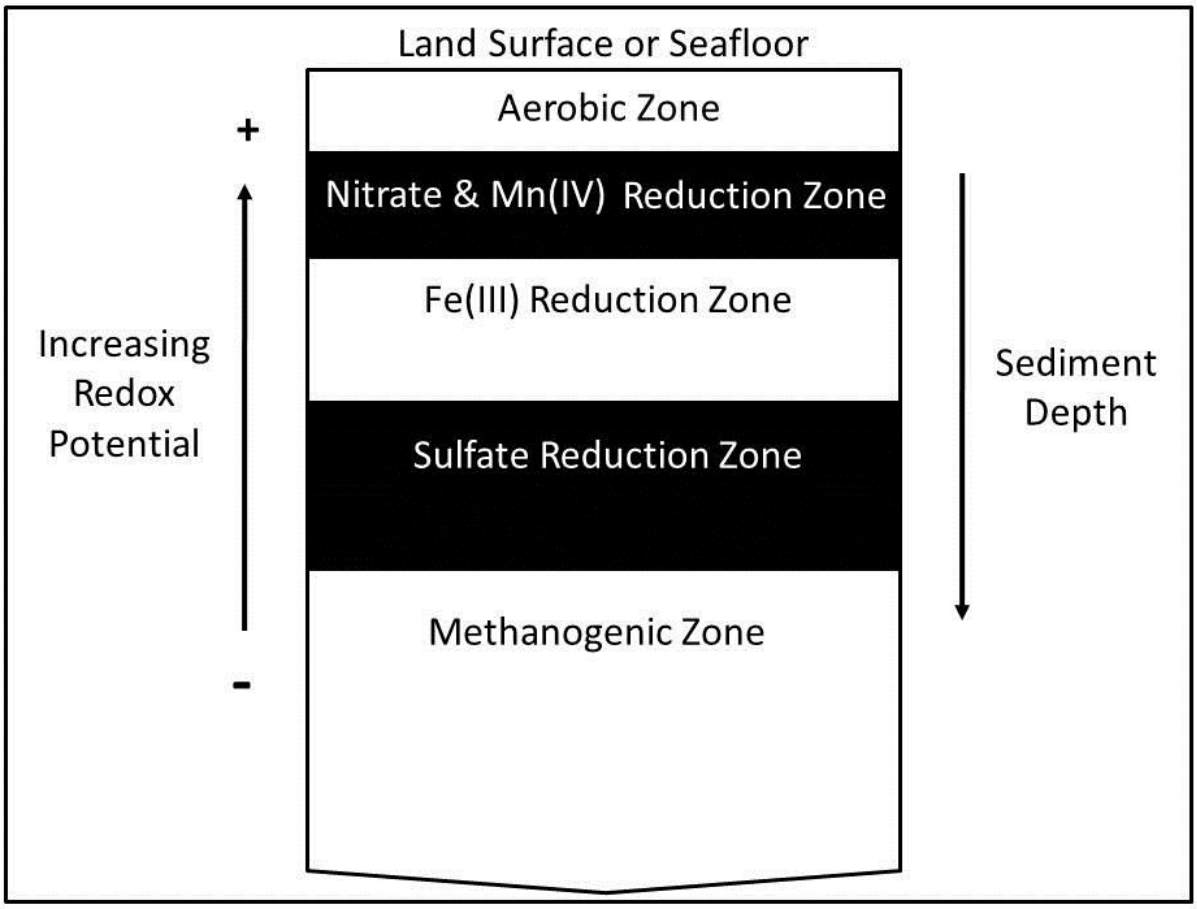

Figure 19. Terminal electron acceptor sequence in wetland sediments (after Lovely and Chapelle, 1995).

Zonation of microbial species, originally thought to be a direct inhibitory process, has since been demonstrated solely as a result of competition for resources and isn't exclusionary in nature (Drever, 1997; Chapelle, 1993). While competitive exclusion is the major factor controlling microorganism zonation, cooperative relationships also have been recognized. In highly organic carbon contaminated locations with sulfidic waters, both Fe (III) reducers and SO_4^{-2} reducers may thrive together (Beeman and Sulflita, 1987). While competitive exclusionary processes limit the activity of microorganisms out of their specific zonation, substrate rich (i.e., carbon) locations may lead to an environment that is conducive to coexistence of bacterium. (Beeman and Sulflita, 1987; Chapelle, 1993). The major biogeochemical reactions and processes evaluated in the current study are mitigated by sulfate- and iron-reducing bacteria.

Sulfate-Reducing Bacteria

Sulfate-reducing bacteria (SRB) are a diverse group of prokaryotes that contribute to and regulate many geochemical processes in various geological environments (Chapelle, 1993). These unicellular organisms that lack a cell nucleus exist as both eubacteria and archea (Madigan et al., 1997, 2003). SRB can be placed into two broad physiological subgroups or four groups based on RNA sequence characteristics (Madigan et al., 1997, 2003). The physiological subgroups are defined based on whether or not the bacteria can oxidize fatty acids, lactate, and succinate all the way to carbon dioxide. The four phylogenic subgroups are Gram-negative mesophilic SRB, Gram-positive spore forming SRB, thermophilic bacterial SRB, and thermophilic archaeal SRB (Castro et al., 1999). The geochemical processes SRB facilitate vary, but they are one of the most important facilitators of carbon and sulfur cycling worldwide by way of dissimilatory sulfate reduction. The sulfur cycle, which includes sulfur in three common oxidation states (-2 for sulfides, 0 for elemental sulfur, and +6 for sulfates), relies heavily on

these reducing bacteria for the storage and release of chemical energy (Chapelle, 1993). SRB also prevent the buildup of fermentative products in sediments by using the fermenter's by-products as a carbon source. This process plays a major role in the cycling of the carbon worldwide.

These obligate anaerobes use sulfate as a terminal electron acceptor in a reduction-oxidation reaction that ultimately produces energy for the prokaryote. This is also known as the terminal electron acceptor process (TEAP). Organic carbon that is oxidized in this process is stripped of electrons by SRB. Electrons are then consumed by the organism's electron transport chain to produce biomass and energy for cell maintenance. The organism then transfers the electrons to a newly reduced agent. This substrate-limited reaction often produces hydrogen sulfide (H_2S) as a product from sulfate (SO_4^{-2}) as electrons are placed on sulfur. This reaction is dependent on adequate amounts of electron donors and acceptors being present (National Research Council, 1993; Chapelle, 2001; Saunders et al., 2005). A generalized bacterially facilitated sulfate-reduction reaction, with acetate as the electron donor, is:

$$CH_3COO^- + SO_4^{-2} + H^+ \rightarrow 2\ HCO_3^- + H_2S_{(aq)} \quad (1)$$

SRB are capable of de-mobilizing dissolved heavy metals as a result of their respiratory activities by way of raising pH levels and producing hydrogen sulfide (H_2S), thus precipitating metals as highly insoluble metal-sulfides. A generalized metal sulfide production reaction with Me^{2+} as a divalent normally reduced form of a metal can be shown as.

$$HS^- + Me^{2+} \rightarrow MeS + H^+ \quad (2)$$

Low-valence or reduced forms of metals present in the aqueous phase often bond to the hydrogen sulfide (H_2S), producing metal sulfides referred to as bacterial produced metal sulfides

(BPMS). These BPMS, such as iron sulfides (pyrite, pyrrhotite, troilite, mackinawite) and zinc sulfides (sphalerite, marmatite) can become a adsorption site for various other divalent metals. In reducing environments, BPMS are incorporated and adsorbed with Pb(II), Cu(II), Cd(II), Zn(II), Ni(II), Fe(II), and As(V) (Huerta-Diaz and Morse, 1992; Jong et al., 2004). BPMS are efficient sinks for various toxic trace metals.

The BPMS in modern marsh sediments are mostly various species and textures of sedimentary pyrite when ample amounts of Fe(II), SO_4^{-2}, and organic carbon are present (Berner, 1970, 1984). Laboratory studies have shown that organic carbon present in the system for bacterial consumption is the most important contributing factor during BPMS growth in terrigenous marine sediments (Berner, 1984).

During nucleation and growth, various pyritic minerals show distinct textures and forms under alternating redox conditions in tidally-influenced salt marshes. BPMS, especially pyrite, evolve into framboidal spheres, fused octahedral pyrite crystals, well developed octahedral crystals, loose euhedral pyrite crystals, and fused framboids. These forms are theorized to indicate differences in oxygen concentrations in coastal and marine sediments during mineral growth (Wilkin et al., 1996). Hence, BPMS forms may be useful for paleoenvironmental analysis. However, recently texture and growth of BPMS have been attributed alternatively to substrate availability, and interplay of several biogeochemical processes (Roychoudhury, 2003).

While SRB are widely considered to create auspicious biotransformative reactions such as trace metal sequestration, several key pathways that are taken by SRB can be extremely toxic and detrimental. This includes the formation of thioarsenate and thioarsenite, known arsenic bearing aqueous compounds, in highly sulfidic waters. Areas with elevated hydrogen-sulfide concentrations often produced by SRB can lead to the formation of these two toxic aqueous

compounds instead of forming insoluble metal sulfides. These aqueous compounds bind the arsenate and arsenite released from arsenic incorporated in iron-oxides by iron-reducing bacteria (Keimowitz et al., 2005).

Recent studies have shown that strongly reducing environments created by SRB can facilitate mercury methylation (USGS Fact Sheet 146, 2000; Mason et al., 2005; Monrreal, 2007). In this process, inorganic mercury and carbon are joined to make methylmercury under strongly reducing environments. SRB are particularly efficient mercury methylators due to their coupling with sulfate reduction. However, the process is poorly understood (Chapelle, 1994). In many Gulf estuaries and coastal watersheds, mercury bioaccumulation from fish consumption already poses a health hazard.

Iron-Reducing Bacteria

Iron-reducing bacteria (IRB) exist in nature as a multitude of anaerobic prokaryotes using various resources as electron donors and acceptors in TEAP. While IRB classifications are currently in a state of flux, it is commonly recognized that there are four members of the delta subdivision of the class Protobacteria: *Geobacter, Desulfuromusa, Pelobacter*, and *Desulfuromonas*, all of which are Gram-negative (Lonergan et al., 1996). In coastal environments, chemoheterotroph species commonly use organic carbon as an electron donor in TEAP (Lovely and Chapelle, 1995; Drever, 1997; Straub et al., 2000). These chemoheterotrophs contribute to one of the most important microbial mediated groundwater redox reactions that occur in wetland sediments (Chapelle, 1993). Reduction of ferric iron (Fe^{+3}) to ferrous iron (Fe^{+2}) by way of iron being an electron acceptor and organic carbon the donor leads to the principal cause of undesirable high concentrations of dissolved iron and associated trace metals in groundwater.

Iron is most commonly introduced to wetland environments by deposition of Fe- and Mn-oxides/hydroxide minerals being derived from terrestrial erosion and run off. These negatively charged clays and silts sorb divalent toxic metals often concentrated by anthropogenic means (Freeze and Cherry, 1979; Drever, 1997). During the TEAP facilitated by IRB, organic carbon is stripped of electrons and then placed on ferric irons that constitute Fe- and Mn-oxides/hydroxide minerals. A generalized bacterium-facilitated iron-reduction reaction, with acetate as the electron donor can be shown as:

$$CH_3COO^- + 8\ FeOOH(s) + 15\ H^+ \rightarrow 2\ HCO_3^- + 8\ Fe^{+2} + 12\ H_2O \quad (3)$$

Toxic metals such as arsenic and mercury are released during iron reduction when Fe- and Mn-oxides/hydroxides breakdown and Fe^{+3} is reduced by IRB. Release of sequestered metals into the environment cause high concentrations of dissolved metals in the IRB environment. In addition to the release of metals, speciation can take place due to reducing conditions. Arsenic can be reduced from As(V) to As(III), the more adsorption-resistant and toxic form of arsenic (Bose and Sharma, 2002; Saunders et al., 2008). *Geobacter metallireducens* has been identified as the major species that metabolize these reactions. However, multiple strains contribute to the process (Lonergan et al., 1996; Chapelle, 1993).

IRB exist in nature where specialized electron donors and acceptors exist in abundance to facilitate its TEAP. The depth at which the reaction flourishes is related to IRB's ability to out-compete deeper microbes while more efficient microbes out-compete IRB in shallower TEAP zones (Figure 19). In iron-rich, sulfate-depleted environments, IRB also have been linked to mercury methylation, although the process is poorly understood. In contrast, sulfate-rich environments, SRB will out-compete IRB for mercury methylation (Kerin et al., 2006; Merritt and Amirbahman, 2009). In iron-limited, sulfate-rich environments (i.e. coastal wetlands)

IRB can co-exist but in most cases are commonly out-competed by SRB. SRB will dominate the environment at these locations (Madigan et al., 1997; Straub et al., 2000).

METHODS

Sample Retrieval and Preparation

Surface-water samples were first drawn via a Van Dorn style sampler from immediately above the sediment surface at each site for in situ analysis. Additional water samples also were collected and placed in sealed bottles for bulk chemical and dissolved organic carbon (DOC) analyses. Water samples were filtered through a 0.45-µm filter, and sub-samples taken for trace element and cation analysis were acidified with trace-grade concentrated HNO_3 acid.

At least eight cores of sediment were taken at each site using a Wildco hand corer with a two-meter extension. Each sediment core was caught and sealed in a 50-cm-tall plastic tube, inside the coring device. The corers metal nose was replaced with a plastic one, and all other parts that came in contact with the sediment were plastic to avoid trace-metal contamination. Cores collected at each sampling site were extracted from the hand corer and surface water was removed. The plastic tube containing the sediment was then capped as quickly as possible. Cores were labeled with their specific site location prefix and additionally labeled with A, B, C, D, E, F, G, and H to differentiate them from one another within their sampling locations (Table 2). The cores were then stored upright in a cooler on ice and transported back to the lab.

Immediately following collection, cores were taken to nearby wet chemistry laboratories for further processing. These labs were chosen based on of their proximity to sampling locations, which permitted rapid processing. All cores were processed within twelve hours of sampling to minimize changes in redox conditions and potential sediment-water reactions. WB, WI, and LB samples were brought to Weeks Bay Reserve Laboratory for processing, while RG and BJS

samples were processed at Southern Mississippi University's Laboratory at Stennis Space Center.

Live marsh plants were collected from each location for stable carbon-isotope analysis. Oil suppressed plants also were collected at each heavily oiled location where oil persisted. All plants collected were either *Juncas* or *Spartina alterniflora.* Bulk sediments from the surface of heavily oiled sites also were collected, and their degradation-resistant polycyclic aromatic hydrocarbons (PAH) were extracted for GC-MS and biomarker analysis.

In Situ Water Analyses

In situ surface-water from each site was analyzed for dissolved oxygen (DO), pH, electrical conductivity, oxidation-reduction potential (ORP), and temperature during each site visit using hand-held meters or with a TROLL 9000 multi-parameters port. Surface water from each location was analyzed at Auburn University's Forestry Department by a Shimadzu TOC-V Combustion Analyzer for DOC contents. Filtered (0.45-µm filter) surface waters from each site were sent immediately after collection to Vassar College for analyses that included major ion and trace metal analyses by ion chromatography (IC) and inductively coupled plasma mass spectrometry (ICP-MS).

Pore-Water Geochemical Analyses

Sediment cores were sectioned at 3-cm intervals to insure 50-ml of sediment volume for each section from the top of the core down to 30 cm. Several of these cores and their component sections were then centrifuged with a Beckman Coulter Allegra X-22 that was transported to each lab in order to separate pore-waters from the sediments (Table 2). To better understand the effect of oil spill on sediments, geochemical analyses were conducted on 10 pore-water samples

extracted from various depth intervals (0-3 cm, 3-6 cm, 6-9 cm, etc.) of each core to delineate any changes with depth. Pore-waters used in anaerobic analyses were sectioned and extracted in nitrogen-filled glove bags. This insured a continued anoxic environment for pore-water geochemistry and trace-metal analyses. Pore-water samples for trace elements and cation analysis were acidified with trace-metal grade concentrated HNO_3. After all pore waters were separated and prepped, they were used for the analyses described below.

A HACH DR/2700 was used immediately in the lab to measure reduced ferrous iron (HACH method 8146) and sulfide (HACH method 8131) concentrations in pore waters. A hand-held pH meter (Hanna 8424) was used to test pH values in pore water from each section. Samples for total and organic mercury analyses were stored in VWR trace clean vials. These samples were shipped and analyzed using a Tekran 2500 Fluorescence Mercury Detector at Woods Hole Oceanographic Institution. Concentrations of fluoride, chloride, nitrite, sulfate, bromide, nitrate, phosphate, lithium, sodium, ammonium, potassium, magnesium and calcium were determined using Ion Chromatography (IC) facilities at Vassar College. Inductively coupled plasma mass spectrometry (ICP-MS) to evaluate trace metal concentrations was performed at Columbia University. Arsenic speciation measurements were conducted at Vassar College using IC-Atomic Fluorescence Spectrometry. A Shimadzu TOC-V Combustion Analyzer at Auburn University's Forestry Department was used for measuring dissolved organic carbon (DOC) in pore water.

Grain-Size and Geochemical Analyses of Sediments

Each of the 30-cm-long cores from 10 coring sites were sectioned into 3-cm segments and hundreds of sediment subsamples were processed for grain size and geochemical analyses (Table 1) to recognize any changes with substrate depth. Sediments utilized for anaerobic analyses

were sectioned in nitrogen-filled glove bags. This insured a continued anoxic environment for trace metal analysis and anaerobic microbial preservation. Unless otherwise noted, sediments were dried in an oven at 30° C to insure minimum volatilization of any metals. After drying, sediments were hand pulverized to pass through a 230-mesh sieve. Ten sets of sediment samples (0-3 cm, 3-6 cm, 6-9 cm etc.) from each site were used in analyses described below.

Samples were shipped to ACME labs to analyze bulk elemental composition by ICP-MS after total acid digestion and removal of organics. Total digestion analysis quantified results for 38 elements, including mercury and arsenic. Additional sediment samples were analyzed for carbon isotope ($^{13}C/^{12}C$) ratios to fingerprint sources of organic matter in the wetlands. Carbon-isotope analyses were performed using a Finnigan MAT delta Plus XP Mass Spectrometer at Florida State University. A LECO carbon analyzer in Auburn University's Sedimentary Geology lab was used to determine total organic carbon (TOC) contents of sediments.

Pulverized sediments from the 0-3 cm, 15-18 cm, and 27-30 cm sections of the core from each site were used to quantitatively analyze mineral composition by a Rigaku XRD housed in the Chemistry Department at Auburn University. Samples were spread with hexane onto a zero background holder to eliminate preferred orientation. Measurements of the intensity of reflections at 2-theta values were recorded from three to sixty-five degrees. Reflections and intensities are determined by unit-cell dimensions, which reveal information about the crystallographic structures of minerals present in each sample. Data was copied into RAW files for input into identification software. The files were then analyzed by a free demonstration version of the Match Crystal Identification software. Background subtraction, K-alpha2 stripping, data smoothing, and 2-theta correction were performed when necessary. Qualitative and semi-quantitative results were recorded for each sample.

Sediments from the 0-3 cm, 15-18 cm, and 27-30 cm sections from one core at each site (15 samples) were analyzed for grain-size by wet-sieve and pipette techniques (Gee and Or, 2002). Sediment samples were wet-sieved through a 230-mesh sieve using distilled water to separate sands and larger organic material from the fines (silt and clay). The distilled water, fines, and 50 ml of deflocculant were added to a 1000-ml graduated cylinder. The sand and organics left in the 230-mesh sieve were washed into a beaker with distilled water and all organics were removed by floating them off the surface.

The sand portion of each section was dried in an oven and weighed. For samples in which sand exceeded 5% by weight, sands were processed by standard dry sieve analysis using one-phi interval screens. The fine portions of each sample were analyzed by standard pipette analysis. Grain-size analyses allowed for quantification of grain sizes from -1 phi to >10 phi in 1- phi intervals.

Sediments from 0-3 cm, 15-18 cm, and 27-30 cm sections from one core at each site were separated in anoxic conditions, packed with ice, and then sent overnight to Dr. Benedict Okeke at Auburn University at Montgomery. These samples were used for culturing and DNA analysis of possible iron- and sulfate-reducing bacteria (Table 2). Microbial analyses included the use of Eppendorf thermo cycler and most probable number/polymerase chain-reaction techniques.

Heavy mineral separation of sediments from Weeks Bay and Bay Jimmy South was conducted at Auburn University's sedimentology laboratories in order to analyze metal-sulfide precipitation. Sediments from greater than 12 cm of core were dried, disaggregated, and then added to tetrabromoethane and placed in 50-ml centrifuge tubes. Tetrabromoethane is a halogenated hydrocarbon that has an unusually high density around 3 g/ml. Samples were centrifuged for fifteen minutes at 3000 rpm and the less dense material was removed from the

top. Additional tetrabromoethane was added and the process repeated until only the >3 g/ml sediment fraction remained. Heavy minerals were removed, washed with acetone, and dried. Heavy minerals were used to make grain-mount thin sections for petrographic identification and photographic documentation of sulfides. Thin sections and gold-sputter coated loose samples were then taken to Auburn University's Material Engineering SEM Laboratory for image and elemental analyses. Energy-dispersive X-ray spectroscopy (EDAX) was employed in conjunction with the SEM to image various metal sulfides and to quantify their approximate chemical compositions.

Selected metal sulfides identified in thin sections were transported to the National High Magnetic Field Lab in Tallahassee, Florida, for laser ablation inductively coupled plasma mass spectrometric (LA-ICP-MS) analysis. Dr. Munir Humayun of Florida State University assisted with all LA-ICP-MS measurements at the National High Magnetic Field Lab Plasma Analytical Facility. Analyses were performed with a UP 193 FXArF (193 nm) excimer laser ablation system (New Wave Research, Fremont, CA, USA) coupled to a Thermo Finnigan Element XR ICP-MS. The ablating spot size ranged from 15-25 μm. All results were normalized to Fe and S, and results of selected metals were recorded.

Gas Chromatography/Mass Spectrometry-Time of Flight & Selected Ion-Mode Analyses

Bulk surface sediments and selected sections (0-3 cm, 12-15 cm, and 27-30 cm) of sediment cores from oiled sites (i.e., BJS, WI, and RG) were prepared at Auburn University's Department of Geology and Geography Sedimentology laboratories for PAH extraction and GC/MS analyses. EPA modified method 3570 was used for PAH extraction from sediments. PAH extraction began with mixing 5 g of anhydrous sodium sulfate, 10 g of dichloromethane (DCM), and 3 g of sediment in a pre-cleaned PTFE extraction tube. The tube was sealed, wrapped with

Parafilm, and then agitated vigorously for 2 minutes. Tubes were placed in a rotating incubator and spun for 24 hours then centrifuged for 10 minutes at 3000 rpm. All supernatant was then pipetted into a glass extraction vial, filtered with a 25-mm 0.2-µm PTFE filter, transferred to a new extraction vial and placed under a fume hood. Samples were then blown with N_2 gas for 30 minutes so as to volatize all DCM. A solvent mixture of hexane and methyl-tert-butyl-ether (1:1) was added to the extraction vials in order to solvate any resultant solute PAHs. A small volume (1.5 ml) of the solvation was then evacuated by a glass syringe and needle into a 2.0 ml auto sampler vial for Gas Chromatography/Mass Spectrometry-Time of Flight and Gas Chromatography/Mass Spectrometry Selected Ion-Mode Analyses analyses.

Oil-suppressed plants collected from heavily oiled locations (BJS) were scraped to recover weathered oil. This weathered oil and BP source MC-252 crude oil were prepared for GC/MS analyses by the following process. The oils were placed into an extraction tube with a solution of hexane (1:200). The extraction tube containing the mixture of oil and hexane was then wrapped with Parafilm and vigorously agitated. The agitated sample was placed on a rotating incubator and spun for 24 hours. The solvation was then filtered through a 25-mm 0.2-µm PTFE filter, and 1.5 ml of solution was placed into a 2-ml auto sampler vial.

All samples (sediment extracts, solvated crude oil, and solvated weathered oil) were analyzed at Auburn University Chemistry Department's Mass Spectrometry Center. A Waters GCT Premier bench-top gas-chromatograph orthogonal acceleration time-of-flight mass spectrometer (GC/MS-ToF) was used to identify and semi-quantify concentrations of organic compounds and hydrocarbons. The GC/MS-ToF originally ran at an initial temperature of 90°C with a 5-degree ramp until 300°C was reached for each sample. After initial interpretation, samples were re-run at a starting temperature of 30° C at a 10 degree ramp until 300 degrees was reached.

Finally, samples that showed positive hydrocarbon content were analyzed at specific starting ranges at a 2 degree ramp in order to evaluate more precisely any chromatograph peaks that indicated hydrocarbon presence.

Selected samples of initial BP crude oil (MC 252 crude), site recovered weathered oil, and oil compounds extracted from core and bulk sediments were analyzed by GC-MS under high sensitivity Selected Ion Mode (SIM) for petroleum biomarkers with specific mass-to-charge ratios (M/Z) of 191, 217, and 218 at Columbia Analytical Labs. These samples were analyzed using a Agilent 5975C gas-chromatograph mass spectrometer (GC/MS) in both full-scan and selected ion modes (SIM). When operated in the SIM mode, a triplequad detector minimizes the background noise and virtually eliminates many of the extraneous peaks, allowing better identification and quantification of target biomarker compounds with specific mass-to-charge ratios (M/Z) of 191, 217, and 218.

Remaining Cores and Samples

Additional cores that were collected but not sectioned are being stored intact in the event additional samples are needed in the future. They are stored upright in a cold room at Auburn University's Funchess Hall. All additional sectioned sediment samples, sediment oil extracts, and crude samples are stored at Auburn University's Department of Geology and Geography Hydrogeology Laboratory.

Table 2. Analyses of pore-water, sediment, plant, and crude oil samples.

Core/ Media	N_2	Analysis	Instrument	Location of Analysis	Analytical/ Preservation
A	X X X	1. Major Ions 2. As Speciation 3. Trace Metals	Ion Chromatography (IC) IC-Atomic Fluorescence MS ICP-MS	Vassar Vassar Columbia	Flash Frozen Flash Frozen Acidified
B	X X X	1. Hg Speciation 2. Fe(II) 3. Sulfide	Tekran Mercury Detector HACH Spectrophotometer HACH Spectrophotometer	Woods Hole Field Field	EPA 1631 HACH 8146 HACH 8131
C		1. Dissolved Organic Carbon 2. Sediment Total Organic Carbon	TOC-V Combustion Analyzer LECO Carbon Analyzer	Auburn Auburn	Filtered Inorganic C Test & Removed
D		1. Grain Size Analyses 2. Mineral Identify 3. Metal Sulfide	Sieve and Pipette Methods X-Ray Diffraction SEM, EDAX	Auburn Auburn Auburn	Statistical MATCH Separation
E		1. Sediment Bulk Composition 2. Sediment $^{13}C/^{12}C$	ICP-MS Finnigan IRMS	ACME Labs Florida State	Total Digestion CO_2 Equilibrium
F	X	Microbial Analysis	Eppendorf Thermal Cycler	AUM	MPN/PCR
G		1. PAH Fingerprinting 2. Bio-Marker Analysis 3. Pyritic Framboid Composition	Gas Chromatography/Mass Spectrometry- ToF & SIM LA-ICP-MS	Auburn CASLAB Florida State	PAH Extraction Statistical Slide Mount
H		Supplemental	Supplemental	Auburn	Freezer
Plant		Plant $^{13}C/^{12}C$	Finnigan IRMS	Florida State	CO_2 Equilibrium
Source & Plant Oil		1. PAH Fingerprinting 2. Bio-Marker Analysis	Gas Chromatography/ Mass Spectrometry-ToF & SIM	Auburn CASLAB Auburn	PAH Extraction Chromatograph Statistical

RESULTS AND DISCUSSION

Results are presented and discussed in the following order. First, sediment grain-size and XRD derived mineralogy is described. Second, water geochemistry including major ions, trace metals, reduced Fe and sulfides, pH of pore waters and oxidation reduction potential (ORP), conductivity, and dissolved oxygen (DO) of surface water is addressed. Third, dissolved organic carbon (DOC) in pore waters and total organic contents (TOC) in sediments are reviewed. Next, sediment geochemistry including bulk chemistry, petrographic and SEM-EDAX analysis, aluminum normalized enrichment factors, and laser ablation analysis of sulfide solids are reported and discussed. Next, gas chromatography mass spectrometry (GC-MS) analysis and geochemical correlation of oil biomarkers are reviewed, then carbon isotope systems of marsh sediments, oils, and plants are presented. Finally, microbiology of analyzed sites is addressed. It is important to reiterate to the reader that five locations were chosen in Alabama and Louisiana's coastal wetlands for this particular study (Walker Island, Longs Bayou, Weeks Bay, Rigolets, and Bay Jimmy South). However, in some instances data for all ten sites is reported for comparison and discussion purposes. Additional data referred to but not reported in this chapter are available in the Appendix sections.

Sediment Grain-Size and XRD Analyses

Sediments from 0-3 cm, 12-15 cm, and 27-30 cm sections at all sites were evaluated for grain size distribution (Figures 20, 21, 22) and mineralology (Tables 6, 7, 8). All sites contained various amounts of fine-grained sand, silt, clay, plant debris, and organic matter (Tables 3, 4, 5).

WB, a pristine site, is characterized by relatively fine sediments. Grain size data indicates that sediments at WB are dominated by mud (49-53% clay and 47-51% silt). LB, another control site, consists mostly of fine-grained sand (69-85% sand) with subordinate clay and silt. The slightly contaminated site WI in Alabama is the sandiest of all sites evaluated, having fine sand contents of 88 to 93%. RG, a slightly contaminated site in Louisiana, shows variations in grain size with depth. Sections 0-3 cm and 12-15 cm at RG are dominated by silty sand and sandy silt (47-57% sand and 53-43% mud), while section 27-30 cm is much finer (68% silt and 32% clay). The coarser grain sizes in the upper part of RG cores may be attributed to wash over of coastal sediments into the estuarine environment during Hurricane Katrina in 2005. BJS, a heavily contaminated site, is characterized by muds. BJS sediments only contain silt (73-77%) and clay (27-23%).

The presence of fine-grained sediments and natural organic matter is important for the retention and transformation of metals and oils in marsh sediments. Trace metals often concentrate in fine-grained sediments (e.g., clay) that have negatively charged, high-surface areas for adsorbing positively-charged metals. Other fine-grained solids, such as Fe sulfides and oxides, also may serve as important sinks for toxic metals such as arsenic. Fine-grained marsh sediments containing high levels of organic matter have a greater potential for mercury methylation and arsenic mobilization (Hammerschmidt et al., 2004; Burnol et al., 2010). BJS and other heavily oiled sites all contain high percentages of clay and silt, with little to no sand. Fine-grained sediments and high organic-carbon concentrations that dominate at oiled sites provide favorable environments for biological and chemical transformation of trace metals.

X-ray diffraction (XRD) analyses of sediments were performed on 0-3 cm, 12-15 cm, and 27-30 cm core sections at all sites (Tables 6, 7, 8). Results indicate that sediments consist mainly of

quartz, clay (phyllosilicate minerals), sulfate, and sulfide minerals. Mineralogical composition correlates with both grain size and bulk chemistry (see Sediment Geochemistry section). Sites that have predominantly coarser sediments (i.e., sand and silt), such as WI, BH, and top-most sections of RG, are dominated by quartz. Sites dominated by fine-grained sediments, such as WB and BJS, are relatively quartz poor and clay rich.

Sulfide minerals increase with core depth, most notably in fine-grained sections. Metal sulfides are present at WB and BJS sites at shallower depths (12-15 cm) under a strongly reducing condition. By contrast, sulfide solids do not occur above depths of 27-30 cm at the coarser-grained sites (i.e., WI, RG, and LB).

The presence of sulfides in the 12-15-cm sections of sites WB (17%) and BJS (31%) indicates that fine-grained, inherently organic-rich sediments allow for the establishment of sulfate-reduction conditions at shallower substrate depths. Increased flux of organics (i.e. oil) into salt marsh environments (such as at BJS) may fuel bacterial sulfate reduction and formation of sulfide solids at shallower depths. The presence of sulfur solids at shallower depths when compared to pristine sites is also evident at other fine-grained oiled sites in Louisiana. The shallower reduction horizon is characterized by accelerated SRB colonization and their reductive activities that produce hydrogen sulfide and high pH pore-water (see Water Geochemistry section). The accelerated TEAP process is theorized to be the cause of increased sulfide production via BPMS.

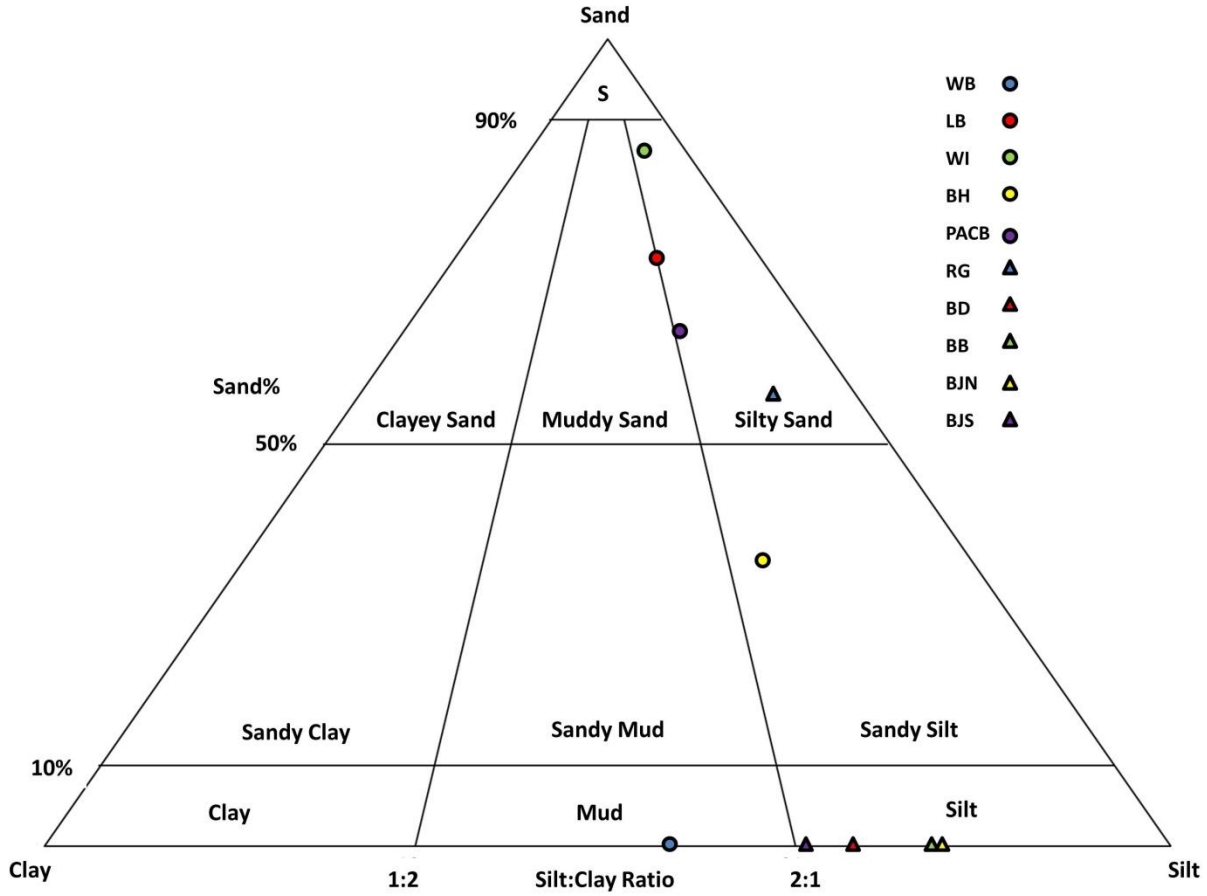

Figure 20. Sediment textures of samples from 0-3 cm depth plotted on Folk diagram.

Table 3. Grain-size characteristics of marsh sediments from 0-3 cm depth intervals.

	Sand %	Silt %	Clay %	Sediment Name	Mode	Textural Group
WB	0.00	54.03	45.97	Mud	Bimodal	Mud
LB	75.25	15.87	8.88	Muddy very fine sand	Unimodal	Muddy sand
WI	88.46	7.93	3.61	Fine silty medium sand	Unimodal	Silty sand
BH	35.87	45.13	19.01	Very fine sandy coarse silt	Trimodal	Sandy silt
PACB	63.68	23.88	12.44	Muddy fine sand	Bimodal	Muddy sand
RG	56.69	34.83	8.47	Very coarse silty very fine sand	Trimodal	Silty sand
BD	0.00	70.31	29.69	Medium silt	Bimodal	Silt
BB	0.00	75.97	24.03	Medium silt	Trimodal	Silt
BJN	0.00	67.34	32.66	Very coarse silt	Trimodal	Silt
BJS	0.00	77.33	22.67	Very coarse silt	Bimodal	Silt

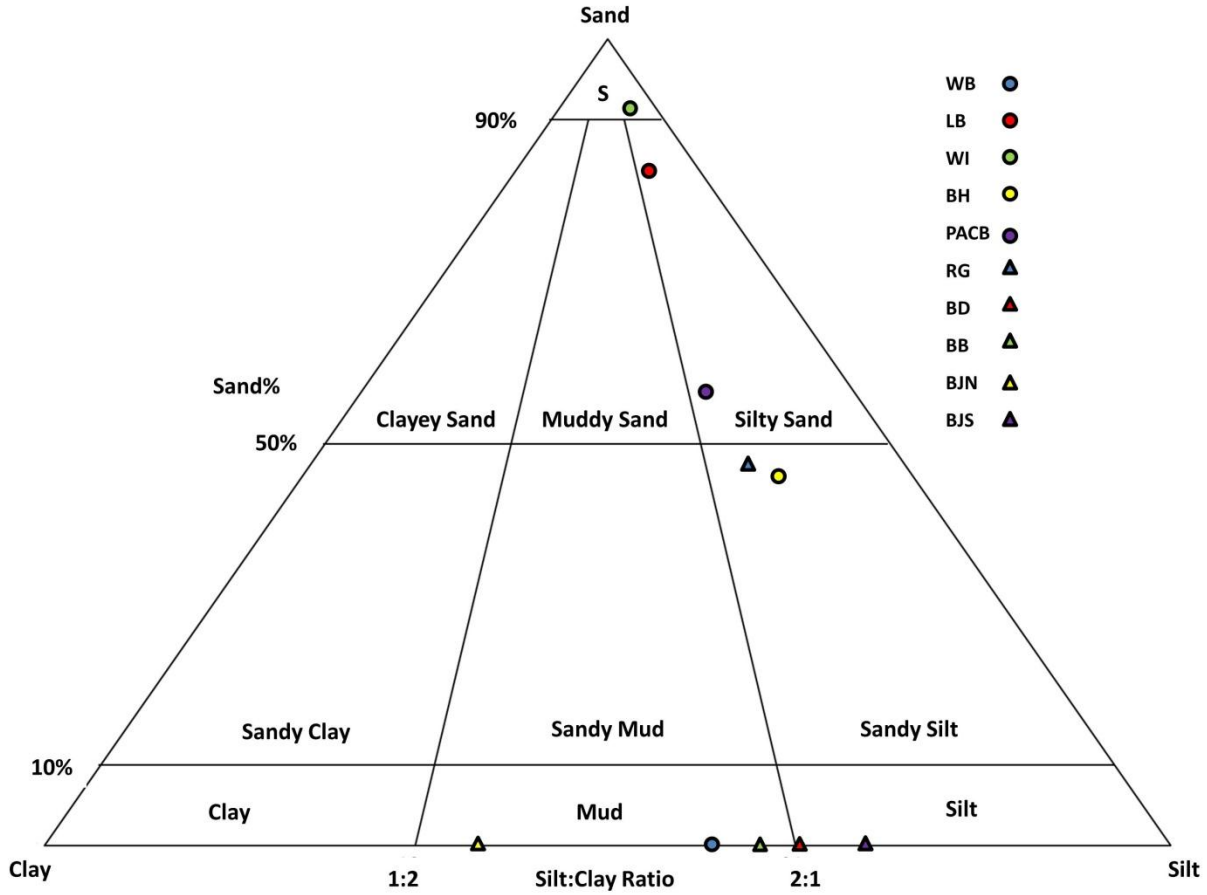

Figure 21. Sediment textures of samples from 12-15 cm depth plotted on Folk diagram.

Table 4. Grain-size characteristics of marsh sediments from 12-15 cm depth interval.

Sample ID	Sand %	Silt %	Clay %	Sediment Name	Mode	Textural Group
WB	0.00	60.78	39.22	Mud	Bimodal	Mud
LB	83.45	11.48	5.07	Very coarse silty very fine sand	Unimodal	Silty sand
WI	93.30	4.00	2.70	Medium sand	Unimodal	Sand
BH	50.63	37.07	12.30	Fine sandy very coarse silt	Bimodal	Sandy silt
PACB	56.02	29.63	14.35	Very coarse silty fine sand	Bimodal	Silty sand
RG	47.49	37.20	15.31	Very fine sandy very coarse silt	Bimodal	Sandy silt
BD	0.00	65.55	34.45	Mud	Bimodal	Mud
BB	0.00	62.09	37.91	Mud	Bimodal	Mud
BJN	0.00	41.37	58.63	Mud	Trimodal	Mud
BJS	0.00	73.57	26.43	Coarse silt	Bimodal	Silt

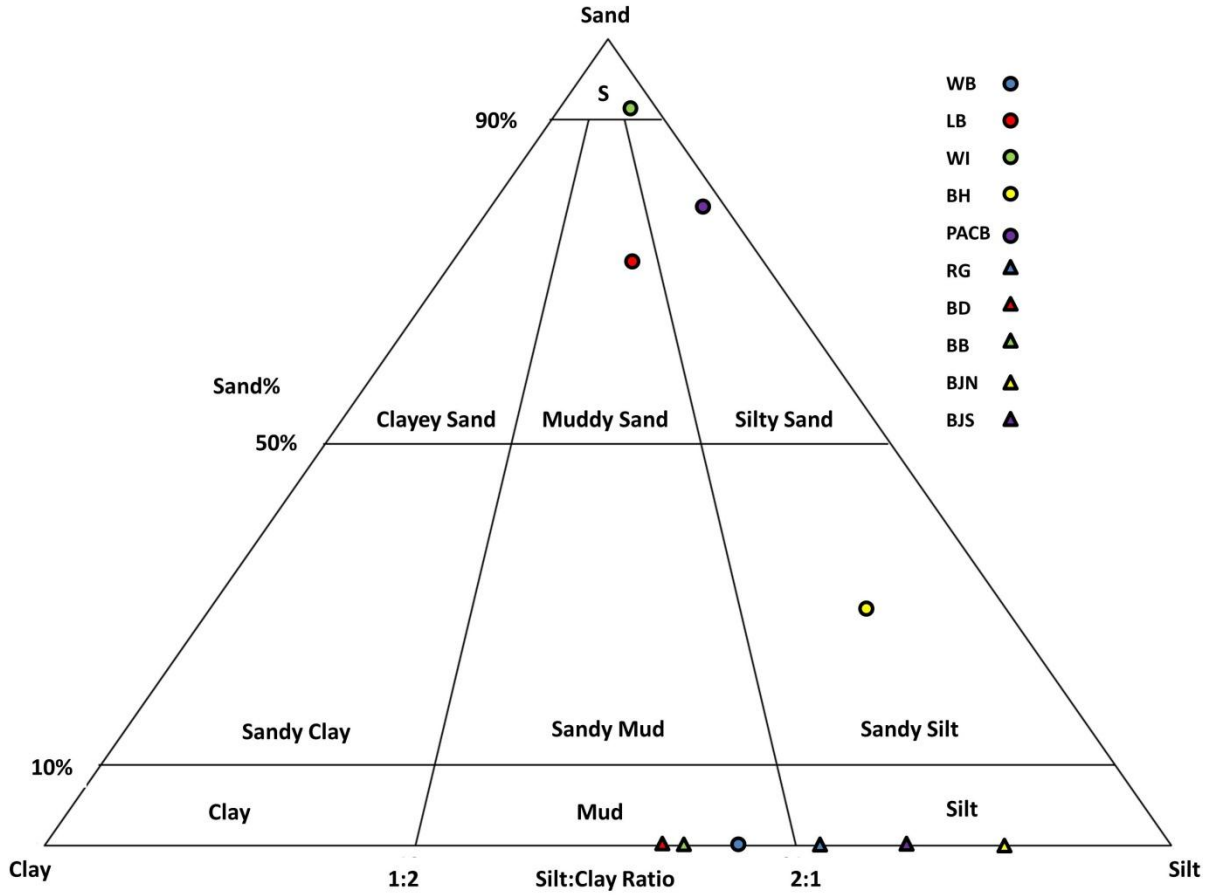

Figure 22. Sediment textures of samples from 27-30 cm depth plotted on Folk diagram.

Table 5. Grain-size characteristics of marsh sediments from 27-30 cm depth interval.

Sample ID	Sand %	Silt %	Clay %	Sediment Name	Mode	Textural Group
WB	0.00	61.73	38.27	Mud	Bimodal	Mud
LB	69.08	17.81	13.11	Muddy fine sand	Bimodal	Muddy sand
WI	92.66	4.66	2.68	Medium sand	Unimodal	Sand
BH	29.04	59.48	11.47	Very fine sandy coarse silt	Trimodal	Sandy silt
PACB	74.08	21.85	4.07	Coarse silty fine sand	Bimodal	Silty sand
RG	0.00	68.05	31.95	Medium silt	Bimodal	Silt
BD	0.00	57.52	42.48	Mud	Trimodal	Mud
BB	0.00	56.71	43.29	Mud	Bimodal	Mud
BJN	0.00	87.16	12.84	Medium silt	Bimodal	Silt
BJS	0.00	73.49	26.51	Coarse silt	Bimodal	Silt

Table 6. Average mineral composition of sediment samples from 0-3 cm of depth determined by XRD.

Minerals 12-15 cm	WB %	LB %	WI %	BH %	PACB %	RG %	BD %	BB %	BJN %	BJS %
Quartz	46	63	75	73	83	53	57	43	57	65
Clay Minerals	48	37	15	27	9	41	27	50	43	15
Sulfates	0	0	10	0	8	6	0	7	0	20
Fe Sulfides	0	0	0	0	0	0	5	0	0	0
Non-Fe Sulfides	0	0	0	0	0	0	0	0	0	0
Others	6	0	0	0	0	0	11	0	0	0

Table 7. Average mineral composition of sediment samples from 12-15 cm of depth determined by XRD.

Minerals 12-15 cm	WB %	LB %	WI %	BH %	PACB %	RG %	BD %	BB %	BJN %	BJS %
Quartz	54	63	88	66	84	41	27	9	29	54
Clay Minerals	20	29	7	26	9	52	15	51	51	15
Sulfates	9	0	5	8	7	7	16	12	7	0
Fe Sulfides	8	0	0	0	0	0	15	9	13	6
Non-Fe Sulfides	9	8	0	0	0	0	27	19	0	25
Others	0	0	0	0	0	0	0	0	0	0

Table 8. Average mineral composition of sediment samples from 27-30 cm of depth determined by XRD.

Minerals 27-30 cm	WB %	LB %	WI %	BH %	PACB %	RG %	BD %	BB %	BJN %	BJS %
Quartz	26	79	82	49	63	56	18	58	49	54
Clay Minerals	42	16	12	23	24	23	41	29	15	19
Sulfates	4	0	0	4	8	0	9	0	0	7
Fe Sulfides	28	1	6	0	5	7	3	0	5	6
Non-Fe Sulfides	0	4	0	3	0	14	29	6	31	14
Others	0	0	0	21	0	0	0	7	0	0

Surface-Water Geochemistry

Surface-water data including temperature, pH, ORP, DO, DOC, and electrical conductivity, from all sites are provided in Table 9. Large variations in surface-water temperature (6.6 to 25.3°C) are directly related to different sampling dates for different sites (Alabama and Mississippi sites, October 2010; Louisiana sites, January 2011). Surface water pH (7.03 to 8.3) and conductivity (>2000 to 13950 µs/cm) data indicate that varying degrees of freshwater and seawater mixing occurs in various salt-marsh settings. ORP (65 to 230 mV) between sites vary slightly but all indicate slightly oxidizing conditions in surface waters. Cold water can hold more DO than warmer water. The total amounts of dissolved oxygen at all Louisiana sites (9.73 to 12.32 mg/kg) measured in January are higher than those at Alabama and Mississippi sites (6.9 to 8.09 mg/kg) measured during the warmer month of September. DOC values indicate variations in total organic loading in filtered water (compounds below 0.45 µm), and the values increase proportionally with the degree of contamination at each site. BJS, a heavily contaminated and more tidally influenced site, shows more than twice the levels of DOC than at WB, a pristine site. These higher DOC levels most likely result from degraded oil that was present along the contaminated shoreline. The degraded oil has leached or dissolved into surface waters during tidal fluctuations or cycles. The DOC levels in surface water (< 45 mg/kg) at contaminated sites, however, are significantly lower than those in pore-water extracted from sediments (up to hundreds of mg/kg, see next section). This indicates that the vast majority of oil contaminant in the water column has been evaporated, dispersed, or degraded by microorganisms months after oil spills.

Table 9. Surface water data gathered from all sites.

Sample ID	Water Depth (cm)	Temp. (°C)	pH	ORP (mV)	DO (mg/kg)	Cond. (µs/cm)	DOC (mg/kg)
WB	85	22.8	8.3	189	8	>2000	17.33
LB	40	25.3	7.03	196	6.98	>2000	26.60
WI	30	25.3	7.53	160	8.09	>2000	33.00
BH	20	21.6	7.54	134	6.9	>2000	32.38
PACB	25	23.1	7.88	135	7.7	>2000	31.29
RG	20	8.78	7.63	230	10.80	16990	23.40
BD	10	11.5	7.73	102	9.73	20000	40.00
BB	10	10.4	7.81	65	10.72	18000	43.43
BJN	5	6.6	7.90	220	12.32	15360	41.79
BJS	5	7.2	8.08	180	11.65	13950	41.85

Pore-Water Geochemistry

Pore water in WB and LB sediments is characterized by high chlorine, sodium, and sulfate contents (see Appendix 3), similar to those of surface water (Monrreal, 2007). The WB pore water has much lower SO_4/Cl ratios (0.018±0.011) compared to those in surface waters (average 0.048) and seawater (~0.052), indicating strong bacterial sulfate reduction. In contrast, SO_4/Cl ratios of pore water in LB are higher (average 0.065) and are close to those of seawater. Relatively higher levels of nitrate and methyl mercury are found in WB's pore water compared to those of WB, indicating that WB receives more nutrients and trace metals from anthropogenic sources. The concentration of NH_4 (28.9-32.8 mg/kg) is higher than those of NO_3^- (<2 mg/kg) in WB pore water, suggesting that bacterial nitrate reduction occurs under reducing conditions. No NO_3^- or NH_4 were detected in LB pore water. Total mercury concentrations in pore water are similar at both sites, however, moderate levels of Me-Hg (0.15-3.52 ng/L) were found in WB pore water relative to those in LB (<1 ng/L).

Iron, arsenic, and total dissolved sulfur levels in pore water were relatively similar at WB and LB sites. Manganese concentrations in pore water are much higher in WB (mean = 1647 μg/L) than in LB (mean = 154 μg/L). Similarly, WB sediments have higher Mn contents than those in LB (see Sediment Geochemistry section). High Mn contents in pore water of WB are likely derived from bacterial reduction of Mn-rich sediments such as Mn-oxyhydroxides. The Mn content of pore-water in Weeks Bay reaches a maximum just below the sediment-water interface, and then remains relatively constant below this depth (Figure 23). This trend is consistent with moderate Mn-reducing conditions just below the sediment-water interface. The pore-water arsenic profile in WB exhibits similar pattern to that of iron and manganese (Figure 23), suggesting that similar biogeochemical processes release Fe, Mn, and As into pore water. It should be noted that Fe and reduced S contents in WB pore water show no strong correlation with As or Mn, implying that pore-water chemistry may be affected by various biogeochemical reactions (i.e., bacterial manganese and iron reduction, sulfate reduction, etc.) and accompanying bio-mineralization processes (see LA-ICP-MS Analysis section below). A perfect correlation among these parameters might be expected if a pore-water profile is dominated by a single biogeochemical or mineral reaction. Recent studies (e.g., Park et al., 2006; Lee et al., 2007), however, found no compelling evidence that the respiration of one type of microbe would exclude others from a particular substrate redox zone. This implies that a change from high-Fe into low-Fe pore-waters over a short distance at depth may result from a minor adjustment in the balance between the activities of iron and sulfate reducers or biomineralization. For example, bacterial sulfate reduction and precipitation of iron sulfides could strip Fe^{2+}, SO_4^{2-}, H^+, and perhaps other trace elements (by co-precipitation) from pore-water in different ratios. Analysis of pore water geochemistry at heavily oiled sites is in progress and the preliminary data show

that trace-metal concentrations are generally low compared to those in sediments (Keimowitz, personal communication).

Reduced Fe and sulfide concentrations in pore waters extracted from sediment cores were measured via a HACH Spectrophotometer DR/2700. Reduced Fe concentrations show that ferrous iron was present at all sites (Figure 24 and Appendix 2). The reduced iron concentrations are fairly low (< 0.02 mg/kg) at the heavily contaminated BJS site with respect to those measured at pristine and slightly contaminated sites WB and WI in Alabama. The presence of reduced Fe and Fe-reducing bacteria (see Microbiology section) at all sites indicates that reducing environments necessary for anaerobic bacterial reduction of Fe- and Mn-oxides/hydroxides were established. Reducing conditions in sediments is facilitated by the terminal electron acceptor process (TEAP) and organic decomposition. During TEAP, electron acceptors (e.g., Fe- and Mn-oxides/hydroxides) are reduced by iron-reducing bacteria (IRB) and adsorbed metals (e.g., arsenic) are released (Freeze and Cherry, 1979; Drever, 1997; Bose and Sharma, 2002; Saunders et al., 2008).

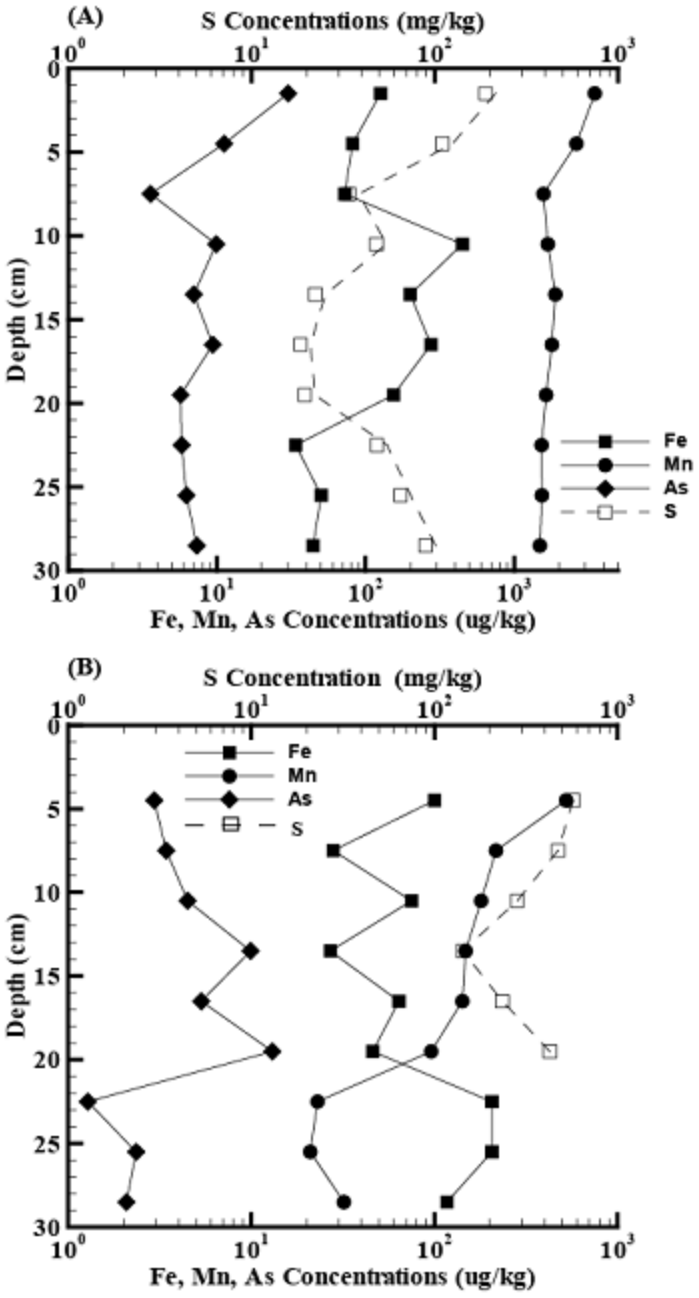

Figure 23. Variations in the concentrations of selected trace metals in pore water with substrate depth at Weeks Bay (A) and Longs Bayou (B) sites.

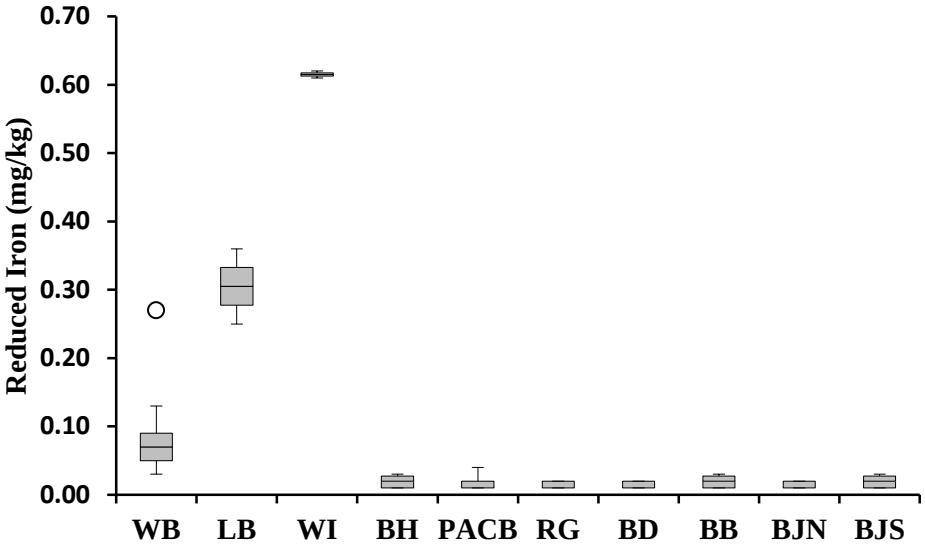

Figure 24. Box and whisker plot of reduced Fe (ferrous iron) in extracted pore waters from ten salt-marsh sampling sites. Contaminated sites (i.e., BJS) show lower levels of reduced Fe compared to those at non-contaminated sites (i.e., LB). Circles designate outliers.

Reduced sulfide concentrations in pore waters are very high at all heavily oiled sites (Figure 25 & Appendix 2). Hydrogen-sulfide contents reached 9 mg/kg at BJS, a heavily contaminated salt marsh in Louisiana. Other nearby contaminated sites (BJN, BB, BD, etc.) show even higher levels of hydrogen sulfides (up to 80-100 mg/kg). Reduced sulfide levels are much lower (< 1 mg/kg) at pristine sites, such as WB. The alarmingly high reduced sulfide concentrations at heavily contaminated locations indicate that bacterial sulfate reduction might have been enhanced by the introduction of spilled oil. Influx of oil in muddy sediments probably provided additional substrate and carbon sources for sulfate reducing bacteria.

Pore-water pH data indicates a mixing of fresh water and seawater. Pore-water pH and sulfide concentrations show similar increases with depth (Figures 26 & 27). Combined, these results indicate that seawater intrusion and enhanced bacterial sulfate reduction are likely

responsible for the high pH values and sulfide concentrations at depth. Bacterial sulfate reduction may be expressed as the following:

$$SO_4^{-2} + 2CH_2O + 2H^+ \rightarrow 2CO_2 + H_2S + 2H_2O \quad (4)$$

Such a reaction is enhanced when massive introduction of oil and organic matter stimulates SRB activity and accelerates the TEAP process. Bacterial sulfate reduction also raises the pH primarily due to the conversion of SO_4^{2-} to H_2S and HCO_3^- production. It should be noted that reduced sulfide concentrations and SRB MPN (see Microbiology section) are relatively low at the BJS site compared to those at other heavily oiled sites, even though BJS shows a similar pH trend with depth (Figure 27). It is not clear to what extent physical environments may affect biogeochemical processes; BJS faces the open ocean and harsh environments there may suppress anaerobic microbial activitiy to some extent.

Elevated sulfate reduction facilitated by sulfate-reducing bacteria results in highly reducing sulfidic waters. High sulfide content in water may transform arsenic into aqueous complexes of thioarsenates and thioarsenites (Hollibaugh et al., 2005; Keimowitz et al., 2005; Lee et al., 2007; Planer-Friedrich et al., 2009; Lee et al., 2007). In Fe-rich environments, reduced sulfide may react with ferrous iron to form sulfide solids (e.g., pyritic minerals) and sequester arsenic and other metals via co-precipitation (Saunders et al., 2008). Strongly reducing environments maintained by SRB can also facilitate mercury methylation (Chapelle, 1994; USGS Fact Sheet 146, 2000; Mason et al., 2005; Monreal, 2007). Favorable reducing conditions for these biogeochemical processes certainly exist at heavily contaminated sites.

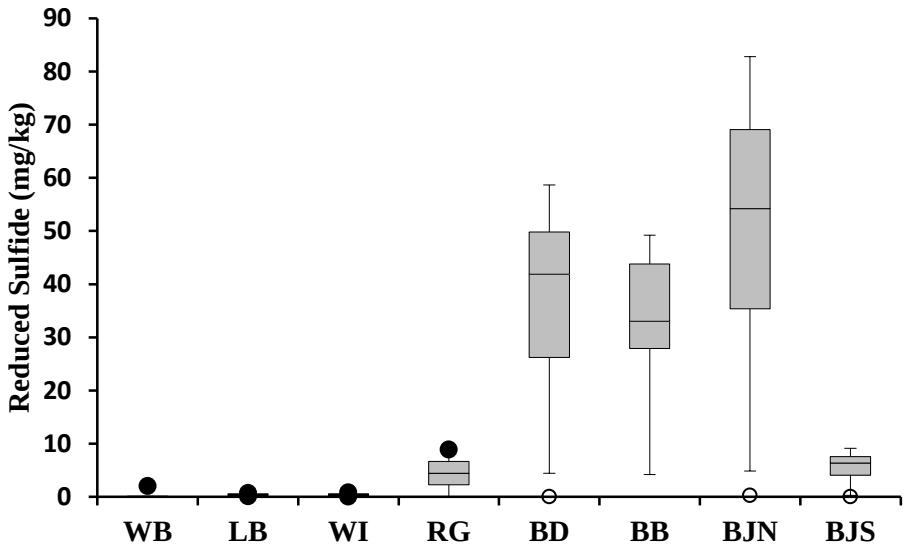

Figure 25. Box and whisker plot of reduced sulfides in extracted pore waters of ten salt-marsh sampling sites. Contaminated sites show much higher levels of sulfides from bacterial sulfate reduction compared to those at non-contaminated sites. Solid circles show scattered measurements at WB, LB, WI, and RG sites. Open circles represent low outliers (with distance from the box > 1.5 times the difference between the third and the first quarter) associated with low concentrations measured at heavily oiled sites BD, BJN, and BJS. PACB and BH are omitted due to lack of data.

Heavily contaminated, highly sulfidic sites such as BJS show less reduced iron in pore waters compared to pristine sites. Low reduced iron and very high levels of sulfide indicate that bacterial sulfate reduction has fixed most reduced Fe and other trace metals by forming solid iron-sulfides. Estuaries and coastal salt marshes can be considered as iron limited, sulfate rich environments. Although IRB have been found to co-exist with SRB in such environments (see Microbiology section), they are often out-competed by SRB due to the ample supply of sulfate from seawater, which favors bacterial sulfate reduction (Madigan et al., 1997; Straub et al., 2000). Due to the competition for available electron donors (i.e., organic matter), iron reducers are probably outcompeted by sulfate reducers in oil-contaminated marsh environments. This, coupled with iron sequestration via metal sulfide precipitation (see Sediment Geochemistry section), explains the low levels of reduced iron at contaminated sites.

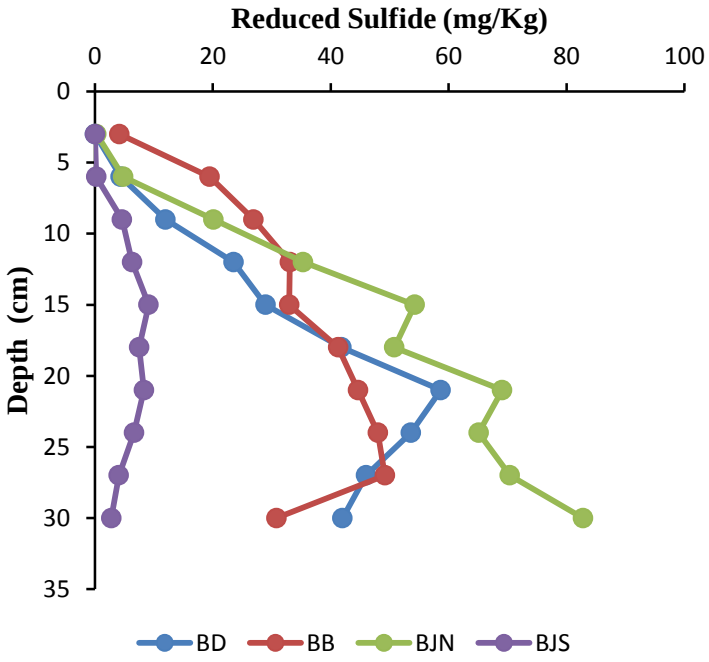

Figure 26. Plot of reduced sulfides in pore waters versus depth at four salt-marsh sampling sites in Louisiana. Sites show higher levels of sulfides from bacterial sulfate reduction with depth. Various sites in Alabama and Mississippi are omitted due to incomplete data.

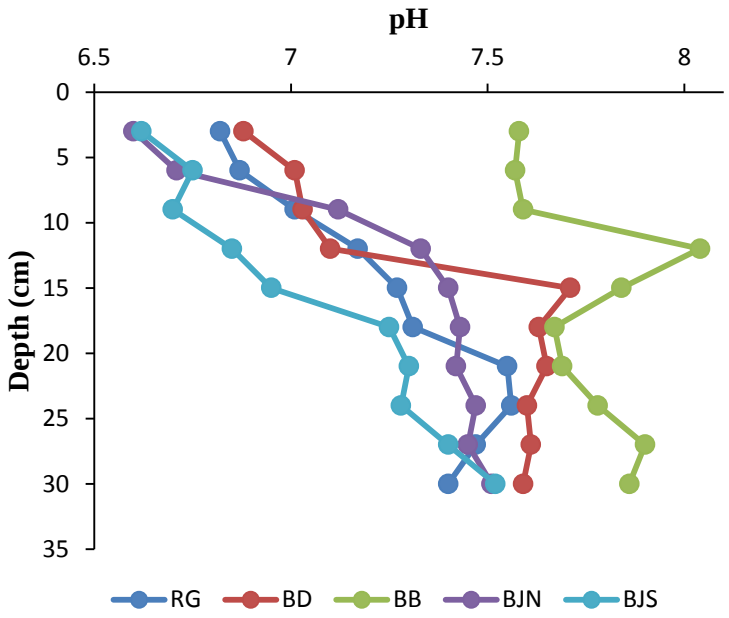

Figure 27. Plot of pH in pore waters versus depth at five salt marsh sampling sites in Louisiana. Sites show increasing pH with depth from sulfate reduction and seawater intrusion. Various sites are omitted due to incomplete data.

Carbon Contents of Pore Waters and Sediments

DOC levels of pore water extracted from sediment cores were also analyzed and the results are compared to those in surface water DOC levels (Figures 28, 29 and Appendix 2). DOC levels at heavily oiled sites, ranging up to hundreds of mg/kg, are on the order of one to two magnitudes higher than those at pristine and slightly contaminated sites. DOC levels increase with depth, possibly indicating saltwater-freshwater mixing near the sediment surface or freshwater recharge from rainfall. The vertical spatial changes in DOC also could indicate that seawater and heavy oil fractions invaded the deeper levels of the marsh sediments due to their higher density with respect to freshwater. DOC levels are also much higher in pore waters than in surface waters (< 50 mg/kg) at heavily oiled sites. This indicates that elevated DOC levels could persist in wetland sediments for a long period of time even after a signification portion of the oil in the surface water has been evaporated, dispersed, or degraded by microorganisms.

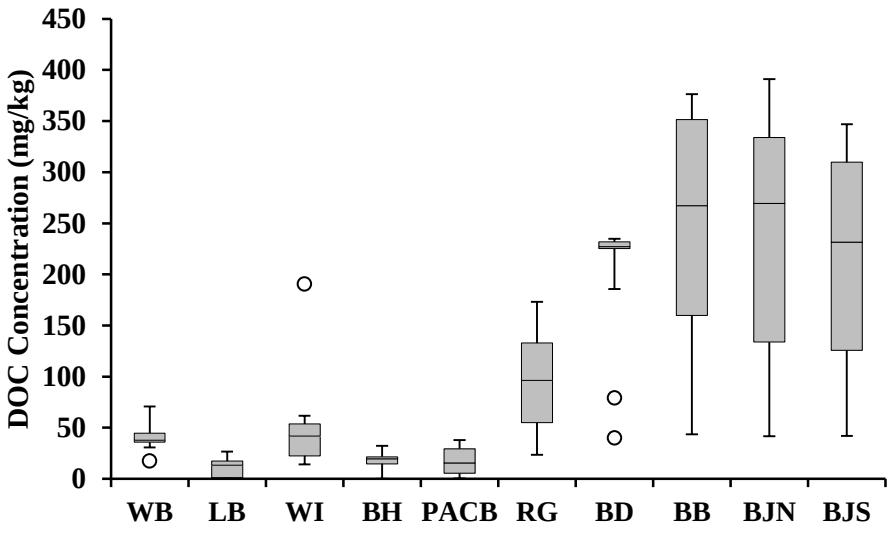

Figure 28. Box and whisker plot of dissolved organic carbon (DOC) in pore water from ten salt-marsh sampling sites. Contaminated sites show significantly higher DOC levels compared to those at non-contaminated sites. Circles designate outliers.

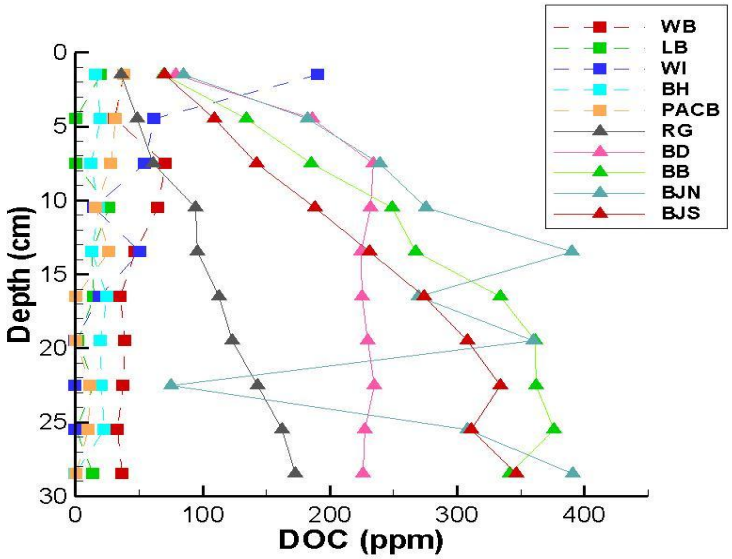

Figure 29. Dissolved organic carbon (DOC) in pore water versus depth at ten salt-marsh sampling sites. Contaminated sites show significantly higher DOC levels compared to those at non-contaminated sites and increasing DOC levels with substrate depth.

TOC values of sediment samples show similar increases with depth at contaminated sites (Figures 30, 31 and Appendix 4). The TOC contents of oiled sediments range from of 4-29%, whereas sediment TOC contents at pristine sites are generally < 3%. Moreover, a linear relationship between DOC and TOC is observed (Figures 28 and 30) although the cause of correlation is not clear. This correlation suggests that either DOC or TOC may be used as an indicator of the level of oil contamination. BJS, a heavily contaminated site, recorded very high TOC values (9.1±3.9%), while LB and WB recorded the lowest (< 4%). Additionally, other nearby heavily contaminated sites show even higher TOC values. For example, TOC contents range up to 29% at the BD site.

Higher TOC values can be attributed to influx of oil, natural organic solid contents, and finer grain sizes at sampled sites. While grain-size characteristics play a vital role in the adsorption of organic carbon in sediments (i.e., smaller platy grains have more adsorbing capability), TOC values show no strong correlation ($R^2 = 0.203$) with clay size contents (Figure 32). This implies that sediment TOC contents may be affected by other factors. The pristine WB site is dominated by clay and silt (Tables 3, 4, 5) but it has much lower TOC contents (<3%) with respect to those at heavily oiled sites. The influx and persistence of oil in contaminated sites remains the key trait that contributes to elevated levels of TOC at contaminated sites. Moreover, the primary adsorptive surface for spilled oil is the fraction of natural organic solids present in the sediments (Dzombak and Luthy, 1984). While clay minerals also provide adsorptive surfaces, there is very limited adsorption of organics or metals on the surfaces of common silicate minerals (e.g., quartz and feldspar) (Ciccioli, 1980).

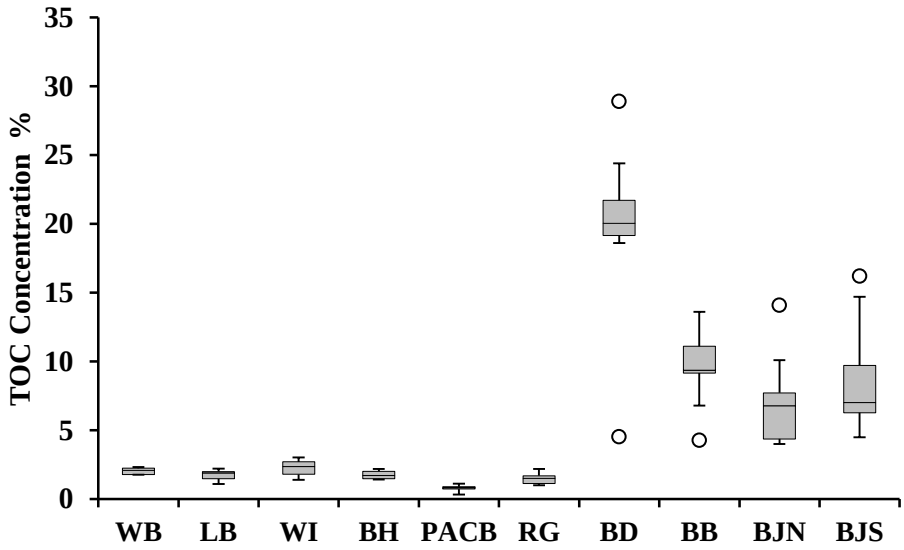

Figure 30. Box and whisker plot of total organic carbon (TOC) in sediments from ten salt-marsh sampling sites. Contaminated sites show significantly higher TOC levels compared to those at non-contaminated sites. Circles designate outliers

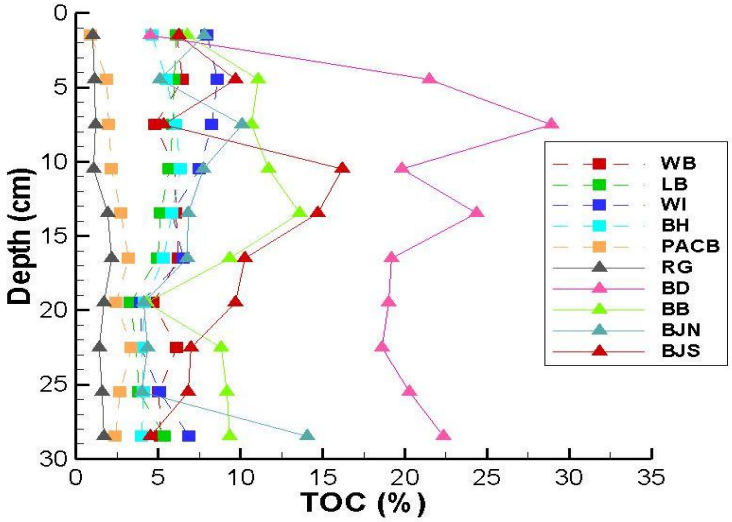

Figure 31. Plot of total organic carbon (TOC) in sediments versus depth at ten salt-marsh sampling sites. Contaminated sites show significantly higher TOC levels compared to those at non-contaminated sites.

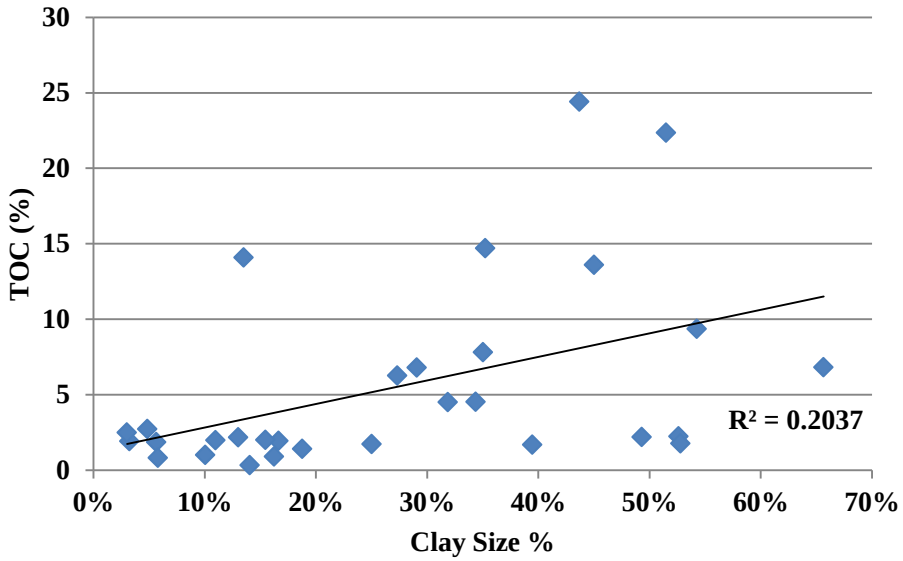

Figure 32. Positive correlation between sediment TOC and percentage of clay sized sediment.

Sediment Geochemistry

Geochemical results from total digestion analysis of 50 sediment samples from sites WB, LB, WI, RG, and BJS show variations in concentrations of major ions and trace elements with depth (Figures 35-41 and Appendix 6, 7). Bulk chemical analyses show that Weeks Bay contains highly elevated levels of trace metals (e.g., Cu, Pb, Zn, Fe, Hg, As, etc.) compared to other pristine sites. Weeks Bay has been the subject of several studies due to its high Hg bioaccumulation potential and the issue of several fish consumption advisories (ADEM, 1996, ADPH, 2008). Bays and estuaries have been considered by many as efficient sinks for metal pollutants (Mason et al., 1994, 1999). This is the case at the WB site in part due to its large freshwater input and constricted mouth leading to the sea (Monrreal, 2007). Large industrial and agricultural activities in Baldwin County represent potential point and non-point sources of trace metals. The fine-grained sediment and relatively high natural organic carbon contents in WB also contribute to the retention and enrichment of trace metals. The analysis of 2001-2009 data of weekly precipitation and associated mercury levels reveal possible sources of Hg in the Weeks Bay and surrounding areas. The data, obtained from the Mercury Deposition Network (MDN) (http://nadp.sws.uiuc.edu/mdn/), include weekly precipitation (mm), total mercury concentrations (ng/L) in precipitation, and total mercury wet deposition (ng/m^2) collected from two Alabama MDN sites AL02 and AL24 near Mobile Bay. Higher mercury deposition clearly correlates with periods of higher precipitation (Figure 33), supporting the hypothesis that the most likely source for mercury in the coastal watershed is from atmospheric deposition.

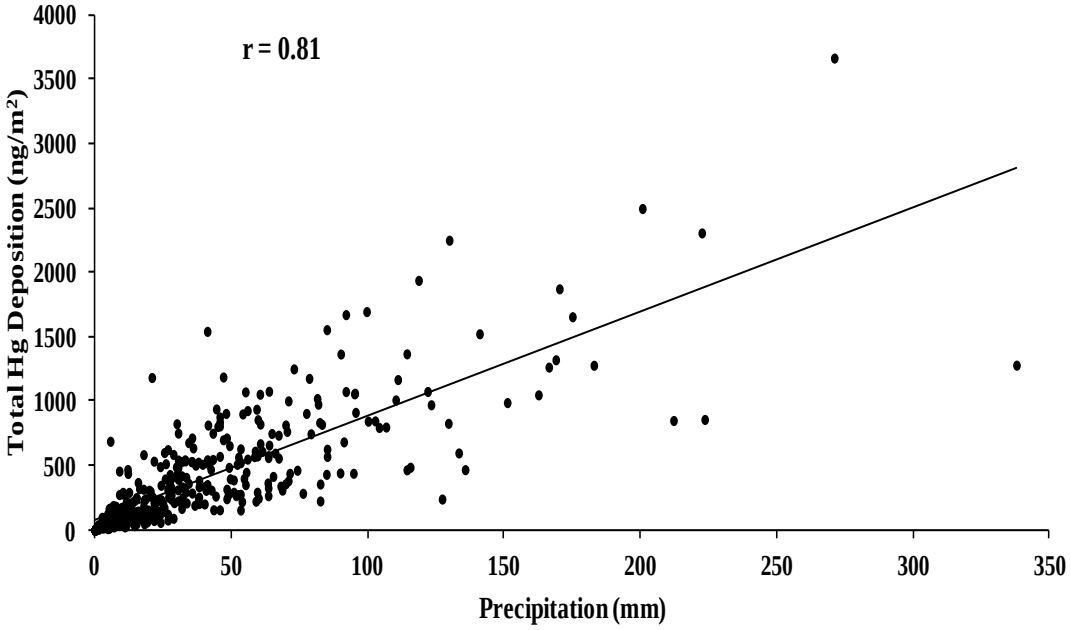

Figure 33. Bivariate scatter plot showing linear relationship between total mercury wet deposition and precipitation. The data was collected from Alabama Mercury Deposition Network site AL02 near Mobile Bay from June 2001 to December 2009.

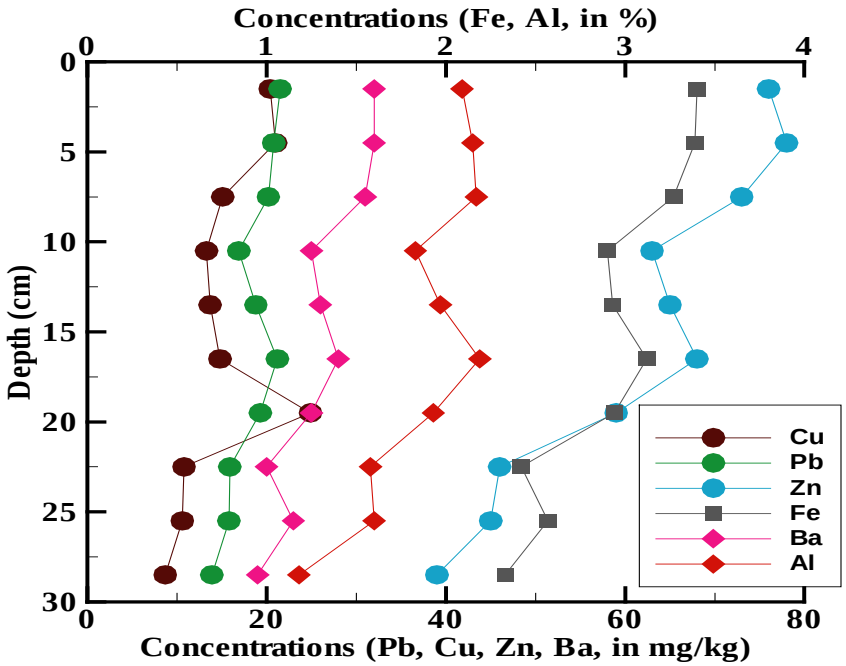

Figure 34, Depth profiles showing the range in concentration and spatial distribution of selected metals in the top 30 cm at the Weeks Bay site.

The enrichment of trace metals in shallow (post-industrial) sediments (< 20 cm of depth, see Figure 34) of Weeks Bay can be attributed to atmospheric deposition and riverine inputs derived from recent industrial activities. Sedimentation rates in coastal marshes are estimated to be less than about 0.3 cm/yr. which would yield about 20 cm of sediments over 60 years of sedimentation (Callaway et al., 1997). Elevated concentrations in Fe and other trace metals in Weeks Bay's sediments most likely are a direct result of the increase of industrialization in Baldwin County. Elevated levels of trace metals and Fe in the bulk sediment analysis clearly show that the chemical constituents for metal cycling and possible formation of bacterially produced metal sulfides (BPMS) are present under reducing environments.

Total digestion analysis of sediment samples also shows approximately 150 to 200 % enrichment of certain trace elements (e.g., Ni, Cu, Pb, Zn, Sr, Co, V, Ba, Hg, As) in heavily oiled zones with respect to less-affected and pristine sites (Figures 35-41). Trace metal levels at heavily oiled Louisiana marshes are even higher than those found in Weeks Bay. At BJS and other Louisiana oiled sites, elevated metal levels extend beyond shallow (post-industrial) profiles to greater depths (down to 30 cm) (Figures 35-41), suggesting that oil and various associated metals have spread through the deeper levels of marsh sediments. Elevated concentrations of arsenic can be weakly correlated with the finer grain sizes ($R^2 = 0.225$) that dominate at BJS and other heavily oiled sites (Figure 42). Fine grained sediments at these sites aid in the retention of trace metals.

While grain size is obviously a contributing factor to elevated metal content, heavily contaminated sites also show elevated levels of Ni, Cu, S, and to a lesser degree V. These four elements are common metals in crude oil and thus can be considered to be indicators of oil contamination. Ni/V ratios have been used in the past as source-rock parameters and as a crude

oil indicator (Barwise, 1990; Lopez et al., 1995). Light or immature crude oils (e.g., BP MC-252) have the highest concentrations of Ni, Cu, V, and S when compared to mature oils. Immature crude contains more trace metals than other crude oil types (Ball et al., 1960; Barwise, 1990; Lopez et al., 1995; 1998).

BJS and other heavily contaminated sites have 150 to 200% more Cu and Ni than pristine sites. The Ni and Cu concentrations of heavily oiled sites are also higher than WB, which retains the most metals derived from industrial activities instead of the oil spill (Figures 35, 36). S and V also are elevated at heavily oiled sites compared to pristine sites such as LB. The elevated S levels at heavily contaminated sites cannot be derived from sea-water intrusion alone, as conductivity measurements show similar sea-water presence at all sites (Figure 40).

BJS and other heavily oiled Louisiana sites all show elevated levels of trace metals and S. These elevated levels may result from a combination of finer-grained sediments that retain metals and the incursion of oil into the sediments. The extent to which increased trace metal concentrations can be attributed to the oil remain unclear. However, it is important to note that high levels of Ni (a common metal in crude oil) correlate well with extremely high TOC contents in heavily oiled sediments (Figure 43). It appears that the incursion of oil has led to a substantial increase in trace metals and S at heavily oiled sites.

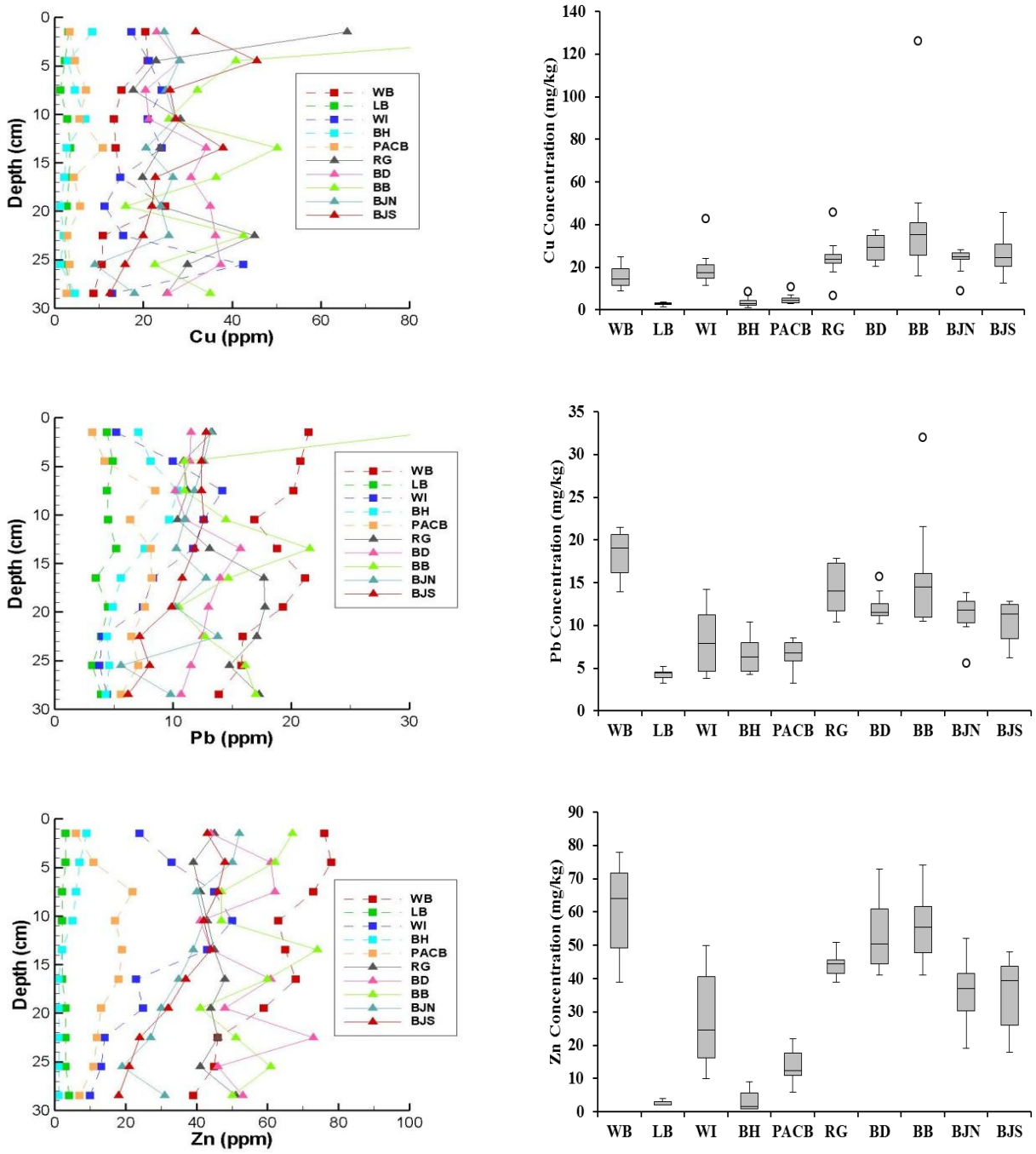

Figure 35. Box plot (left) and depth profiles (right) show the range in concentration and spatial distribution of Cu (top), Pb (middle), and Zn (bottom) in sediments at 10 sampling sites. Heavily-oiled sediments contain higher levels of trace metals compared to those at less-affected sites. Higher metal concentrations in shallow sediments of Weeks Bay are derived from industrial sources via atmospheric deposition and riverine inflow. Circles designate outliers.

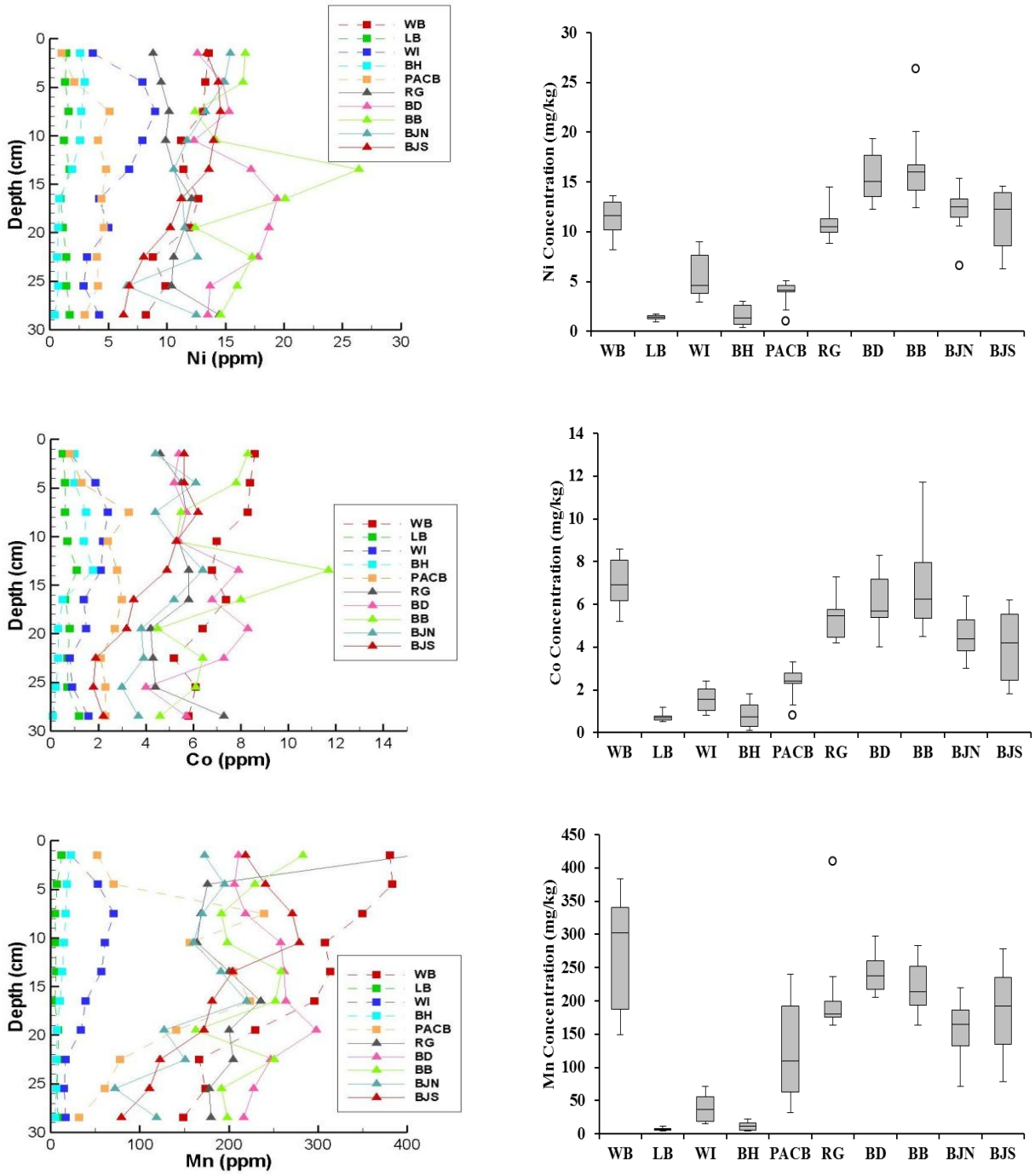

Figure 36. Box plot (left) and depth profiles (right) show the range in concentration and spatial distribution of Ni (top), Co (middle), and Mn (bottom) in sediments at 10 sampling sites. Heavily-oiled sediments contain higher levels of trace metals compared to those at less-affected sites. Higher metal concentrations in shallow sediments of Weeks Bay are derived from industrial sources via atmospheric deposition and riverine inflow. Circles designate outliers.

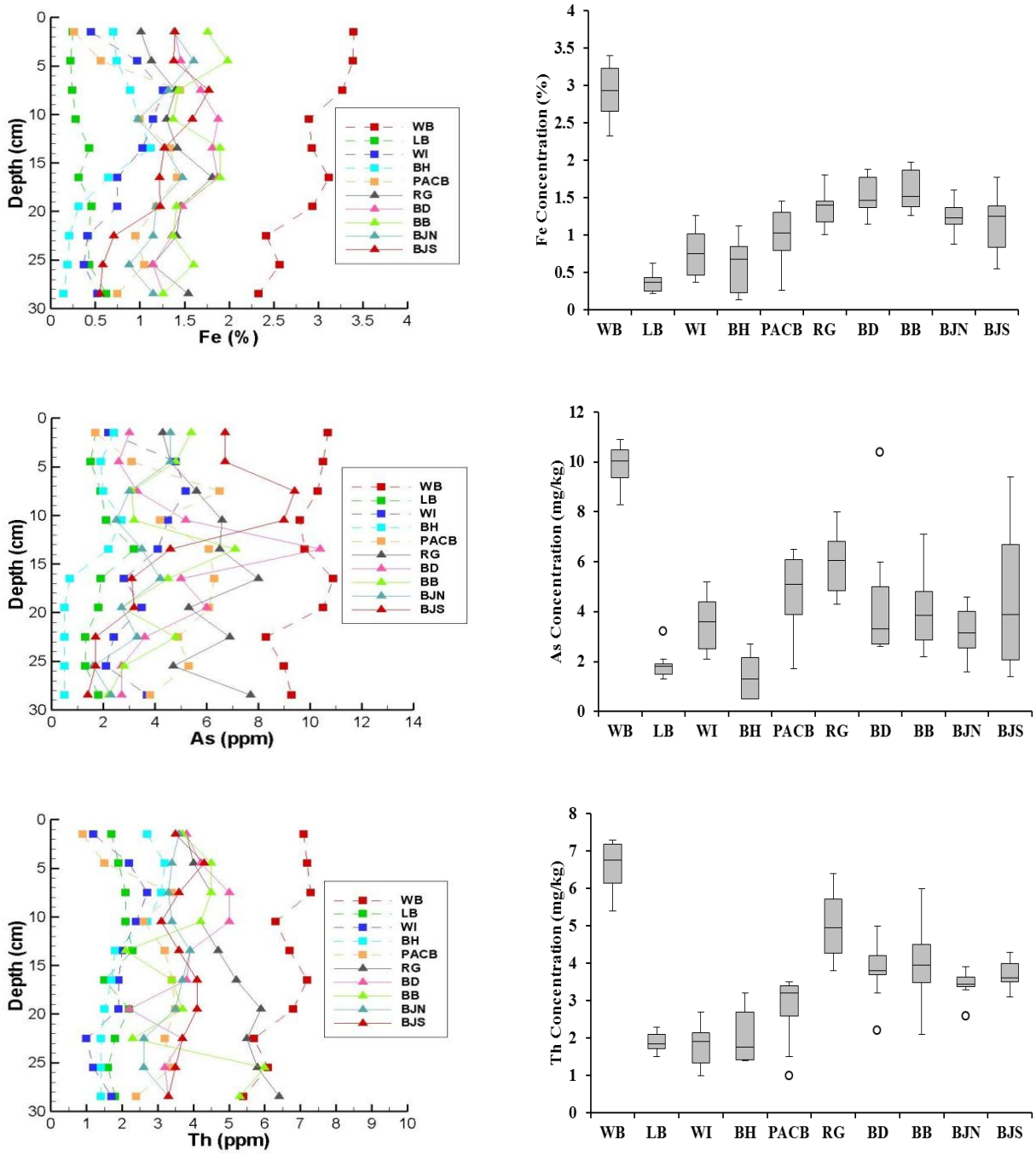

Figure 37. Box plot (left) and depth profiles (right) show the range in concentration and spatial distribution of Fe (top), As (middle), and Th (bottom) in sediments at 10 sampling sites. Heavily-oiled sediments contain higher levels of trace metals compared to those at less-affected sites. Higher metal concentrations in shallow sediments of Weeks Bay are derived from industrial sources via atmospheric deposition and riverine inflow. Circles designate outliers.

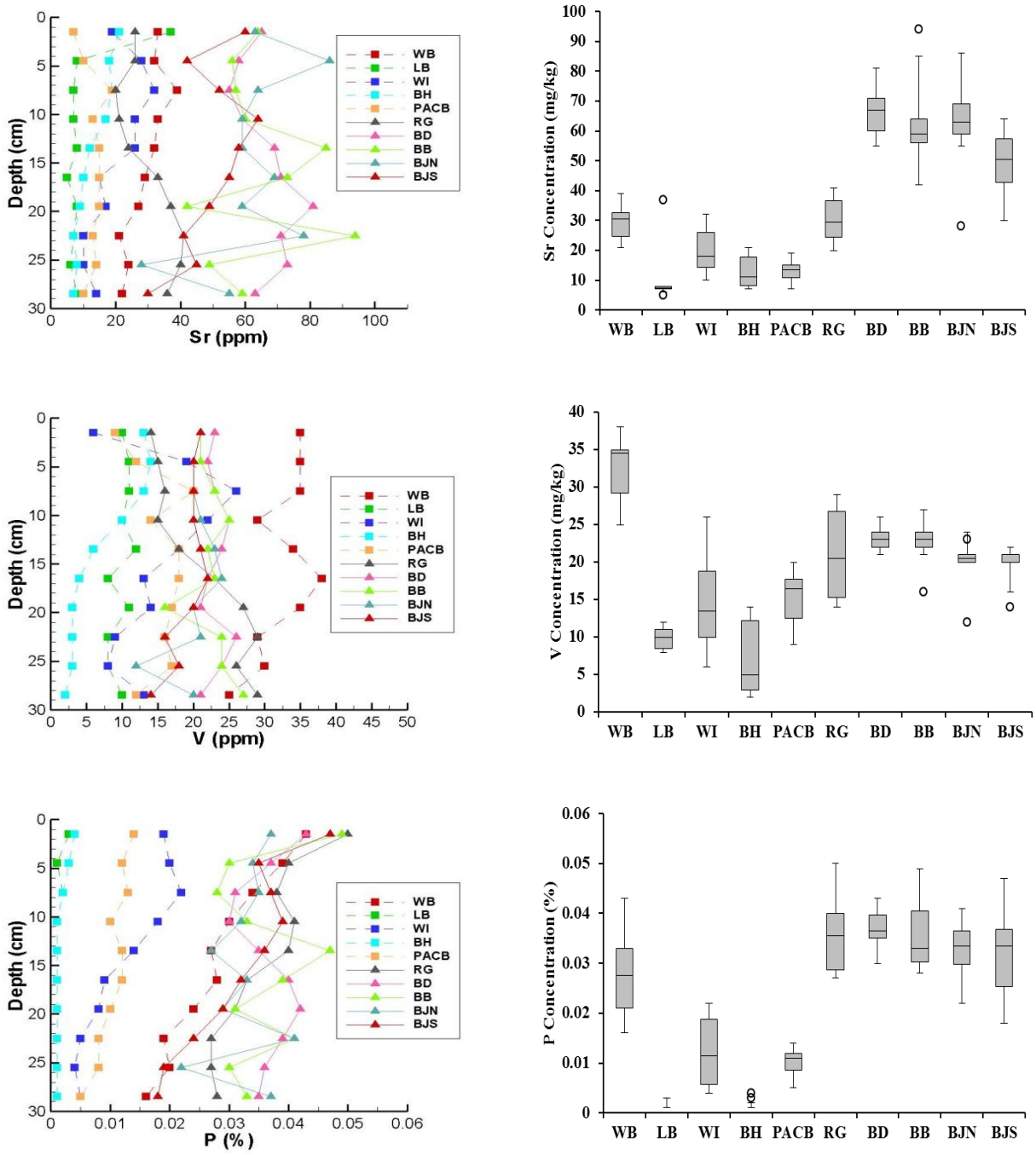

Figure 38. Box plot (left) and depth profiles (right) show the range in concentration and spatial distribution of Sr (top), V (middle), and P (bottom) in sediments at 10 sampling sites. Heavily-oiled sediments contain higher levels of trace metals compared to those at less-affected sites. Higher metal concentrations in shallow sediments of Weeks Bay are derived from industrial sources via atmospheric deposition and riverine inflow. Circles designate outliers.

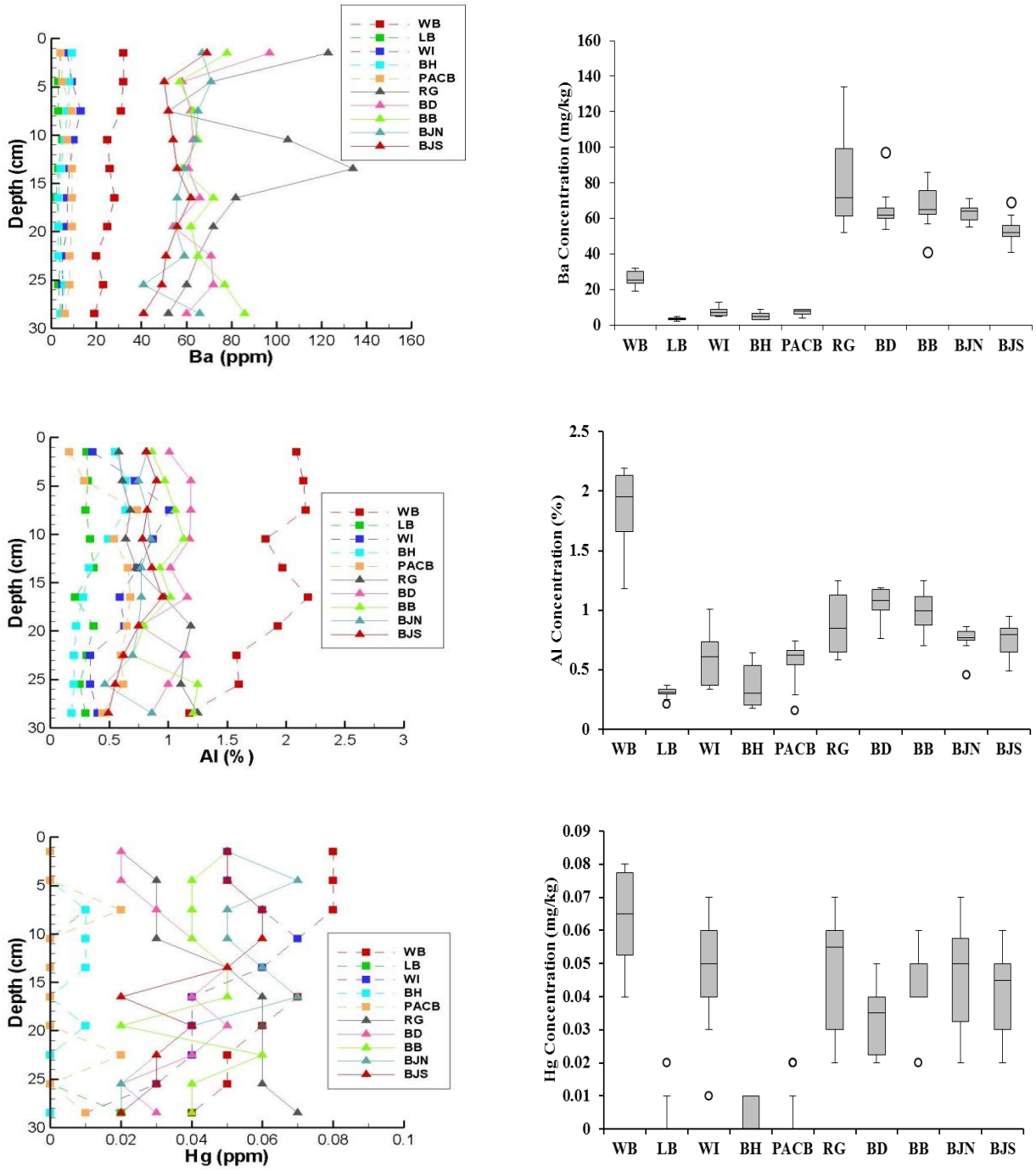

Figure 39. Box plot (left) and depth profiles (right) show the range in concentration and spatial distribution of Ba (top), Al (middle), and Hg (bottom) in sediments at 10 sampling sites. Heavily-oiled sediments contain higher levels of trace metals compared to those at less-affected sites. Higher metal concentrations in shallow sediments of Weeks Bay are derived from industrial sources via atmospheric deposition and riverine inflow. Circles designate outliers.

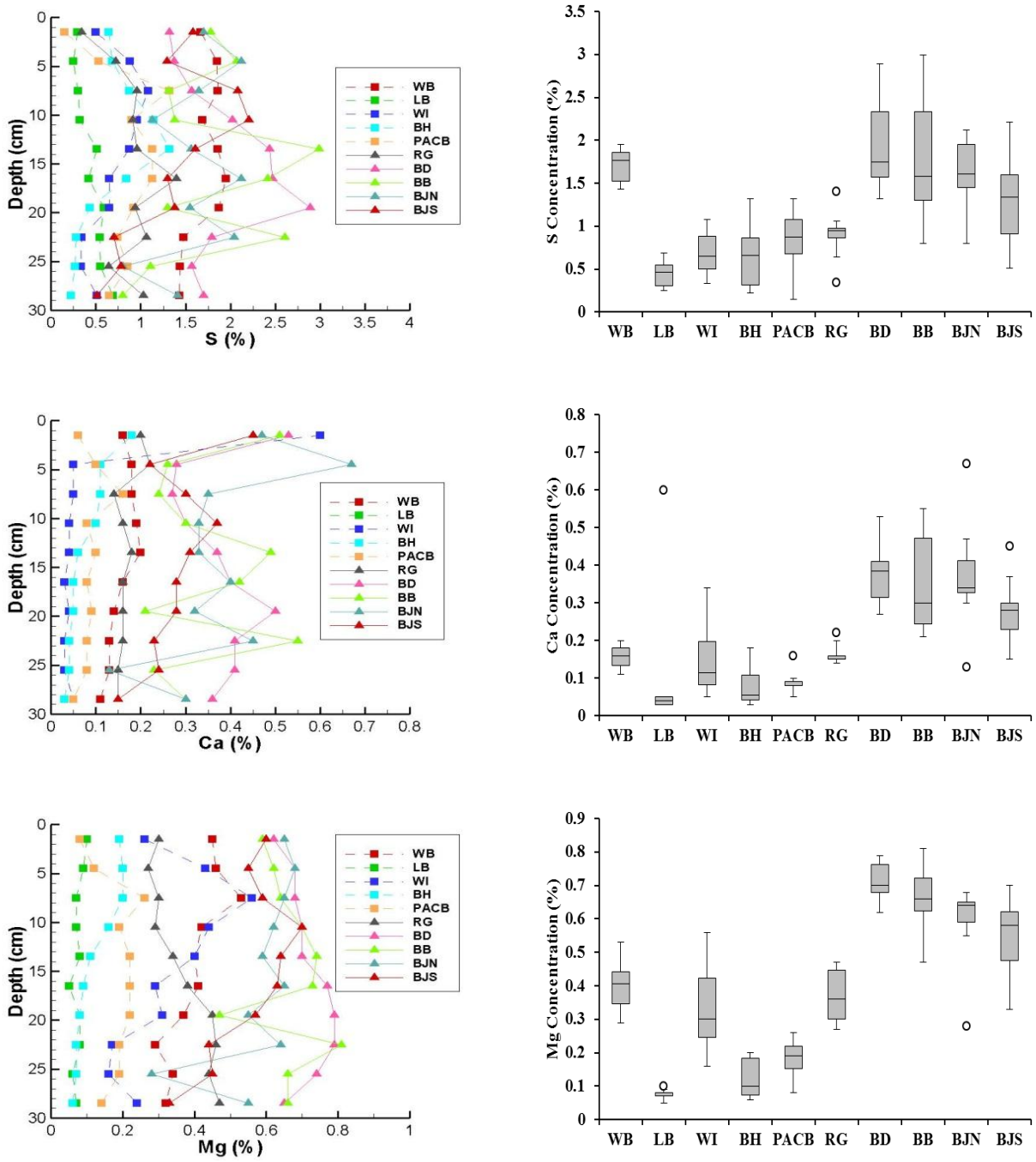

Figure 40. Box plot (left) and depth profiles (right) show the range in concentration and spatial distribution of S (top), Ca (middle), and Mg (bottom) in sediments at 10 sampling sites. Heavily-oiled sediments contain higher levels of trace metals compared to those at less-affected sites. Circles designate outliers.

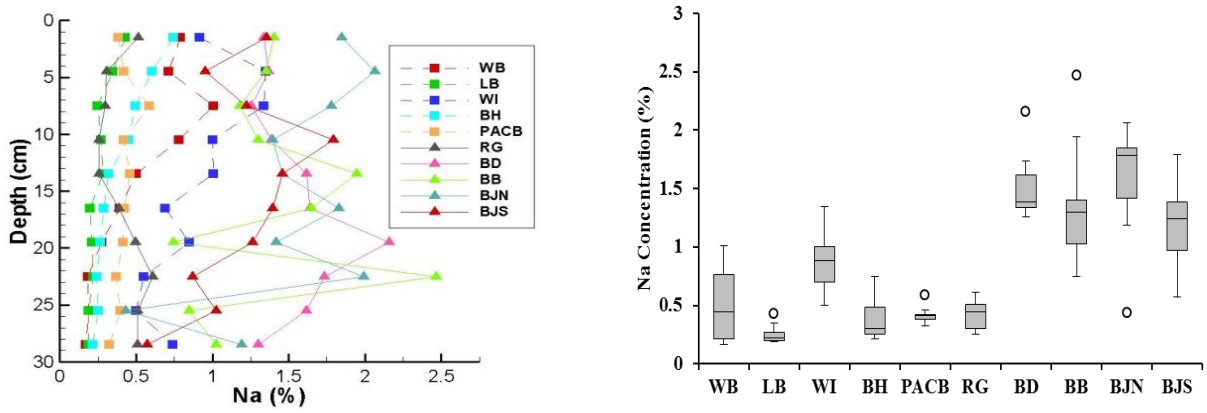

Figure 41. Box plot (left) and depth profiles (right) show the range in concentration and spatial distribution of Na in sediments at 10 sampling sites. Heavily-oiled sediments contain higher levels of trace metals compared to those at less-affected sites. Circles designate outliers.

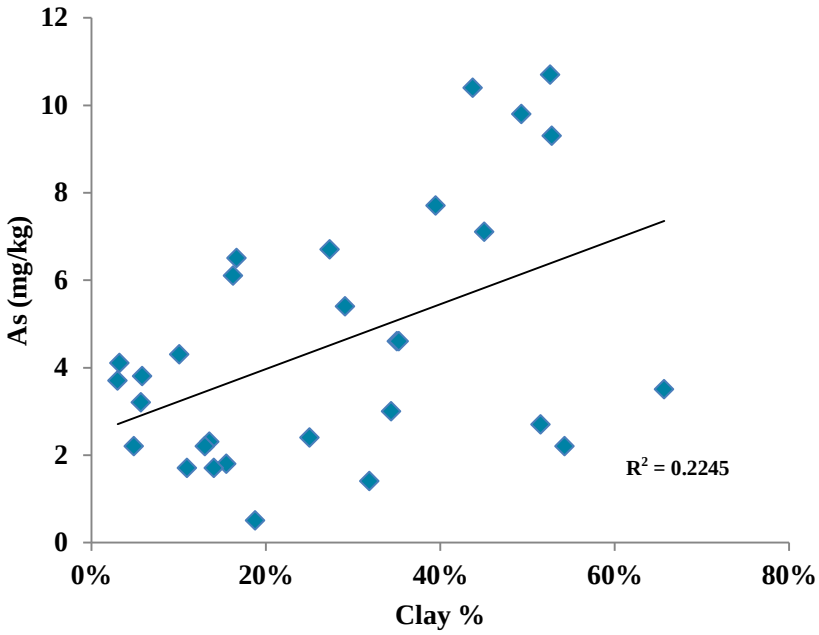

Figure 42. Positive correlations between As and clay content indicating that fine-grained sites retain metals more effectively than coarser grained sites.

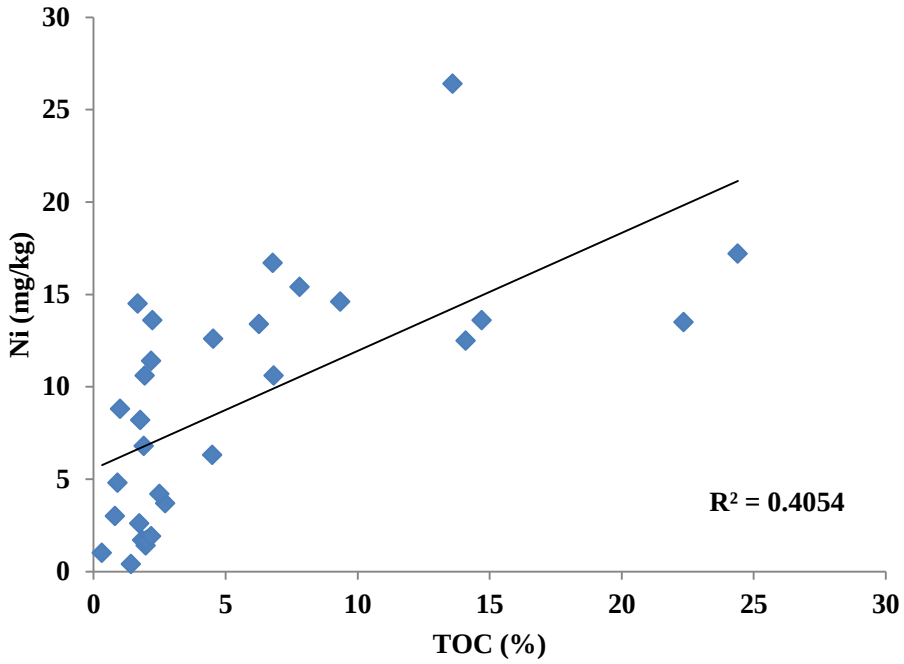

Figure 43. Plot showing positive correlation between Ni concentrations (a common metal in crude oil) and TOC contents in oiled sediments indicating oiled sites have elevated concentrations of Ni.

The aluminum-normalized enrichment factor (ANEF) was calculated from the bulk geochemical data in an attempt to determine the influence of anthropogenic input of trace metals at all sites (Table 10). ANEF, which to a large degree filters out inputs from terrigenous (natural) sediment sources, has been demonstrated to be effective in quantifying trace-metal inputs from post-industrial pollution. The following equation selects aluminum (Al) as the referenced element to calculate ANEF for various metals:

$$\frac{Me_{sample} / Al_{sample}}{Me_{crust} / Al_{crust}}$$

Here *Me* represents trace metal content of sediments and crustal abundance. *Al* represents aluminum content of sediments and crustal abundance. Crustal concentrations of various

elements were calculated and compiled by Wedepohl (1995). Since Al has no known anthropogenic sources to sediments, quantification of any metal from the equation that results in a positive ANEF number can be inferred as having anthropogenic inputs (non-crustal sources). Estuarine sediments that have shown to be trace metal sinks would have positive ANEF anomalies for anthropogenic-introduced trace metals.

ANEF results indicate that there is substantial anthropogenic input of several trace metals particularly at WB and oiled sites (i.e., BJS and RG). Elevated trace metal contents at WB can be directly related to industrial input, atmospheric deposition, and riverine inflow as discussed earlier. Additionally, all sites record positive ANEF values for trace-metals to some degree. This can be directly related to the estuarine environment acting as a trace-metal sink. However, oiled sites show higher ANEF values for Ni, Cu, and V (common components in crude oils) compared to those at pristine sites including WB. Other trace elements such as Pb, Zn, As, and Hg also display relatively high ANEF values (>4) at contaminated sites.

Elevated ANEF values of S exist to some degree at all sites partially due to the presence of sea-water and the precipitation of sulfates and evaporites. The sulfur ANEF values, however, are more elevated at oiled sites. Since sulfur is a main constituent of crude oil, ANEF values of sulfur thus may be used an indicator of oil contamination.

While bulk geochemical and ANEF analyses indicate elevated levels of trace metals in sediments at highly contaminated sites, concentrations of trace metals are generally low in pore-waters extracted from heavily contaminated sediments (Allison Keimowitz, personal communication, 2012). One possible notion for the low concentrations in pore waters is enhanced bacterial sulfate reduction, which removes reduced aqueous metals by precipitating them into metal sulfides (see next section).

Table 10. Average calculated normalized aluminum enrichment with respect to major and trace elements.

Element	WB	LB	WI	BH	PACB	RG	BD	BB	BJN	BJS
Cu	4.40	4.95	21.91	5.68	5.68	20.68	15.49	24.89	16.27	18.43
Pb	4.53	6.32	6.04	8.92	5.87	7.61	5.39	7.64	6.70	6.28
Zn	4.85	1.34	6.79	1.14	3.95	7.98	7.62	8.65	7.15	6.89
Mn	2.12	0.34	0.90	0.47	3.44	3.93	3.46	3.42	3.06	3.59
Fe	3.97	3.04	3.16	3.95	4.59	4.07	3.70	4.17	4.17	3.80
Ba	0.16	0.13	0.15	0.18	0.17	1.22	0.74	0.82	0.93	0.85
Hg	4.71	1.76	10.94	1.55	1.15	7.17	4.63	6.24	8.38	7.52
As	20.97	23.48	23.78	13.62	35.28	27.73	16.92	16.79	16.58	23.34
S	75.51	120.86	92.14	153.08	122.59	85.22	153.72	155.79	173.73	141.57
Sr	0.38	0.81	0.82	0.88	0.64	0.85	1.60	1.66	2.01	1.63
Ni	2.55	1.88	3.83	1.64	2.87	5.34	6.30	7.25	6.63	6.15
Co	2.53	1.64	1.76	1.35	2.91	4.33	4.04	4.77	4.11	3.47
V	2.57	4.74	3.58	2.53	4.56	3.49	3.26	3.39	3.92	3.79
Th	2.69	4.67	2.37	4.54	3.89	4.38	2.71	2.98	3.36	3.80
Ca	0.22	0.82	0.61	0.53	0.49	0.55	1.00	0.99	1.30	0.99
Mg	1.23	1.40	3.14	1.92	2.04	2.45	3.97	3.95	4.43	4.21
Na	0.77	2.55	4.74	3.28	2.82	1.44	4.58	4.52	6.08	4.77
Al	1.00	1.00	1.00	1.00	1.00	1.00	1.00	1.00	1.00	1.00

Petrographic, SEM-EDS, and Laser-Ablation ICP-MS Analysis

Petrographic, scanning electron microscope based-energy dispersive analysis (SEM-EDS), and laser-ablation ICP-MS analyses were conducted on sediments recovered from metal-rich sites WB and BJS. Analyses aim at investigating chemical composition, grain size, and texture of metal sulfides formed from pore-water under sulfate-reducing conditions. Sediments from shallow depths of WB and BJS (12-20 cm) were slide- and puck-mounted for analysis. Bacterially produced metal sulfides (BPMS) are clearly evident at both sites. Pyrite with distinct framboidal forms were recognized in petrographic analyses (Figure 44) and SEM imaging (Figure 45). During nucleation and growth, the various pyritic minerals take on distinct textures (Wilkin et al., 1996).

EDS analysis of puck-and slide-mounted framboidal pyrites consistently result in peaks for Fe and S, confirming the petrographic analysis that they are pyritic minerals (Figures 46-49, and Table 11). The formation of BPMS in modern marsh sediments has been demonstrated to take place when ample amounts of Fe(II), SO_4^{-2}, and organic carbon are present (Berner, 1970; 1984). Laboratory studies have shown that organic carbon required for bacterial growth is the most important contributing factor during BPMS formation in marine sediments (Berner, 1984). Thus, the incursion of oil into heavily contaminated sites most likely enhanced BPMS production and, in turn, sequestered reduced trace metals (e.g., Fe, As) that were present in pore water.

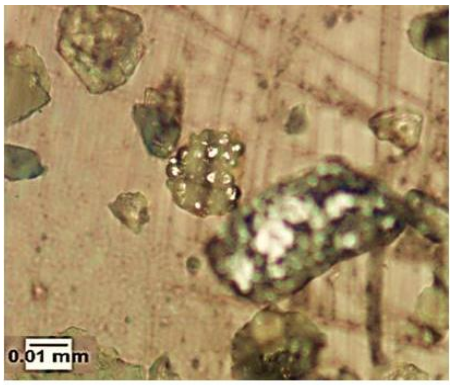

40x Reflected Light BJS

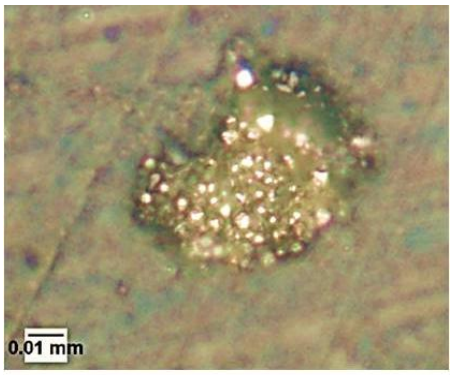

40x Reflected Light BJS

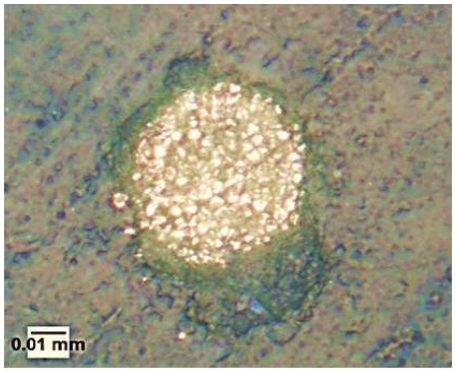

40x Reflected Light WB

Figure 44. Photomicrographs of biogenic pyrite formed in Bay Jimmy South (top) and Weeks Bay (bottom).

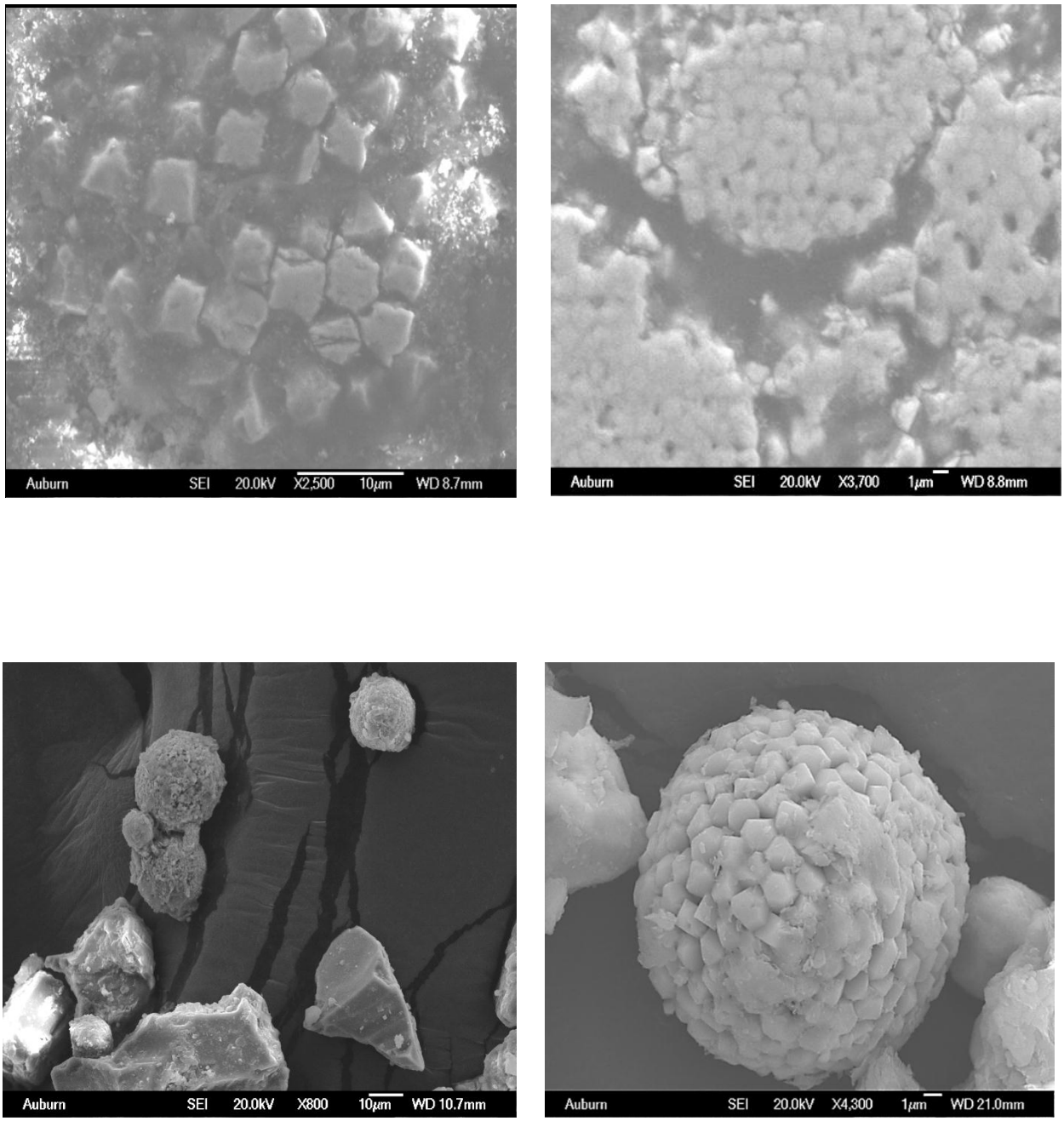

Figure 45. SEM images of slide mounted (BJS top left, WB bottom right) and puck mounted (BJS bottom left, WB bottom right) framboidal pyrite formed by sulfate-reducing bacteria in WB and BJS sediments. SEM image shows framboidal texture of pyrite with pyrite microcrystal (crystal size ranges from 0.5-2 µm) aggregates.

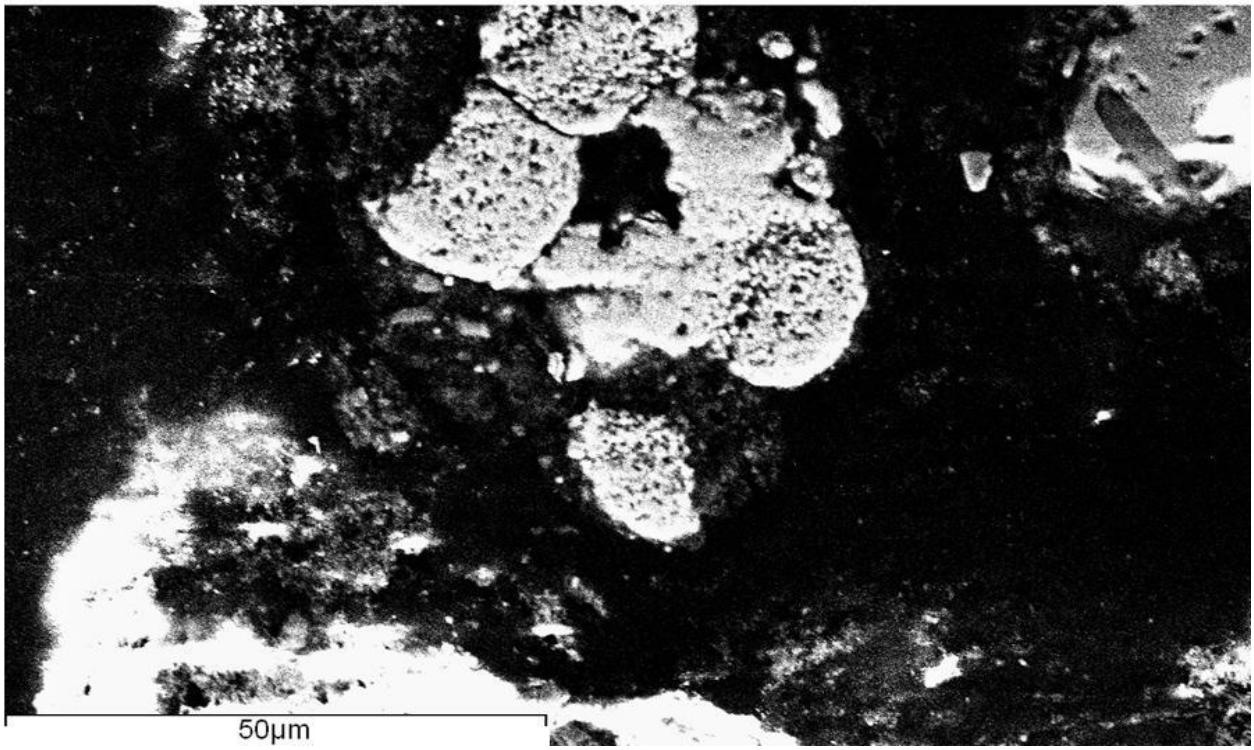

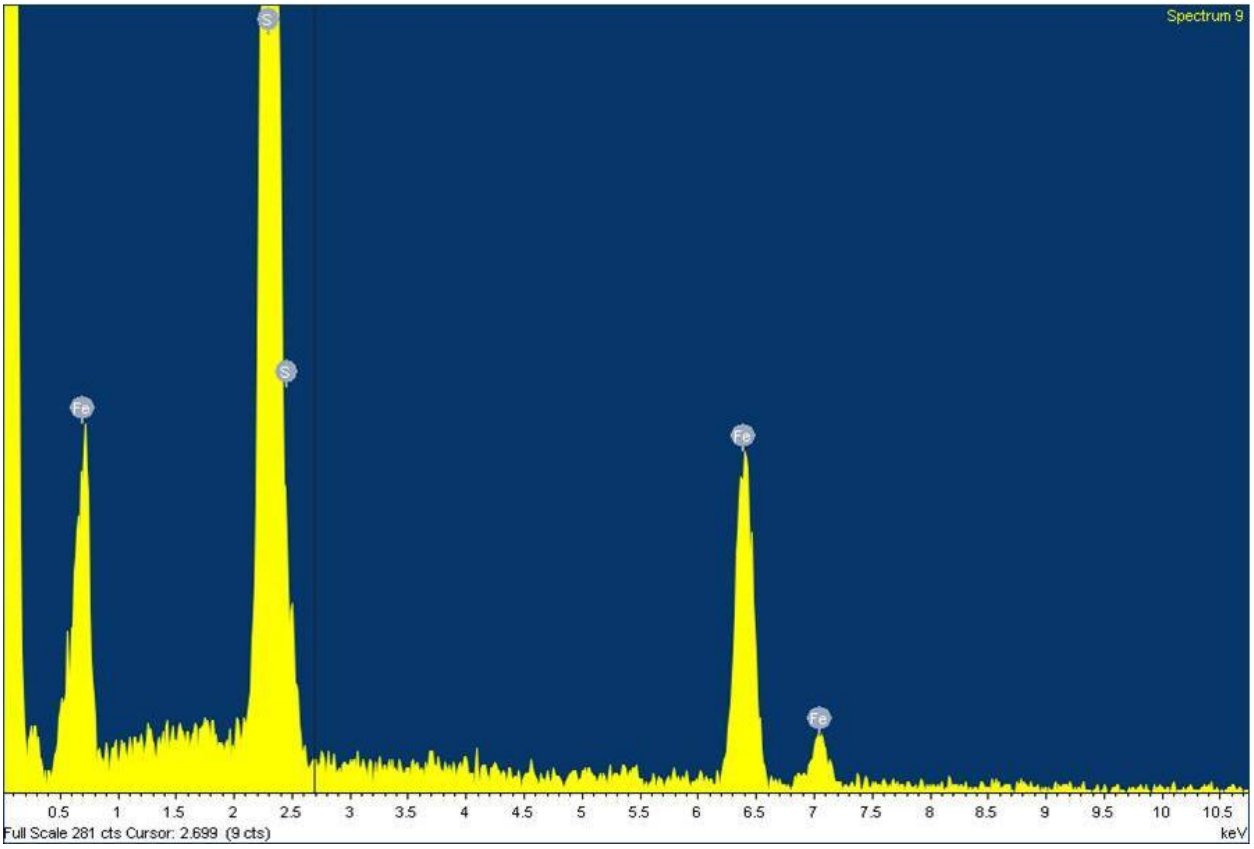

Figure 46. SEM photo and energy dispersive x-ray (EDS) spectra of framboidal pyrite formed by sulfate-reducing bacteria in Weeks Bay (sample WB S-1 Spectrum 5).

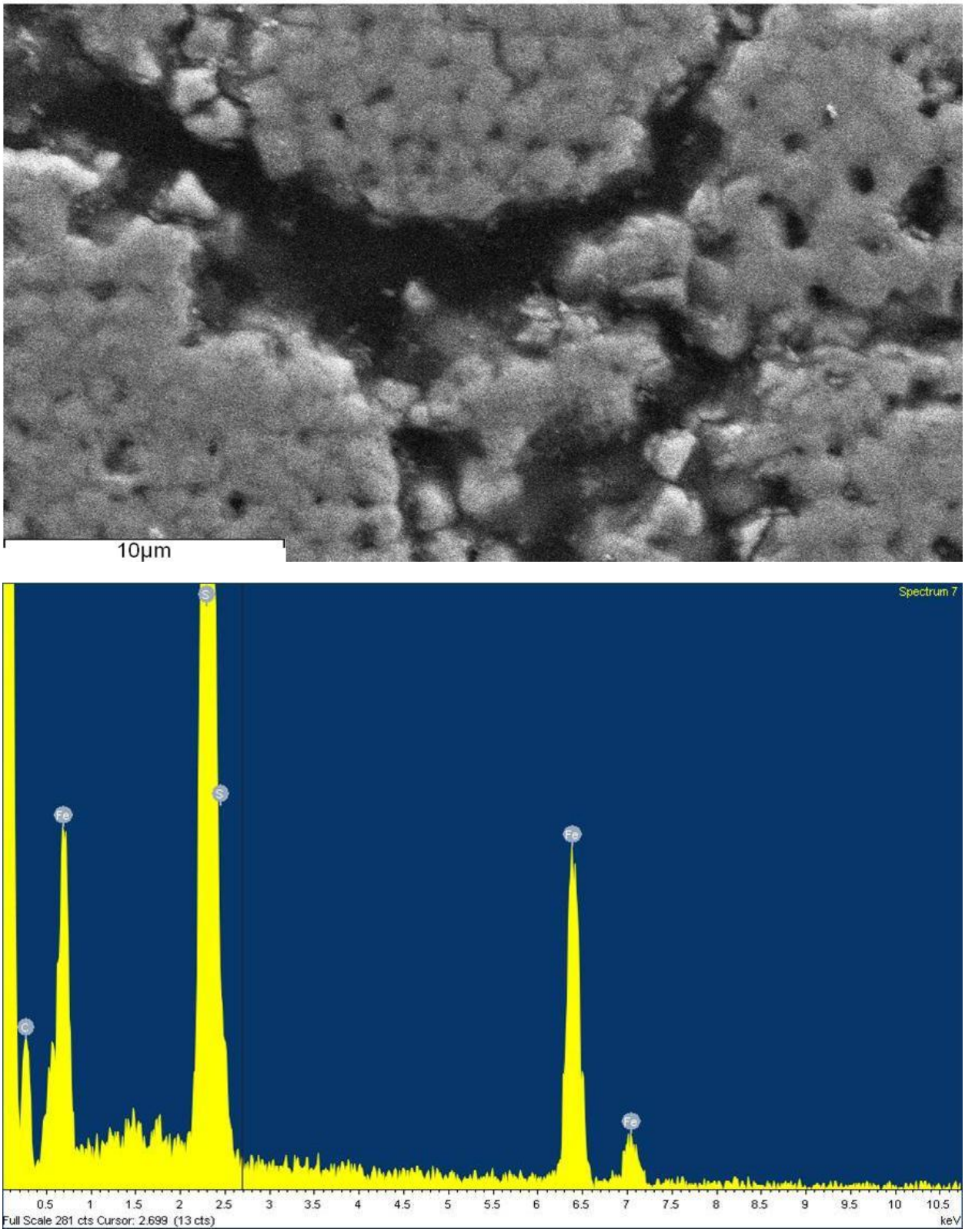

Figure 47. SEM photo and energy dispersive x-ray (EDS) spectra of framboidal pyrite formed by sulfate-reducing bacteria in Weeks Bay (sample WB S-3 Spectrum 2).

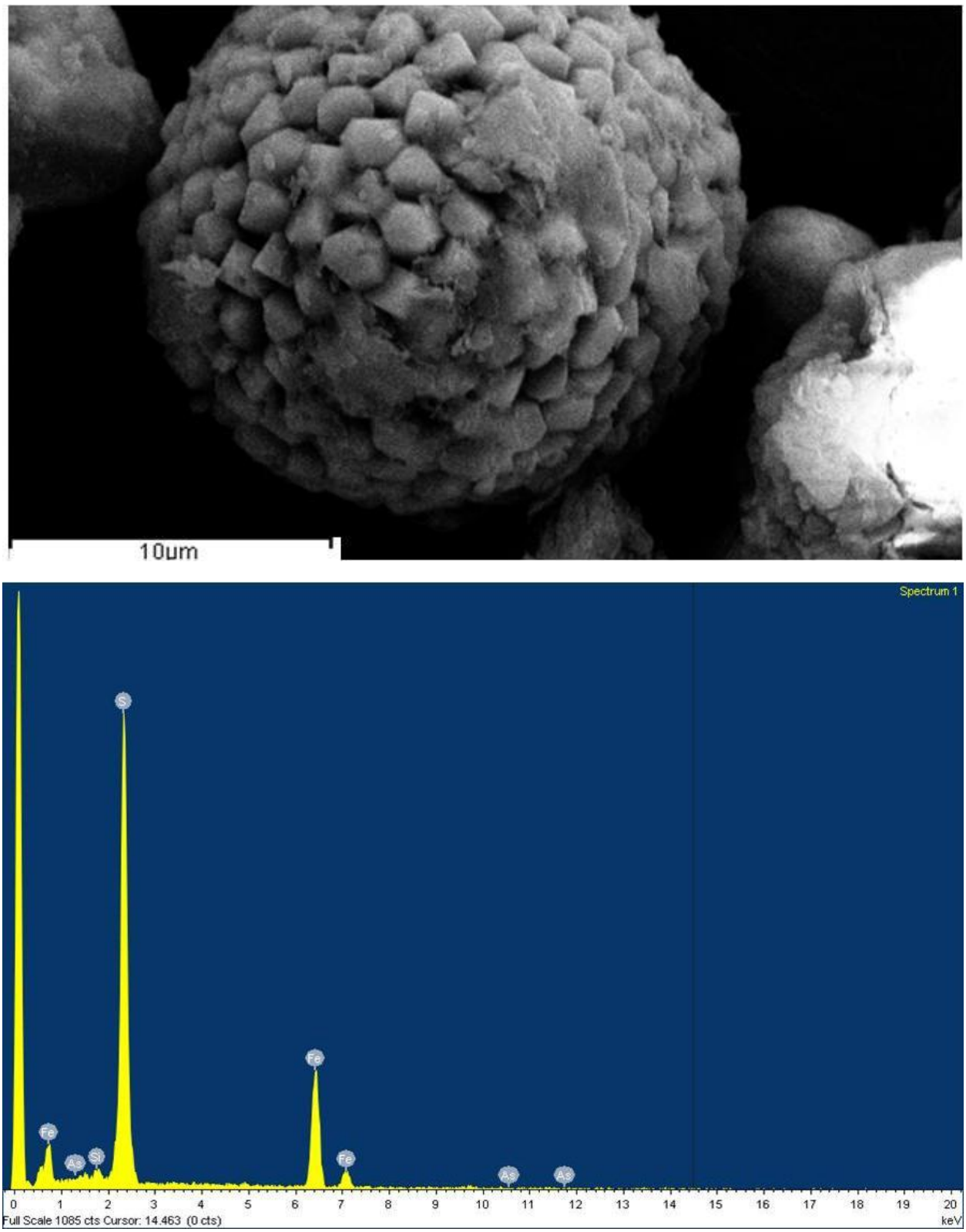

Figure 48. SEM photo and energy dispersive x-ray (EDS) spectra of framboidal pyrite formed by sulfate-reducing bacteria in Weeks Bay (sample WB P-1 Spectrum 1).

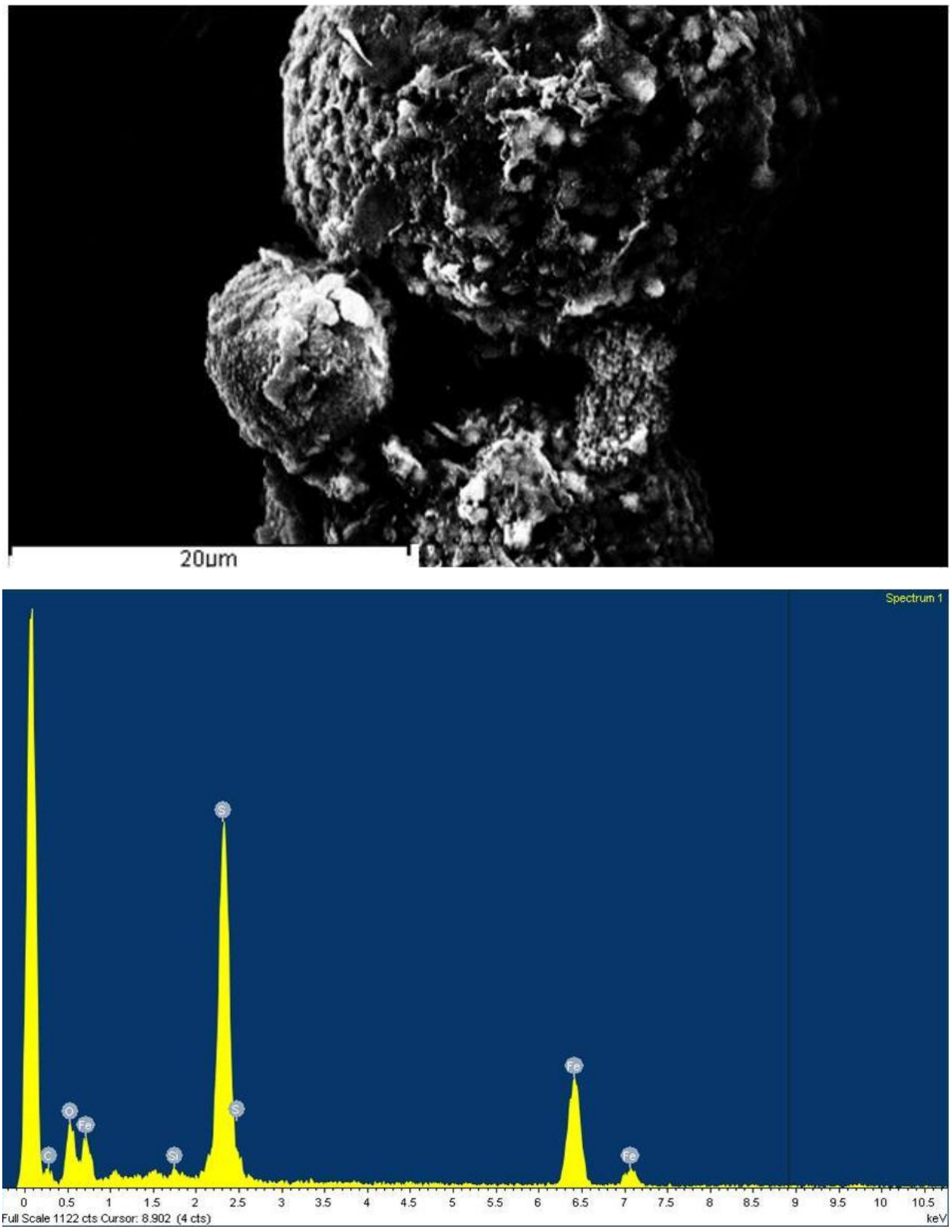

Figure 49. SEM photo and energy dispersive x-ray (EDS) spectra of framboidal pyrite formed by sulfate-reducing bacteria at Bay Jimmy South site (sample BJS P-1 Spectrum 1).

Table 11. Elemental composition by mass percentage of various slide-mounted and puck-mounted grains.

Sample ID	Fe %	S %	Si %	Al %	Total %
Slide-Mounted					
BD S-2 Spectrum 2	62.51	37.49			100.00
BD S-2 Spectrum 7	64.11	35.89			100.00
WB S-1 Spectrum 5	65.11	34.89			100.00
WB S-3 Spectrum 2	63.35	36.65			100.00
Puck-Mounted					
BD P-1 Spectrum 1	53.90	46.10			100.00
WB P-1 Spectrum 1	67.97	32.03			100.00
BJN P-1 Spectrum 1	32.64	55.10	8.80	3.46	100.00
BJS P-1 Spectrum 1	50.61	48.24	1.15		100.00

Recent laboratory and field studies (Huerta-Diaz et al., 1990; Jong et al., 2004) found significant uptake of metals Pb, Cu, Cd, Zn, Ni, Fe, and As by BPMS. Bulk sediment trace metal concentrations (Appendix 7) in WB and at heavily oiled sites indicate that BPMS probably co-precipitated trace metals in much less abundance with respect to Fe and S.

Although EDS analysis shows limited trace metal content, the sensitivity of EDS analysis is not suited for quantifying trace-metal at low concentrations. High-resolution laser ablation-inductively coupled plasma mass spectrometry (LA-ICP/MS) analyses were conducted to quantify the elemental compositions of detrital and framboidal pyrites. Results from LA-ICP/MS analyses show that trace metals are incorporated and adsorbed to the biogenic framboidal pyrites present in WB (Figures 50, 51, 52) and heavily contaminated sites (Keevan et al., 2011) (Appendix 10).

Average S and Fe concentrations in framboid pyrite formed in WB are 37.9 and 57.4 %, respectively. Mn, Pb, Zn, and V are the most abundant trace elements (average concentrations >

1,000 mg/kg) in the analyzed framboid pyrites (Tables 12, 13). The samples also contain various amounts of Co, Ni, Cu, As, Se, Hg, Mo, and Cd. Hg and Te are present but their concentrations are not calculated due to the lack of standard references. Chemical compositions of detrital pyrite identified in thin section (Tables 12, 13) are different from those of framboid pyrite grains. The average trace-metal contents are much lower in detrital pyrites than those in the framboidal form. Mn, Zn, Ni, and As are the most abundant trace elements in the analyzed detrital pyrites. However, their maximum concentrations are less than 65 mg/kg. Early stage framboidal iron sulfides in amorphous form are capable of adsorbing and incorporating trace metals into their structure. However, over time, iron-sulfide grains may lose their sorbing capability as they age and re-organize into larger and better-defined crystals. Moreover, while the Fe/S molar ratios of detrital pyrite are in a remarkably narrow range (0.52-0.58) consistent with pyrite stoichiometry, those of framboidal pyrite grains vary and do not have the stoichiometric Fe/S ratio for either pyrite (FeS_2) or marcasite (FeS). This again implies poorly-defined crystal structures and abnormal stoichiometric compositions for the early-formed framboids. The large variations in chemical composition also suggest a biogenic origin for framboid pyrite. Opportunistic microorganisms such as sulfate reducers may take advantage of desired geochemical conditions (i.e., with abundant electron donors/acceptors and available carbon sources) to grow and quickly and randomly assemble nearby elements into pyrite with unique framboid form. It is also important to note that aggregates of framboid pyrite are "zoned" with respect to certain metal concentrations (Figure 52). The zoned pattern suggests that toxic metals are preferentially sequestered from pore water during bacterial sulfate reduction as pyrite begins to grow (Saunders et al., 2005). Chemical constituents of these biogenic pyrites indicate that they show little to no preference when incorporating reduced trace metals into their structure (Tables 12, 13). The

abundance and variety of metals incorporated into their poorly defined crystalline structure indicate that these framboids most likely are amorphous and biogenic in nature, versus detrital.

Low-valence or reduced forms of metals present in pore-water may be sequestered as amorphous metal sulfides (MeS) via the following biogeochemical reaction:

$$HS^- + Me^{2+} \rightarrow MeS + H^+ \quad (5)$$

Here, Me^{2+} represents a divalent metal. The amorphous MeS solid formed will transform with time to more stable sulfide minerals such as pyrite (FeS_2), the main end product. Reaction (5) is very important since it limits the mobility of trace metals and their dissolved loads in pore-water.

The increased organics present via the incursion of oil not only provided additional carbon as electron donors but also most likely increased the concentration of trace metals in reduced forms via a reductive pathway. Hydrogen sulfide produced by bacterial sulfate reduction could react with reduced metals to form framboidal amorphous metal sulfides. The incursion and persistence of oil at heavily contaminated sites like BJS may lead to increased production of metal sulfides. WB's accelerated BPMS production (i.e., not related to the oil spill) most likely is derived from high terrestrial trace metal and carbon inputs from industrial sources, atmospheric deposition, and riverine inflow.

Bacterially-mediated redox reactions involving organic carbon, Fe, and S may lead to cycling of trace metals between solid minerals and pore water. As reducing conditions fluctuate with availability of limiting substrates, oxidation can lead to the dissolution of BPMS. This oxidation combined with the aging and restructuring (into a more stable form) of amorphous BPMS could lead to the expulsion of metals into pore water. As oil degrades over the long term, sulfate-reducing horizons are likely to shift back to a deeper location due to the degradation of organic material in shallow sediments. Shifting reducing horizons to more oxidizing ones and

subsequent oxidation of metal sulfides may release acidic and trace metal-rich waters into the estuarine environment (Johnston et al., 2011).

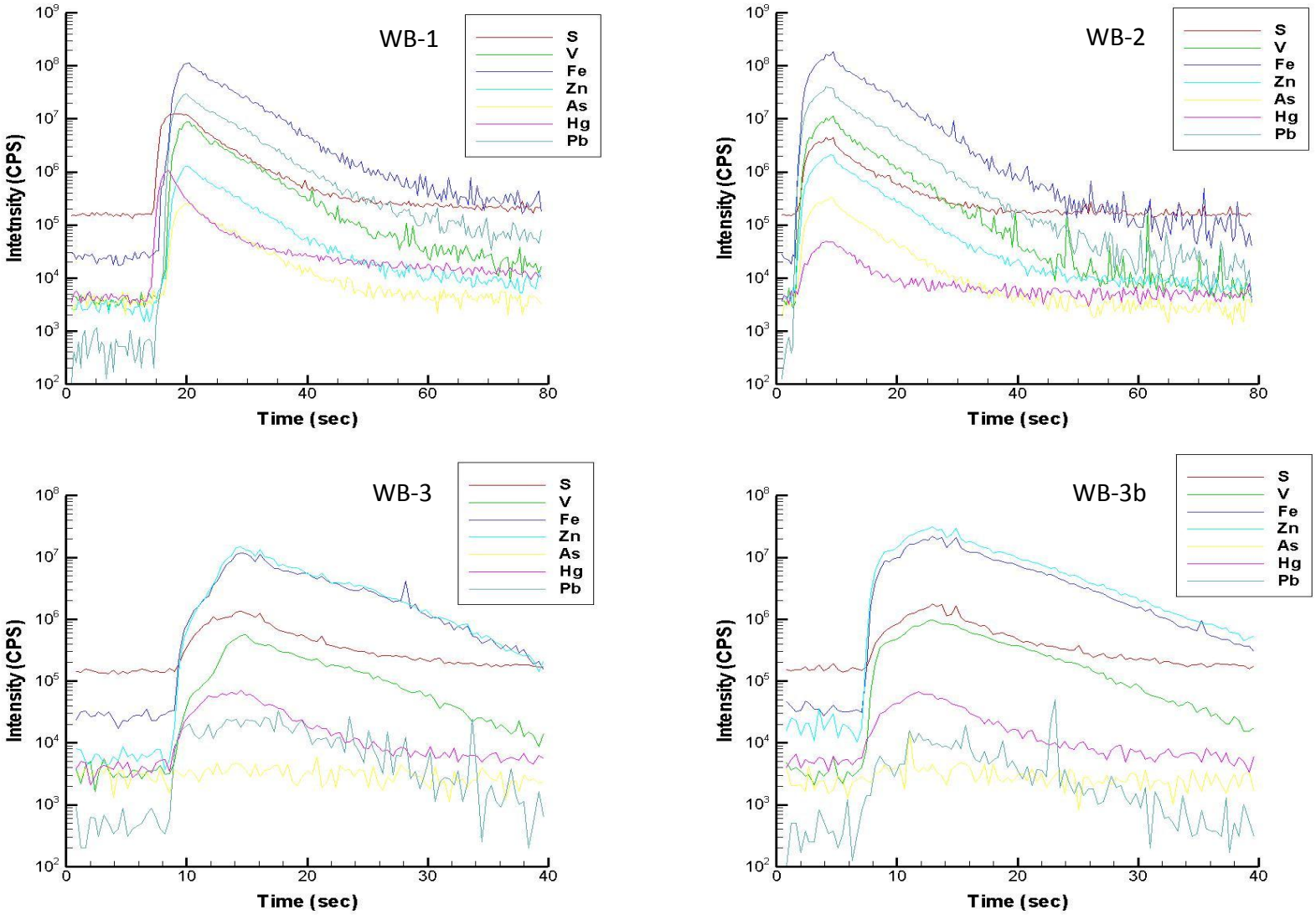

Figure 50. Plots showing LA-ICP/MS spectra of pyrites from WB.

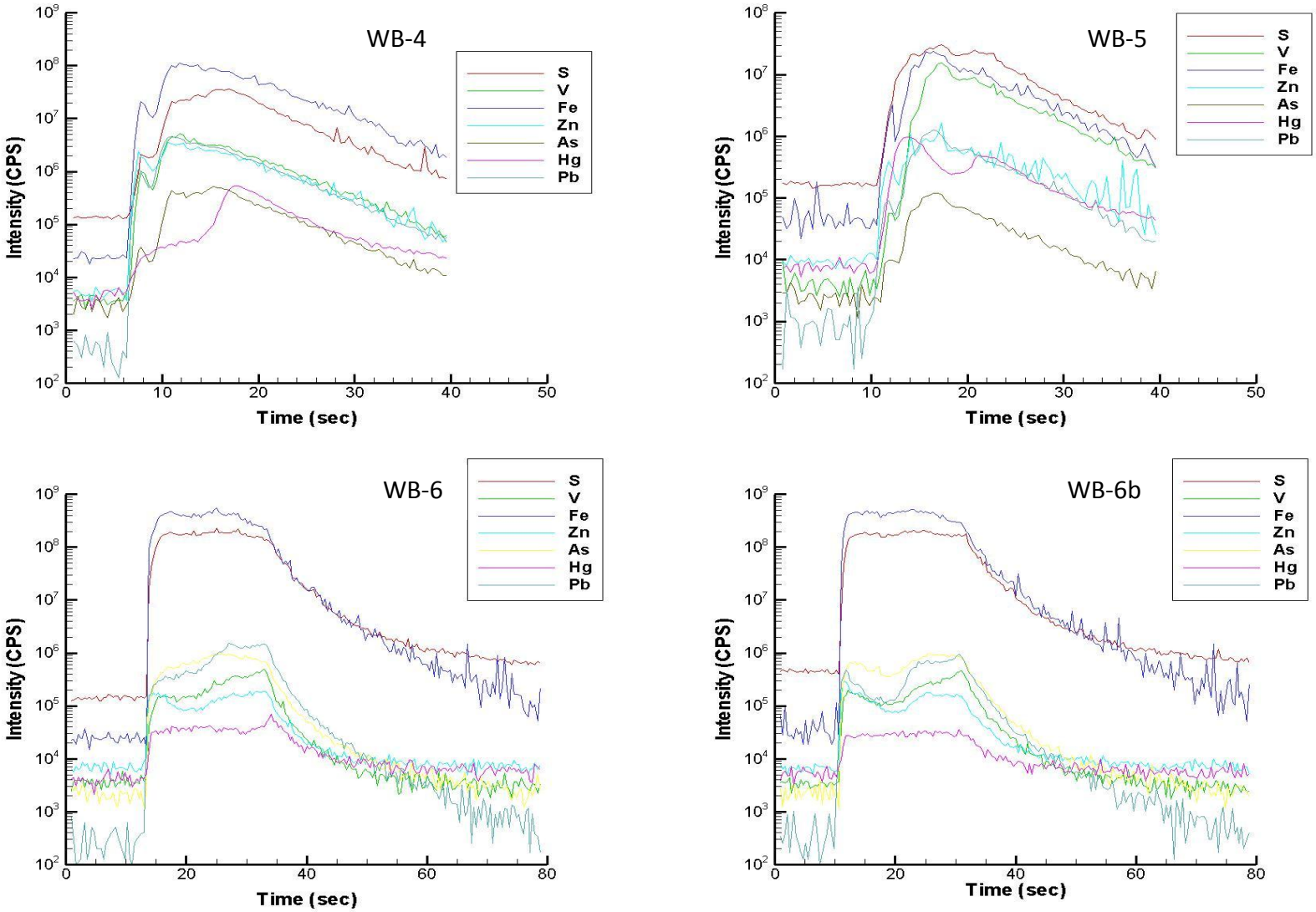

Figure 51. Plots showing LA-ICP/MS spectra of pyrites from WB.

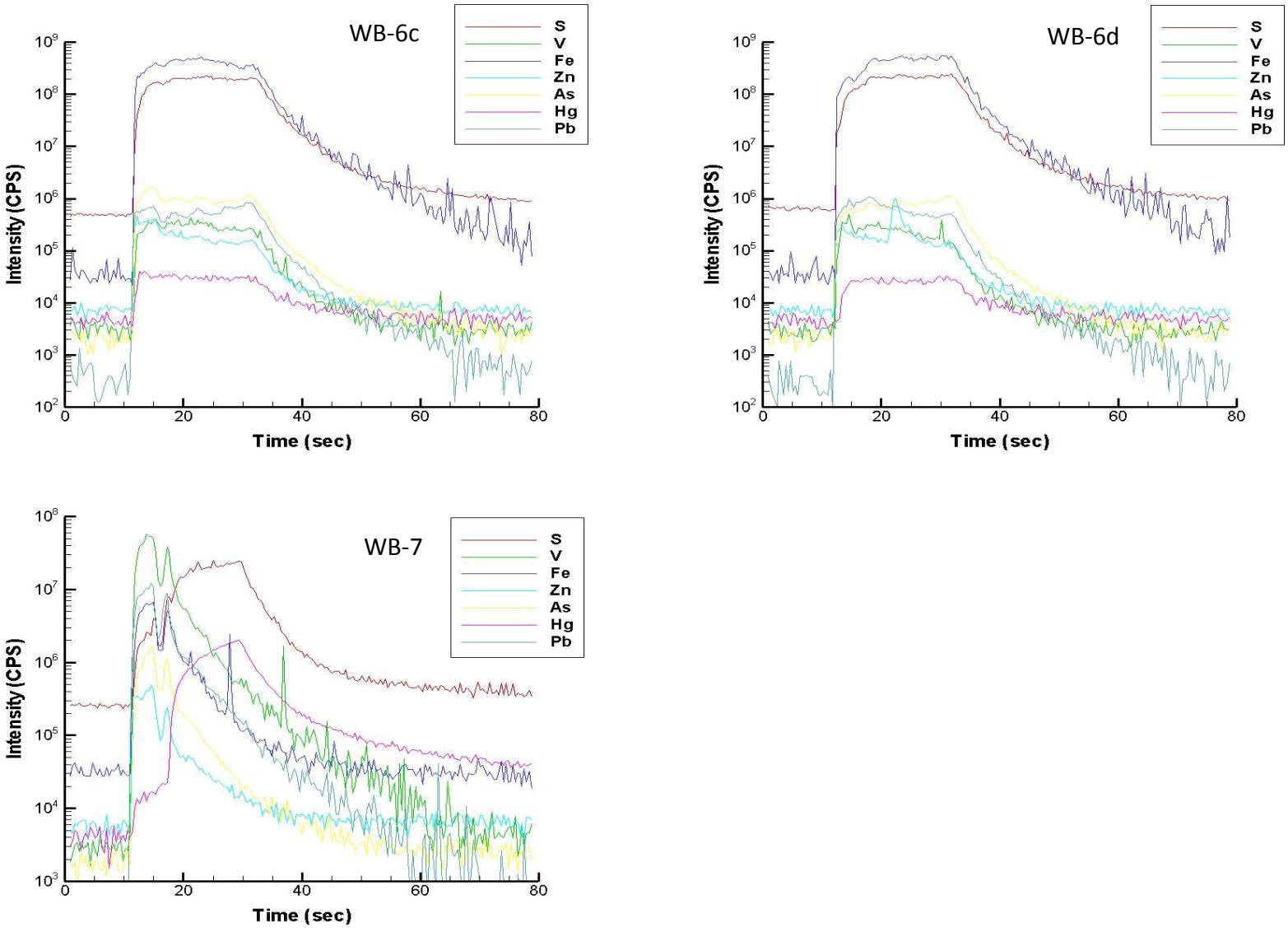

Figure 52. Plots showing LA-ICP/MS spectra of pyrites from WB.

Table 12. Average elemental concentrations measured from LA-ICP/MS analysis of pyrites from WB. Results are normalized to Fe.

Metal	Conc.	WB 1	WB 2	WB 3	WB 3b	WB 4	WB 5	WB 6*
S	**wt. %**	**21.6**	**5.2**	**15.3**	**10.2**	**39.7**	**78.6**	**52.0**
V	mg/kg	924	950	559	612	359	2010	6
Mn	mg/kg	8224	9736	7763	8630	46103	3918	67
Fe	**wt. %**	**77.1**	**93.2**	**74.1**	**76.8**	**55.4**	**20.6**	**48.0**
Co	mg/kg	339	426	618	659	60	45	9
Ni	mg/kg	8	151	2144	1015	140	259	40
Cu	mg/kg	101	158	296	28	89	104	12
Zn	mg/kg	937	1294	94334	118370	1950	1249	21
As	mg/kg	114	119	0	0	164	66	62
Se	mg/kg	31	0	0	0	18	49	3
Mo	mg/kg	77	72	0	0	13	6	4
Cd	mg/kg	10	7	5	4	8	18	0
Te125(LR)**	mg/kg	-	-	-	-	-	-	-
Hg202(LR)**	mg/kg	-	-	-	-	-	-	-
Pb	mg/kg	2901	3153	35	8	286	147	17

*detrital grain

** standard reference for calibration is not available

Table 13. Average elemental concentrations measured from LA-ICP/MS analysis of pyrites from WB. Results are normalized to Fe.

Metal	Conc.	WB 6b*	WB 6c*	WB 6d*	WB 7
S	**wt. %**	**49.9**	**52.4**	**51.5**	**94.2**
V	mg/kg	5	6	4	5736
Mn	mg/kg	64	85	37	861
Fe	**wt. %**	**50.1**	**47.5**	**48.4**	**4.8**
Co	mg/kg	5	5	5	2
Ni	mg/kg	23	21	20	143
Cu	mg/kg	7	9	6	77
Zn	mg/kg	20	28	30	344
As	mg/kg	56	84	61	631
Se	mg/kg	2	3	3	175
Mo	mg/kg	11	24	12	400
Cd	mg/kg	0	0	0	26
Te125(LR)	mg/kg	-	-	-	-
Hg202(LR)	mg/kg	-	-	-	-
Pb	mg/kg	9	11	11	1086

*detrital grain

GC/MS analysis and geochemical correlation of oil

Gas-chromatograph mass-spectrometry time of flight and selected ion-mode analyses (GC/MS-ToF, GC/MS-SIM) were conducted to determine the source and degradation of crude oil compounds present at all sampling sites. In addition, a sample of initial Macondo-1 MC-252 oil was analyzed to provide a control for comparison. Extraction of oil compounds from core sections of 0-3, 12-15, 27-30 cm, at all sites as well as bulk surface sediments, were processed via EPA modified method 3570 of microscale solvent extraction. Resultant extractions from sediments and hexane-cut (200:1) degraded oil and initial MC-252 crude were analyzed via GC/MS-ToF in full-scan mode.

Pristine and slightly contaminated sites such as WB, WI, LB, and RG all returned negative results, indicating little or no petroleum-related hydrocarbons in any sediments. MC-252 oil and oil extractions from BJS surface sediments and sediments from other heavily contaminated sites returned chromatograms that clearly show the presence of various hydrocarbons. The complete chromatograms of degraded oil indicate that heavier hydrocarbons are present while lighter ones have largely been degraded. This is evident from the higher intensity returns of heavier compounds on the right side of the chromatograms (over 14-21 minute range of higher temperatures) (Figures 53, 54). By contrast, full-scan chromatograms from the initial MC-252 crude reflect higher percentages of lighter compounds (Figure 53). These results clearly indicate that heavier compounds persist in sediments, while lighter compounds were preferentially biodegraded by natural microbes or evaporated within months after the oil spill.

The results of GC-MS analysis of degraded oil and MC-252 crude oil are consistent with previous studies, which show that natural microbes preferentially attack the single bonds in the lighter molecules first, especially n-alkanes (Jobson et al., 1972; Bailey et al., 1973). Although

most light compounds of oil may be easily degraded by natural microbes on the short term, saturated heavy oil (e.g., asphaltenes, resins, polycyclic aromatics, etc.) and those adsorbed by sediments can persist in the environment for decades (e.g., Oudot and Chaillan, 2010). Some heavier hydrocarbon compounds eventually may be broken down by bacterial sulfate reduction. However, this degradation process is much slower than aerobic degradation (Shmonova and Shaks, 1971; Bailey et al., 1973). The heavy compounds that persist in BJS and other contaminated sediments can lead to increased microbial activity over the long term as the oil acts as an electron donor and carbon source for slow anaerobic biodegradation.

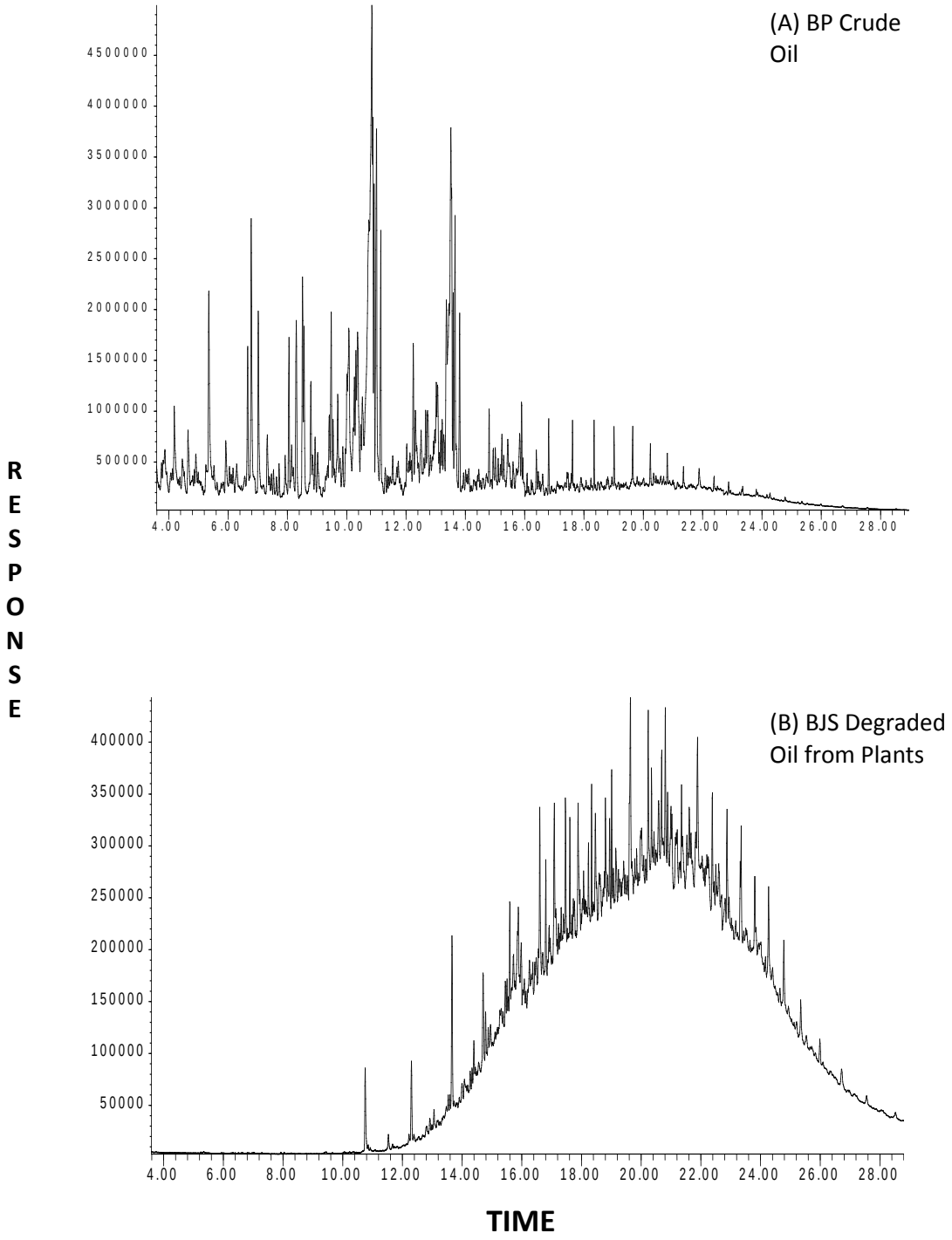

Figure 53. Chromatograms of initial BP MC-252 crude (A) and degraded oil from plants at BJS (B) sampled six months after the spill ceased. Analysis shows that heavier compounds persist in sediments while lighter compounds have been preferentially biodegraded by natural microbes.

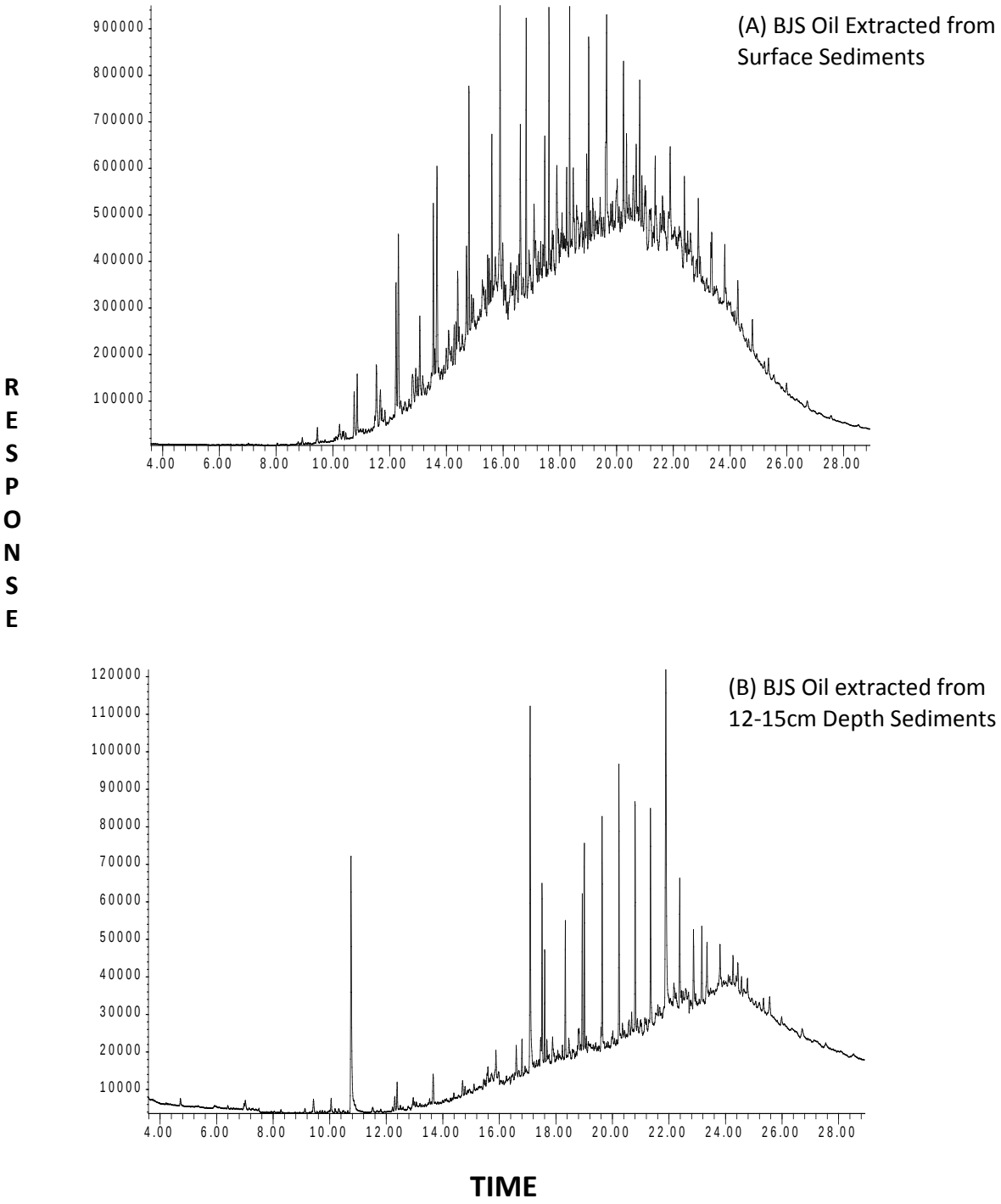

Figure 54. Chromatograms of extracted oil from surface sediments at BJS (A), and oil extracted from 12-15cm depth at BJS (B) sampled six months after the spill ceased. Analysis shows that heavier compounds persist in sediments while lighter compounds have been preferentially biodegraded by natural microbes.

Degraded oil recovered from BJS and initial MC-252 crude were analyzed by GC-MS in the Single Ion Monitoring (SIM) mode. The GC/MS-SIM mode has much higher sensitivity compared to the full scan and ToF modes. GC-MS-SIM also minimizes the background noise and virtually eliminates many of the extraneous peaks, allowing better identification and quantification of target biomarkers in the complex chromatographs. This results in an increased sensitivity factor of 10 to 100 times while analyzing dwell times of specific mass to charge ratios (m/z) (CAS Lab, 2011). All samples were analyzed for specific oil compounds (known as biomarkers) with unique mass-to-charge ratios (m/z) of 191, 217, and 218. These specific m/z ratios contain proven biomarker fragments (Wang et al., 1999).

Variations in source factors, microbial activity and environmental deposition lead to a unique chemical make-up for each crude oil (Wang et al., 1999). This distinct chemical make-up, also known as a fingerprint, can help in the analysis of oil source, original organic matter, thermal maturity, migration, depositional environment, and source-rock age correlations (Peters et al., 1986; 1991; Morrison et al., 2006). Ratios of organic molecule fragments present in the crude that elute, such as terpanes, steranes, and acyclic isoprenoids and their isomers (known as bio-markers), can be analyzed to construct a chemical signature or fingerprint. The selected bio-markers used for fingerprinting show little change in structure during prolonged weathering and oxidation when introduced to the environment (Peters et al., 2005; Morrison et al., 2006; Wang et al., 2007).

GC/MS SIM results clearly correlates MC-252 crude to oil extracted from sediments down to 15 cm as well as to degraded oils recovered from surface sediments. This is evident when comparing specific bio-marker ratios (i.e., associated with m/z 191) such as Ts/Tm (18α-22,29,30-trisnorneohopane/17α-22,29,30-trisnorhopane), 24Tri/23Tri (C24 tricyclic terpane/C23

tricyclic terpane), C29/C30 (17α,21β(H)-30-norhopane/17α,21β(H)-hopane), and 29D/29H (18α(H)-30-norneohopane/17α,21β(H)-30-norhopane)(Figures 55, 56). Although the fragmentogram patterns of M/Z 191 vary among samples, biomarker ratios of selected parameters calculated from peak heights of GC/MS spectra are all in a remarkably narrow range and can be used to correlate spilled oils with initial BP oil (Table 14). All surface sediment oil extracts and degraded oils recovered from BJS and other heavily contaminated sites statistically match the MC-252 oil from the Macondo-1 well. Oil extracts from BJS at the 12-15 cm depth show the presence of MC-252 oil with a possible slight mixing of other oil types (Table 14). Sediments deeper than 15 cm and from other heavily contaminated sites were not analyzed and further investigation is needed. GC/MS-SIM analyses of spilled oil indicate that the degradation of lighter oil compounds has proceeded to varying degrees, while a significant fraction of heavier hydrocarbon compounds still persists in sediments.

Presence of BP oil and high TOC/DOC contents in sediments from 12-15 cm depth at site BJS suggest that not all the spilled oil rose to the surface and evaporated. A portion of the oil spread in the water column and became adsorbed by sediments. Deeper sediments that tested positive for hydrocarbons (down to 15 cm) at BJS and other heavily contaminated sites clearly reside in strongly reducing zones. This is evident when comparing similar patterns with depth for concentrations of reduced hydrogen sulfide and the presence of BPMS. The spilled oil at these depths most likely is undergoing slow degradation by SRB, whose activities have been limited by available substrates (i.e., reactive organic carbon and sulfate).

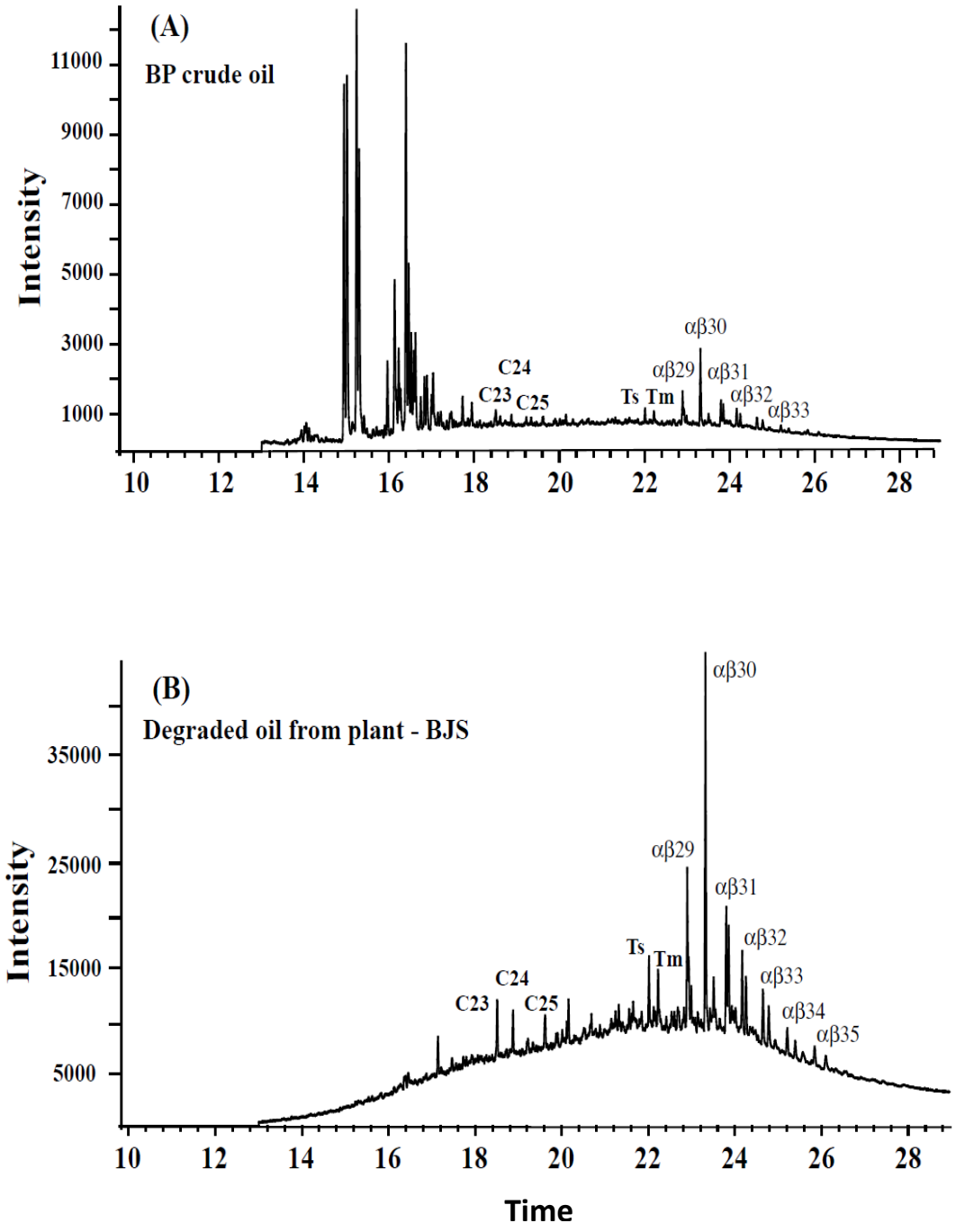

Figure 55. Fragmentograms of BP, MC-252 oil (A) and oil recovered from suppressed plants at BJS (B). Selected ion monitoring (SIM) fragmentograms of m/z 191; hopanes and tri-cyclic terpanes are identified on the fragmentograms for bio-marker analysis.

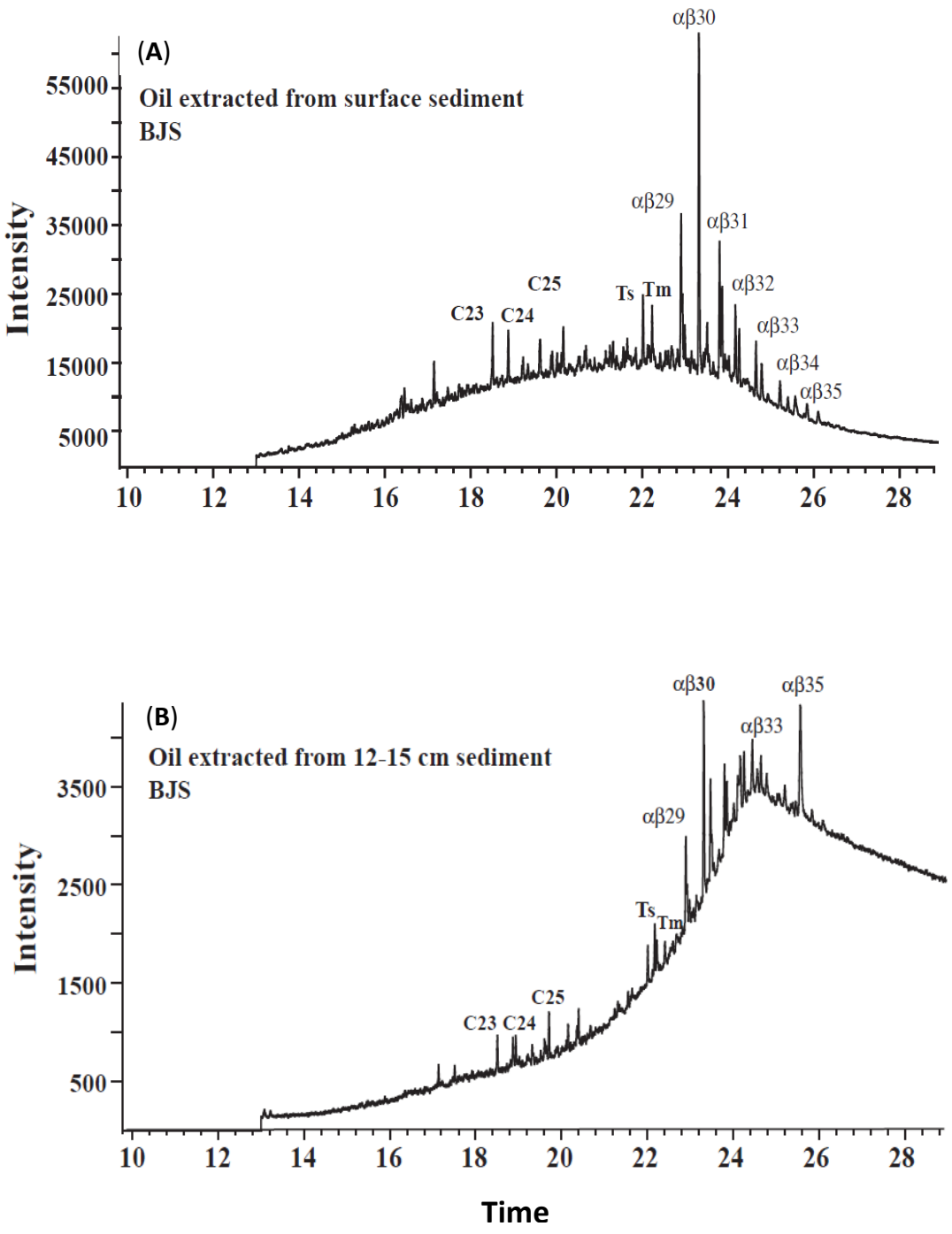

Figure 56. Fragmentograms of oil extracted from surface sediments at BJS (A) and oil extracted from 12-15cm depth of sediments at BJS (B). Selected ion monitoring (SIM) fragmentograms of m/z 191; hopanes and tri-cyclic terpanes are identified on fragmentograms for bio-marker analysis.

Table 14. Biomarker ratios of selected fragmented compounds calculated from peak heights of GC/MS spectra. Although the chromatograph patterns of m/z 191 vary among samples, biomarker ratios fall in a remarkably narrow range and can be used to correlate spilled oils with initial BP-252 crude. Possible slight mixing of oils is evident in BJS and BD 12-15 cm C29/C30 ratio.

Sample Location of Extracted Oil	Ts/Tm (18α-22,29,30-trisnorneohopane/17α-22,29,30-trisnorhopane)	24Tri/23Tri (C24 tricyclic terpane/C23 tricyclic terpane)	C29/C30 (17α,21β(H)-30-norhopane/17α,21β(H)-hopane)	29D/29H (18α(H)-30-norneohopane/17α,21β(H)-30-norhopane)
BP MC-252 Crude	1.07	0.91	0.58	0.56
BJS Plant Recovered	1.07	0.91	0.54	0.56
BJN Plant Recovered	1.06	0.91	0.53	0.56
BJS Surface Sediment	1.07	0.94	0.58	0.56
BJN Surface Sediment	0.96	1.00	0.59	n/a
BJS 12-15cm Sediment	0.90	1.04	0.77	n/a
BD 12-15cm Sediment	0.96	0.98	0.70	n/a

Carbon-Isotope Systems of Marsh Sediments, Oil, and Plants

Carbon-isotope analysis was conducted on the organic matter from every section of cored sediments at all sites, dominant live marsh plants at all sites, and site recovered degraded oil (Appendix 4). Stable carbon-isotope ($^{13}C/^{12}C$) ratios can be used to fingerprint the sources of organic matter in marsh sediments (i.e., plant or oil). Sites dominated primarily by C_4 plants (i.e., *Spartina patens* and *Spartina alterniflora),* which include WI, RG, and BJS, were analyzed by comparing isotopic composition from the organic matter of the sediments and plants to oil. Sites dominated by C_3 Plants (i.e., *Juncas*), which include WB, and LB, were evaluated but could not be used to assess the presence of oil because the lighter isotopic composition of *Juncas* ($\delta^{13}C$ signatures <-24 ‰) is similar to those of Gulf crude oils.

The stable carbon isotopic composition of organic matter in marsh sediments is primarily controlled by the type of vegetation growing in the marsh. Coastal salt marshes dominated by C_4 plants (i.e., primarily *Spartina patens* and *Spartina alterniflora*) have $\delta^{13}C$ signatures of -14.4 to -17.7‰ (Chmura et al., 1987). Slightly contaminated C_4 sites WI and RG returned live plant isotopic $\delta^{13}C$ signatures of -14.4‰ and -15‰ respectively. Sediments from these slightly contaminated sites returned more negative average isotopic signatures of -22.28‰ and -21.53‰ respectively, clearly indicating the influence of isotopically light crude oil. Non-contaminated sites WB and LB, dominated by C_3 plants, returned very similar signatures with regard to sediments and plants (within .04‰ and 2‰), respectively. In addition, very similar isotopic signatures for sediments and plants exist at other non-contaminated locations.

The lighter isotopic signatures of sediments in contaminated C_4 dominant sites can be directly related to the presence of oil. Depending on the source of the oil, crude oils have a more negative $\delta^{13}C$ value (-23 to -32‰) than C_4 plants (-14.4 to -17.7‰) (Stahl, 1977; Macko and

Parker, 1983; Jackson et al., 1996). The reported $\delta^{13}C$ values of crude oils from different reservoir rocks of the southern USA and the Gulf of Mexico range from -26.6 to -33.0‰ (Stahl, 1977; Macko and Parker, 1983), which are very different from the $\delta^{13}C$ signatures of sedimentary carbon in salt marshes along the Louisiana coast (Chmura et al., 1987). The influx of MC-252 oil, which has a $\delta^{13}C$ value of -27‰, can shift the average isotopic signatures of marsh sediments to be more negative than non-contaminated counterparts. Hence, isotopic signatures can be used to recognize the presence of oil in sediments (Figure 57, 58). BJS, like other salt-marshes along Louisiana coast, is dominated by *Spartina sp.* (with $\delta^{13}C$ values of -14.8±0.6 ‰). Thus, the sediment carbon isotopic signatures of BJS sediment (-20.6±1.4 ‰) most likely reflect the influence of the spilled oil.

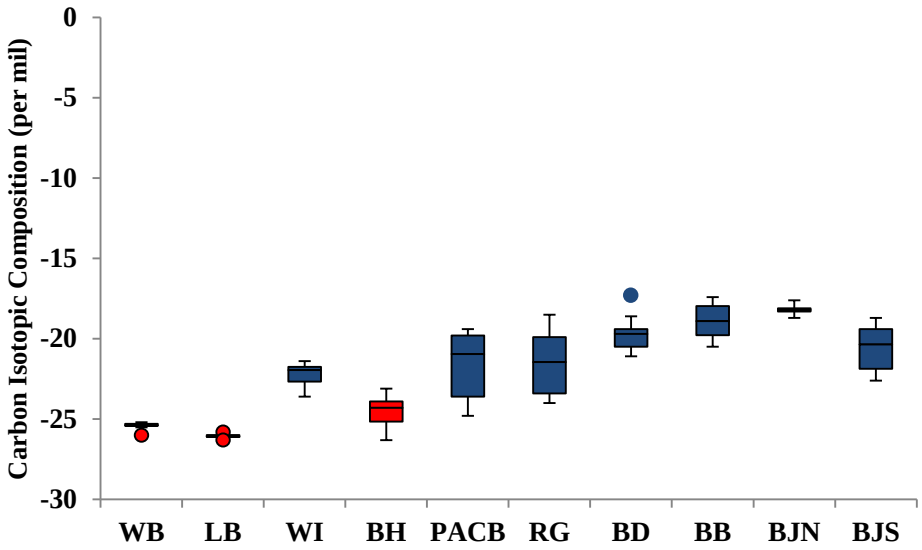

Figure 57. Box and whisker plot showing variations in carbon isotopic compositions of organic matter in sediments. Blue boxes indicate sites dominated by C_4 *Spartina* plants with $^{13}C/^{12}C$ ratios (-14.8±0.6 ‰) heavier than that of BP crude oil (mean = -27‰). Red indicates C_3 *Juncas* plants with lighter isotopic compositions ($\delta^{13}C$ signatures < -24 ‰) that are similar to oil and cannot be used for analysis. Circles designate outliers.

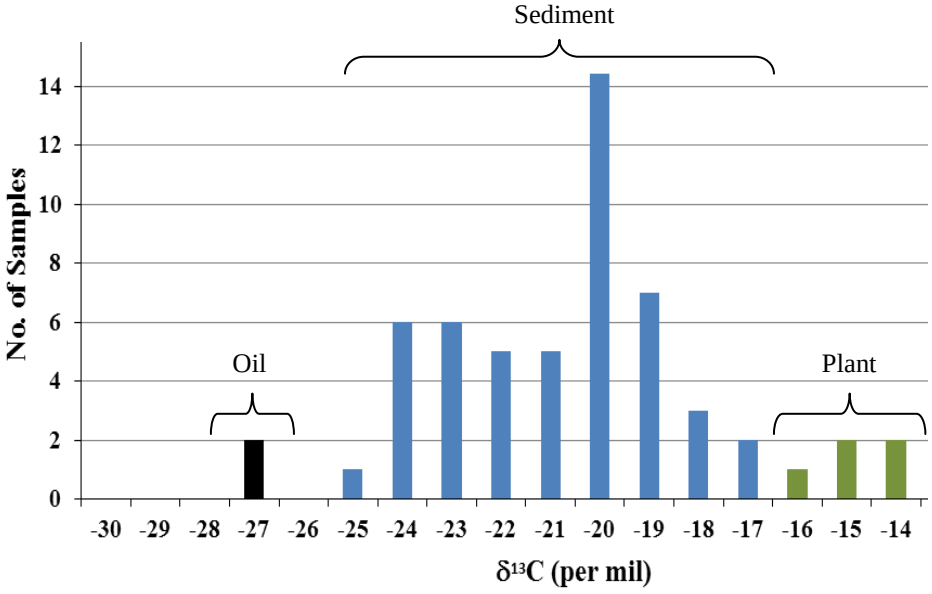

Figure 58. Carbon-isotope histogram showing that $\delta^{13}C$ values of sediment organic matter (blue) collected from five oiled sites (i.e., BB, BD, RG, WI, PACB) dominated by C_4 *Spartina* plants were significantly lighter (-20.8±2.0‰) than those of their marsh plants (-14.8±0.6 ‰, green) but heavier than the initial BP MC252 oil (-27±0.2 ‰) or weathered oil scrapped off the oiled plants (mean = -26.7 ‰, black).

Microbiology

Strongly reducing conditions attributed to the influx of oil likely enhanced the activities of IRB and SRB at contaminated sites. This is evident from the high MPN SRB counts, formation of BPMS, and extremely elevated accumulation of sulfides at heavily contaminated sites. While IRB and SRB via TEAP have proven to be able to alter the chemical evolution and mobility of trace metals, organics (i.e., oil) will stimulate microbial growth that then can lead to the release and complexation of toxic metals (Keimowitz et al., 2005; Schuster et al., 2008; Lee, 2011).

The most probable number (MPN) technique was used to quantify both IRB and SRB present in the 0-3, 12-15, 27-30 cm sections of sediment cores from all sites. MPN results indicate IRB were present at all sites (>1600 IRB/g) and in all sediment core sections (Appendix 9). This indicates that iron reduction is taking place at all sediment depths to various degrees at all sites. The presence of IRB also indicates that the iron reducing conditions necessary to release toxic trace metals into the environment have been established. SRB also were present at all sites, and their population counts generally decrease with depth (Appendix 8). Slightly contaminated site RG recorded the highest numbers of SRB. SRB numbers at highly contaminated sites were similar but slightly lower than RG.

SRB are expected to be most abundant in the deeper levels of sediments due to more strongly reducing conditions and competition with IRB. However, highest MPN numbers (> 900 MPN/g) for SRB at contaminated sites are recorded in the uppermost 0-3 cm of the sediment (Figure 59). This suggests that the influx of oil has accelerated the growth and colonization of SRB and produced strongly reducing conditions near the water-sediment interface. Oil that acts as an electron donor on the sediment surface most likely provides an abundant supply of electrons and organic carbon as needed in TEAP. The reducing horizon depths that generally exist in marsh

sediments have been altered by the influx of oil. The introduction of oil results in a more strongly reducing condition that exists at the water-sediment interface. It is also possible that organic matter derived from terrestrial sources and biological activity settles on sediment surfaces where it is mineralized by sediment microbial populations (Wollast, 1991; Ravenschlag, 2000). Thus at the top of marsh sediments, microbial activity may be enhanced by higher organic matter content (Westrich and Berner, 1984). It should be noted that SRB MPN and reduced sulfide concentrations are lower at the BJS site compared to other heavily oiled sites (see Appendix 8 and Figure 59). It is not clear to what extent physical environments may affect biogeochemical processes; BJS faces the open ocean and harsh environments there may suppress microbial activities to some extent.

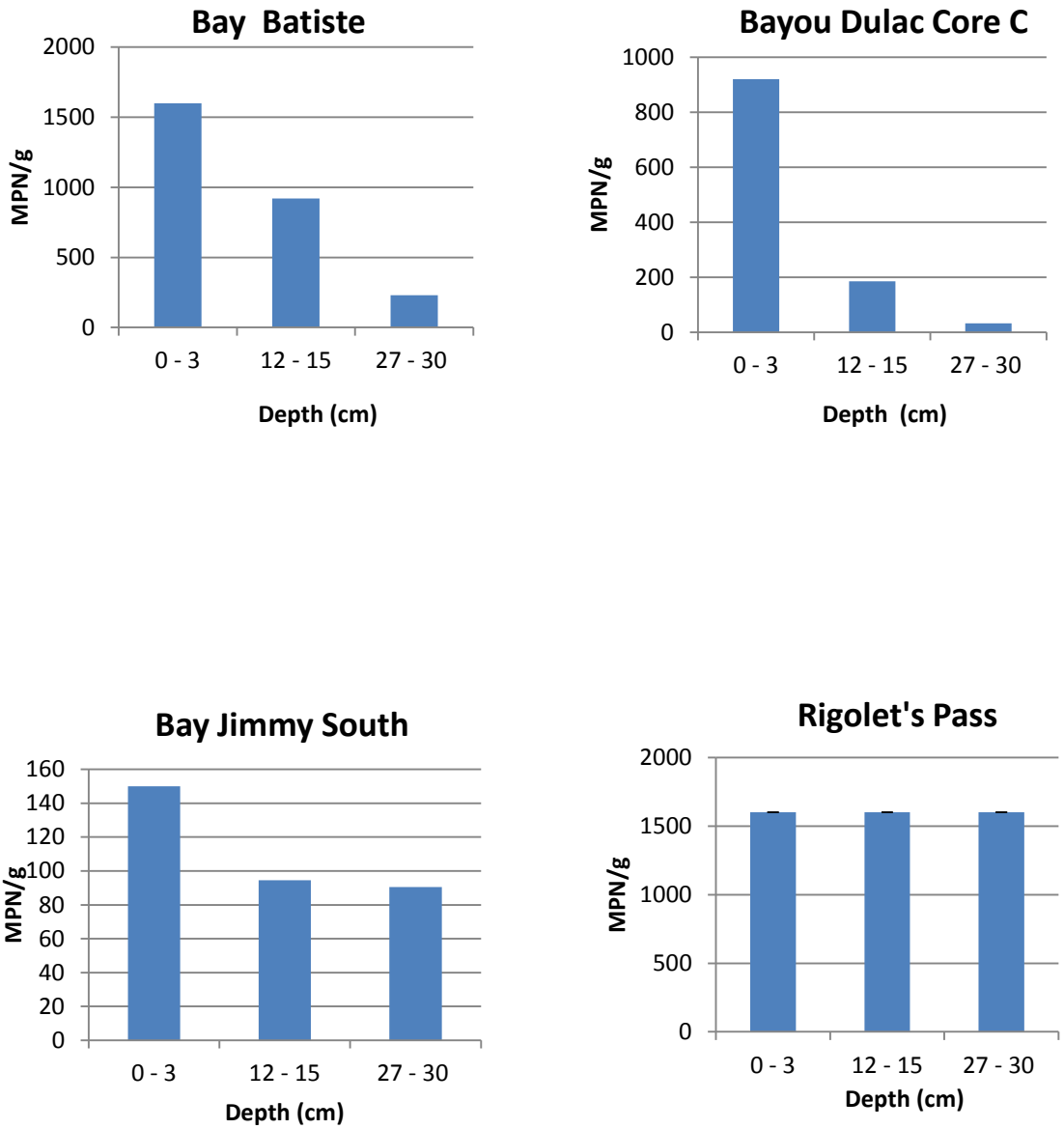

Figure 59. Most probable number (MPN) of sulfate-reducing bacteria (SRB) in heavily (BJS, BB, and BD) and slightly (RG) contaminated sites. Results show populations decrease with depth indicating the possible acceleration of growth and colonization in shallower horizons.

CONCLUSIONS

Ten Gulf salt marsh sites were evaluated for the impacts of the 2010 BP Macondo-1 Deepwater Horizon oil spill. Results indicate that influx of oil has contributed to significant geochemical, hydrological, and microbial transformations in these ecologically sensitive marsh environments. Of the ten sites evaluated, five were discussed in this thesis. These include a heavily contaminated site in Louisiana (Bay Jimmy South: BJS), two intermediate sites in Alabama (Walker Island: WI), and Louisiana (Rigolets: RG), and two pristine sites in Alabama (Weeks Bay: WB, Longs Bayou: LB).

At BJS, a heavily contaminated site where degraded oil still persisted six months after the spill, hydrocarbons are present in sediments down to at least 15 cm. Gas chromatography mass spectrometry (GC/MS) analyses of geochemical biomarkers used to fingerprint the presence of oils in BJS and other heavily contaminated sediments reveal preferential biodegradation of lighter compounds. The spilled oil is quickly degraded by natural microbes or evaporated, while the heavier fractions of oil still remain adsorbed by sediments. GC/MS selected ion mode (SIM) results indicate a positive correlation between source BP MC-252 oil, site recovered oil, and all oil extracts from cored sediments and bulk surface sediments. The ratios of selected biomarkers calculated from the gas chromatograph spectra for spilled oils and BP MC-252 crude fall in a remarkably narrow range.

Whereas BJS and other heavily contaminated sites indicate the presence of BP MC-252 oil, C_4 plant dominated intermediate sites (RG and WI) are characterized by lighter than normal sedimentary $\delta^{13}C$ values. Intermediate (RG and WI) and heavily (BJS) oiled sites $\delta^{13}C$ values

(-20.8±2.0 ‰) have been shifted significantly lower compared to their marsh plants (-14.8±0.6 ‰) $\delta^{13}C$ values. This shift reflects the influence of isotopically lighter oil (-27±0.2 ‰). The presence of oil compounds at these heavily and intermediately contaminated sites can be recognized by the shift in $\delta^{13}C$ values that are more negative than those of vegetation in the area. In contrast, $\delta^{13}C$ values for sediment and vegetation at pristine sites WB and LB are virtually identical (within .04‰ and 2‰), indicating no oil.

The influx of oil at BJS led to elevated levels of dissolved organic carbon (DOC) and total organic carbon (TOC) compared to pristine sites WB and LB. Pore waters separated from heavily oiled Louisiana wetland sediments at BJS show extremely high DOC concentrations that reach as much as 347 mg/kg, compared to those (< 50 mg/kg) at pristine sites WB and LB. DOC levels at BJS are much higher in pore waters (mean = 228 mg/kg) than in surface water (mean = 42 mg/kg) and increase significantly with depth in the substrate. These results indicate near-surface sediments may be flushed by freshwater recharge from rainfall or shallow groundwater. Elevated DOC levels could persist in deeper wetland sediments for a long period of time after a significant portion of the oil in the surface water has been evaporated, dispersed, or degraded by microorganisms. Denser seawater may also push oils into deeper portions of the marsh sediments due to salinity stratification. Elevated TOC concentrations in sediments also can be attributed to oil intrusion into sediments at BJS and other heavily contaminated sites. BJS TOC analysis showed a maximum of 16%, while TOC at pristine sites (LB and WB) is considerably lower < 4%. Notably, other heavily contaminated sites show even higher TOC values up to 29%. Clearly, the intrusion of oil has resulted in organic contamination of sediments that, in turn, has fueled microbial processes that rely on organic carbon as an electron donor.

Heavily oiled sites are all characterized by high sulfide concentrations (up to 80-100 mg/kg) and an abundance of sulfate-reducing bacteria. Pristine sites WB and LB have much lower sulfide concentrations (< 1 mg/kg). The abundance of sulfides at oiled locations indicates accelerated bacterial sulfate reduction caused by the increase in organic carbon (i.e., oil). Whereas iron-reducing bacteria are present at all sites (MPN >1600 IRB/g), the relatively low reduced Fe and metal contents and high sulfide concentrations indicate that bacterial sulfate reduction has fixed most reduced Fe and other trace metals by forming solid iron sulfides.

Elevated concentrations of trace metals are found in BJS and WB sediments. The elevated levels in WB sediments can be attributed to large industrial and agricultural activities in Baldwin County, all of which are potential point and non-point sources of metal pollutants. The fine-grained sediments in WB also contribute to the retention and enrichment of trace metals. BJS and other heavily contaminated sites are elevated in certain trace metals and elements (Cu, Pb, Zn, Fe, Hg, As, V, Ni, and S) compared to pristine sites LB and intermediate sites RG and WI. Heavily oiled sites like BJS, are characterized by metal concentrations that are 150 to 200% higher than those at pristine site LB. One factor contributing to the elevated trace metal concentrations at BJS and other heavily oiled sites is finer grain sizes that dominate there. These finer, inherently more organic carbon-rich sediments, aid in the retention of trace metals through adsorption. Fine-grained heavily contaminated sites also show increased levels of Ni, Cu, S, and, to a lesser degree V. These four elements are considered to be indicators of oil contamination. Sediments at BJS and other heavily contaminated sites have Cu and Ni contents that are 150 to 200% higher than those at pristine sites. The Ni and Cu concentrations of heavily oiled sites are all substantially higher than WB levels. This is notable because WB's results show that it has the most elevated trace metal content of all sites, other than Cu and Ni. Elevated

S and V levels are recognized at heavily oiled sites; elevated levels of Ni, Cu, S, and V may result from a combination of the absorption capabilities of fine-grained sediments and incursion of oil in sediments. The specific contribution of trace metals by oil remains unclear. Nevertheless, it is evident that the incursion of oil has led to an increase of trace metals and S at heavily oiled sites.

Reduced trace-metal concentrations in pore water are fairly low with respect to trace-metal concentrations in sediments. Trace metals at BJS and other heavily contaminated sites have been sequestered into solid forms. The altered sulfate reduction horizon created by the oil influx and increased microbial activity resulted in an accelerated sequestration of trace metals into sulfur solids. The low concentrations of reduced iron and high sulfide contents at BJS and other highly contaminated sites indicate that bacterial sulfate reduction has fixed most reduced Fe and other trace metals by forming solid iron sulfide. Biogenic sulfide minerals, such as pyrite with distinct framboidal form, are abundant at BJS and in other oiled marsh sediments. Laser-ablation inductively coupled plasma mass spectrometry (LA-ICP-MS) analysis of these pyrite spheroids consistently yield peaks for Fe and S, along with high levels of sequestered trace metals such as arsenic, mercury, and lead. BPMS production may have prevented toxic aqueous complexes like thioarsenites from forming by the sequestration of arsenic into sulfide solids.

Whereas sediments at BJS and other heavily contaminated sites still contain enough oil to be sensed by GC/MS-ToF techniques, sediments at intermediate sites WI and RG do not. Nevertheless, isotopic signatures reveal that oil was present at intermediate sites at the time of sampling. It is possible that intermediate sites WI and RG received substantial organic contamination from the oil. However, coarser grain size and lower organic carbon contents of RG and WI sediments precluded the retention of the oil and its trace metals. Local conditions

also likely played a vital role in oil retention; BJS and other heavily contaminated sites are less influenced by tides than sites RG and WI. The flushing of seawater from storm and tidal action in higher energy environments may have helped to cleanse these sites.

Results from all Louisiana sites are troubling from an environmental standpoint. Continued evaluation of ecologically sensitive estuarine environments is needed to fully understand the long-term effects of the oil spill. Heavier components of crude oil continue to exist in Louisiana sediments. The potential impacts of biodegradation of this oil over the long term and possible oxidation of biogenically produced metal sulfides along with the resultant re-mobilization of adsorbed trace metals are unclear. Recent studies have shown that shifting reducing zones to more oxidizing ones by limiting electron donors, such as the long term degradation of the oil, can shift sulfate-reducing horizons back to a deeper and more natural location. Johnston et al. (2011) have shown that the oxidation of sulfides as a result of downward shifts in the sulfate-reduction zone can release acidic waters and reduced trace metals in the estuarine environment. This process is of particular concern as microbes continue to degrade the remaining oil and will eventually run out of electron donors. Thus, it is important to monitor the evolution of oil and its impact on the concentration, speciation, and release of metals in wetlands impacted by the spill for years to come.

REFERENCES

ADEM, 1996, The ADEM fish tissue monitoring program 1991-1995: Alabama Department of Environmental Management, Montgomery, AL, 36 pp.

ADPH, 2008, Alabama Department of Public Health issues 2008 fish consumption advisories: Alabama Department of Public Health, Montgomery, AL, 8 pp.

Amos, J., 2010, SkyTruth: http://mcbi.org/news/PR-Norse-Amos-2010.pdf (accessed November 10, 2010).

Ball, J.S., Wegner W.J., Hyden, H.J., Horr, C.A., and Myers, A.T., 1960, Metal Content of Twenty-Four Petroleums: Journal of Chemical Engineering, v. 5, p. 553–557.

Bailey, N.J.L., Jobson, A.M., and Rogers, M.A., 1973, Bacterial degradation of crude oil: comparison of field and experimental data. Chemical Geology, v. 11, p. 203–221.

Barwise, A.G., 1990, Role of Nickel and Vanadium in Petroleum Classification: Energy and Fuels, v. 4, p. 647-652.

Beasley, L.R., 2010, Interaction of groundwater, surface water and seawater in Wolf Bay, Weeks Bay, and Dauphin Island Coastal Watersheds, Alabama. [M.S. Thesis]: Auburn University, 65 pp.

Beeman, R. E., and Sulflita, J. M., 1987, Microbial ecology of a shallow unconfined ground water aquifer polluted by municipal landfill leachate: Microbial Ecology, v. 14, p. 39-54.

Berner, R. A., 1970, Sedimentary pyrite formation: American Journal of Science, v. 268, p. l-23.

Berner, R. A., 1984, Sedimentary pyrite formation: an update. Geochimica et Cosmochimica Acta, v. 48, p. 605–615.

Benoit, J. M., Gilmour, C.C., Mason, R.P., Riedel, G.S., and Riedel, G.F., 1998, Behavior of mercury in the Patuxent River estuary: Biogeochemistry, v.40, p. 249-265.

Burnol, A., and Charlet, L., 2010, Fe(II)-Fe(III)-bearing phases as a mineralogical control on the heterogeneity of arsenic in Southeast Asian groundwater: Environmental Science & Technology, v. 44, p. 7541–7547.

Bose, P., and Sharma, A., 2002, Role of iron in controlling speciation and mobilization of arsenic in subsurface environment: Water Research, v. 36, p. 4916-4926.

Callaway, J.C., DeLaune, R.D., and Patrick, W.H. Jr., 1997, Sediment accretion rates from four coastal wetlands along the Gulf of Mexico: Journal of Coastal Research, v. 13, p. 181-191.

Chapelle, F., 1993, Groundwater Microbiology and Geochemistry: John Wiley and Sons, Inc. New York, N.Y. p. 48-274

Chmura, G., Socki, R., and Abernethy, R., 1987, An inventory of ^{13}C abundances in coastal wetlands of Louisiana, USA: Vegetation and sediments: Oecologia, v.74, p. 264-271.

Chandler, R.V., Gillet, B., and DeJarnette, S.S., 1996, Hydrogeologic and Water-Use Data for Southern Baldwin County, Alabama: Geologic Survey of Alabama, 188 pp.

Crone, T.J., and Tolstoy, M., 2011, Magnitude of the 2010 Gulf of Mexico oil leak: Science, v. 330, p. 634.

Ciccioli, P.W., Cooper, T., Hammer, P.M., and Hayes, J.M., 1980, Organic solute-mineral surface Interaction; A new method for the determination of groundwater velocities: Water Resources, v.16, p. 217-223.

Cohen, T., Que Hee, S.S., and Ambrose, R.F., 2001, Trace metals in Fish and Invertebrates of three California Coastal Wetlands: Marine Pollution Bulletin, v. 42, p. 224-232.

Columbia Analytical Services, 2011, GCMS-SIM: http://www.caslab.com/News/gcms-full-scan-vs-cgms-sim.html (accessed September, 2011).

Dzombak, D. A., and Luthy, R. G., 1984, Estimating adsorption of polycyclic aromatic hydrocarbons on Soils: Soil Science, v. 137, p. 5-12.

Drever, J., 1997, The Geochemistry of Natural Waters; Surface and Groundwater Environments: 2nd Ed. Prentice Hall, Upper Saddle River, New Jersey, 436 pp.

Environmental Protection Agency, 2000, EPA Fact Sheet: http://www.epa.gov/safewater /arsenic/regulations_techfactsheet.html (accessed October, 2010).

The Examiner News, 2010, Gulf oil spill: http://www.examiner.com/environmental-news-in-national/gulf-oil-spill-update- noaa-forecast-oil-on-pointe-aux-chenes-waveland-pass-christian-pictures. (accessed October, 2010).

Folk, R.L., 2005, Nannobacteria and the formation of framboidal pyrite; Textual evidence: Journal of Earth Systems Science, v. 114, p. 369-374.

Freeze, R.A., and Cherry, J.A., 1978, Groundwater: Prentice-Hall, Englewood Cliffs, New Jersey, 604 pp.

Griffin, J.R., 2000, Reactive transport of solutes and isotopes in the Eutaw aquifer, western Alabama. [M.S. Thesis]: Auburn University, 75 pp.

Haeselera, F., Behar, F., Garnier, D., and Chenet, P., 2010, First stoichiometric model of oil biodegradation in natural petroleum systems: Part I – The BioClass 0D approach: Organic Geochemistry, v. 41, p. 1156-1170.

Hammer, D., 2010, Tar balls reach Lake Pontchartrain: http://search.nola.com /David+hammer/5/?date_range=all (accessed December, 2011).

Hammerschmidt, C.R., Fitzgerald, W. F., Lamborg, C.H., Balcom, P. H., and Visscher, P.T., 2004, Biogeochemistry of methylmercury in sediments of Long Island Sound: Marine Chemistry, v. 90, p. 31-52.

Huerta-Diaz, M., and Morse, J., 1992, Pyritization of trace metals in anoxic marine sediments: Geochimica et Cosmochimica Acta, v.56, p. 2681—2702.

Hollibaugh, J.T., Carini, S., Gürleyük, H., Jellison, R., Joye, S.B., LeCleir, G., Meile, C.,Vasquez, L., and Wallschläger, D., 2005, Arsenic speciation in Mono Lake, California; response to seasonal stratification and anoxia: Geochim. Cosmochim. Acta, v. 69, p. 1925–1937.

Islam, F., Gault, A., Polya, C., David, A., Charnock, D., Chatterjee, D., and Loyd, J., 2004, Adsorption of As(III) and As(V) onto vivianite; evaluation as a sink for arsenic in Bengali aquifers: Geochimica et Cosmochimica Acta, v. 71, p. 432.

Jackson, A., Pardue, J., and Araujo, R., 1996, Monitoring crude oil mineralization in salt marshes: Use of stable carbon isotope ratios: Environmental Science Technology, 1996, v. 30, p. 1139-1144.

Jobson, A., Cook, F.D., and Westlake, D.W.S., 1972, Microbial utilization of crude oil: Applied Microbiology, v. 23, p. 1082–1089.

Jong, T., and Parry, P., 2004, Adsorption of Pb(II), Cu(II), Cd(II), Zn(II), Ni(II), Fe(II), and As(V) on bacterially produced metal sulfides: Journal of Colloid and Interface Science, v. 275, p. 61-71.

Johnston, S.G., Keene, A., Bush, R., Burton, A., Sullivan, L., Isaacson, L., McElnea, A., Ahern, R., D., Smith, D., and Powell B., 2011, Iron geochemical zonation in a tidally inundated acid sulfate soil wetland: Chemical Geology, v. 280, p. 257–270.

Keevan, J., Natter, M., Lee, M.-K., Keimowitz, A., Okeke, B., Sarvda, C., and Saunders, J.A., 2011, Biogeochemical and hydrological controls on fate and distribution of trace metals in oiled Gulf salt marshes: AGU Annual Fall Meeting, San Francisco.

Keimowitz, A., Simpson, H., Stute, M., Data S., Chillrud, S., Ross, J., and Tsang, M., 2005, Naturally occurring arsenic: Mobilization at a landfill in Maine and Implications for remediation: Applied Geochemistry, v. 20, p. 1985-2002.

Kerin, E.J., Gilmour, C.C., Roden, E., Suzuki, M.T., Coates, J.D., and Mason, R.P., 2006, Mercury methylation by dissimilatory iron-reducing bacteria: Applied and Environmental Microbiology, v. 72, p. 7919-7921.

King, J., Harmon, S., Fu, T., and Gladden, J., 2002, Mercury Removal, Methylmercury Formation, and Sulfate–Reducing Bacteria in Wetland Mesocosms: Chemosphere, v. 46, p. 859-870.

Lee, M.-K., Saunders, J., and Wilkin, R., 2005, Geochemical modeling of arsenic speciation and mobilization: Implications for bioremediation: Advances in Arsenic Research, v. 915, p. 398 - 413.

Lee, M.-K., Griffin, J., Saunders, J.A., Wang, Y., and Jean, J., 2007, Reactive transport of trace elements and isotopes in Alabama coastal plain aquifers: Journal of Geophysical Research, v. 112, G02026.

Lee, M-K., 2011, Quarterly Interim Report of MESC BPGRI Grant : Assessing the Effects of Oil/Dispersant on Mobility and Biotransformation of Toxic Metals in Gulf Coastal Wetlands: Department of Geology and Geography, Auburn University.

Lonergan, D.J., Jenter, H.L., Coates, J.D., Phillips, E.J.P., Schmidt, T.M., and Lovley, D.R., 1996, Phylogenetic analysis of dissimilatory Fe (III)-reducing bacteria: Journal of Bacteriology, p. 2402-2408.

López, L., Mónaco, S., Galarraga, Lira, A., and Cruz, C., 1995, V/Ni ratio in maltene and asphaltene fractions of crude oils from the west Venezuelan basin: correlation studies: Chemical Geology, v. 119, p. 255-262.

López, L., Mónaco, S., and Richardson, M., 1998, Use of molecular parameters and trace elements in oil-oil correlation studies, Barinas sub-basin, Venezuela: Organic Geochemistry, v. 29, p. 613-629.

Lovley, D.R., and Chapelle, F.H..,1995, Deep subsurface microbial processes: Reviews of Geophysics, v. 33, p. 365-381.

Macko, S., and Parker, P., 1983, Stable nitrogen and carbon isotope ratios of beach tars on south Texas barrier island: Marine Environmental Resources, v.10, p. 93-103.

Madigan, M., Martinko, J., and Parker, J., 1997, Brock Biology of Microorganisms: Eighth Ed. Prentice Hall, Upper Saddle River, New Jersey, 986 pp.

Mason, R., Fitzgerald, W., and Morel, F., 1994, The biogeochemical cycling of elemental mercury; anthropogenic influences: Geochimica et Cosmochimica Acta, v. 58, p. 3191-3198.

Mason, R., Lawson, N., Lawrence, A., Leaner, J., Lee, J., and Sheu, G., 1999, Mercury in the Chesapeake Bay: Marine Chemistry v. 65, p. 77-96.

Merritt, K. A., and Amirbahman, A., 2009, Mercury methylation dynamics in estuarine and coastal marine environments — A critical review: Earth Science Reviews, v. 96, p. 54-66.

Monrreal, R.H., 2007, Hydrology and Water Chemistry in Weeks Bay, Alabama: Implications of Mercury Bioaccumalation [M.S. Thesis]: Auburn University, 65 p.p.

Morrison, R. and Murphy, B., 2006, Environmental Forensics: Elsevier Publishing. Boston, Ma. p. 340-429.

McArthur, J. M., Banerjee, D.M., Hudson-Edwards, K.A., Mishra, R., Purohit, R., Ravenscroft, P., Cronin, A., Howarth, R.J., Chatterjee, A., Talukder, T., Lowry, D., Houghton, S., and Cadha, D.K., 2004, Natural organic matter in sedimentary basins and its relation to arsenic in anoxic ground water: The example of West Bengal and its worldwide implications: Applied Geochemistry, v. 19, p. 1255–1293.

National Research Council, 1993, In situ bioremediation--When does it work?: Washington, D.C., National Academies Press, v.17, 224 p.p.

Nickson, R.T., McArthur, J.M., Burgess, W.G., Ahmed, K.M., Ravenscroft, P., and Rahman, M., 1998, Arsenic poisoning of Bangladesh groundwater: Nature, v.395 p. 338-389.

Nickson, R. T., McArthur, J.M., Ravenscroft, P., Burgess, W.G., and Ahmed, K.M., 2000, Mechanism of arsenic release to groundwater, Bangladesh and West Bengal: Applied Geochemistry, v.15, p. 403– 413.

Oudot, J., and Chaillan, F., 2010, Pyrolysis of asphaltenes and biomarkers for the fingerprinting of the amico cadiz oil spill after 23 years: Comptes Rendus Chimie, v.13, p. 548–552.

Park, J., Sanford, R.A., and Bethke ,C.M., 2006, Geochemical and microbiological zonation of the Middendorf aquifer, South Carolina: Chemical Geolology, v. 230, p. 88-104.

Planer-Friedrich, B., and Wallschläger, D., 2009, A critical investigation of hydride generation-based arsenic speciation in sulfidic waters: Environmental Science and Technology, v. 43, p. 5007–5013.

Peters K.E., Moldowan, J.M., Schoell, M., and Hempkins, W.B., 1986, Petroleum isotopic and biomarker composition related to source rock organic matter and depositional environment: Advances in Organic Geochemistry, v. 10, p. 17–27.

Peters, K.E., and Moldowan, J.M., 1991, Effects of source, thermal maturity and biodegradation on the distribution and isomerization of homohopanes in petroleum: Organic Geochemistry, v. 17, p. 47–61.

Peters, K.E., Walters, C.C., and Moldowan, J.M., 2005, The Biomarker Guide. Volume 1, Biomarkers and Isotopes in the Environment and Human History: Cambridge University Press, 1132 p.p.

Ravenschlag, K., Sahm, K., Knoblauch, C., Jorgensen, B.B., and Amann, R., 2000, Community structure, cellular rRNA content, and activity of sulfate-reducing bacteria in marine arctic sediments: Applied Environmental Microbiology, v. 66, p. 3592-3602.

Rittmann, B., and P. McCarty, 2001, Environmental Biotechnology: Mcgraw-Hill Publishing, Boston, Massachusetts, p. 2-78.

Roychoudhury, A.N., Kostka, J.E., and Van-Cappellen, P., 2003, Pyritization: a palaeoenvironmental and redox proxy reevaluated: Estuarine, Coastal and Shelf Science, v. 57, p. 1183-1193.

Rosenbauer, R. J., 2010, Reconnaissance of Macondo-1 well oil in sediment and tarballs from the northern Gulf of Mexico shoreline, Texas to Florida, U. S. Geological Survey- Open File Report 0196-1497, 22 p.p.

Saunders, J.A., Lee, M-K., Wolf, L.A., Morton, C.M., Feng, Y., Thomson, I., and Park, S., 2005, Geochemical, microbiological, and geophysical assessments of anaerobic immobilization of heavy metals: Bioremediation Journal, v. 9, p. 33–48.

Saunders, J.A., Lee, M.K., Shamsudduha, M., Dhakal, P., Uddin, A., Chowdury, M.T., and Ahmed, K.M., 2008, Gochemistry and mineralogy of arsenic in (natural) anaerobic groundwaters: Applied Geochemistry, v. 23, p. 3205-3214.

Shmonova, N.I., and Shaks, I.A., 1971, Alteration of the asphalt-tar fractions of petroleum under the effect of micro-organisms under aerobic and anaerobic conditions: Vses. Neft. Nauchno-Issled. Geologorazved. Inst., Tr., v. 294, p. 4–19.

Schuster, P.F., Shanley, J.B., Marvin-Dipasquale, M., Reddy, M.M., Aiken, G.R., Roth, D.A., Taylor, H.E., Krabbenhoft D,P, and DeWild J.F., 2008, Mercury and organic carbon dynamics during runoff episodes from a northeastern USA watershed: Water, Air, & Soil Pollution, v.187 p. 89-108.

Smedley, P.L. and Kinniburgh,D.G., 2002, A review of the source, behavior and distribution of arsenic in natural waters: Applied Geochemistry, v.17, p. 517-568.

Stahl, W., 1977, Carbon and nitrogen isotopes in hydrocarbon research and exploration: Chemical Geology, v. 20, p. 121-149.

Straub, K. L., Benz, M., and Schink, B., 2000, Iron metabolism in anoxic environments at near neutral pH: FEMS Microbiology Ecology, v. 34, p. 181-186.

Sunderland, E. M., F. A. P. C. Gobas, A. Heyes, B. A. Branfireun, A. K. Bayer, R. E. Cranston, and Parsons, M.B., 2004, Speciation and Bioavailability of Mercury in Well-Mixed Estuarine Sediments: Marine Chemistry, v. 90, p. 91-105.

Ullricha, M.S., Tantona, T.W., and Abdrashitova, S.A., 2001, Mercury in the Aquatic Environment: A Review of Factors Affecting Methylation: Critical Reviews in Environmental Science and Technology, v. 31, p. 241-293.

United States Department of the Interior, 2010, Flow Rate Technical Group: http://www.doi.gov/news/pressreleases/Flow-Rate-Group-Provides- Preliminary-Best-Estimate-Of-Oil-Flowing-from-BP-Oil-Well.cfm (accessed October, 2010).

United States Geological Survey, 2000, USGS Fact Sheet 146: http://www.usgs.gov/themes /factsheet/146-00/ (accessed October 2010).

Wang, Z., Fingas,M., and Page,D., 1999, Oil spill identification: Journal of Chromatography, v. 843, p. 369-411.

Wang, Z. and Stout, S., 2007, Oil Spill Environmental Forensics Fingerprinting and Source Identification: Elsevier Publishing. Boston, Massachusetts, p. 1-146.

Welch, A., Lico, M., and Hughes, J., 1988, Arsenic in ground water of the western United States: Ground Water, v. 26, p. 333-347.

Westrich, J,T., and Berner, R.A., 1984, The role of sedimentary organic matter in bacterial sulfate reduction: the G model tested: Limnology and Oceanography, v. 29, p. 236–249.

Wilkin, R. T., Barnes, H. L., and Brantley, S. L.,1996, The size distribution of framboidal pyrite in modern sediments: an indicator of redox conditions: Geochimica et Cosmochimica Acta vol. 60, p. 3897–3912.

Wollast, R., 1991, The coastal organic carbon cycle: Fluxes, sources, and sinks: Mantoura, R.C.E. (Eds.), Ocean Margin Processes in Global Change: John Wiley and Sons Inc., New York, New York, p. 365-382.

APPENDIX 1

Appendix 1a. Surface water chemistry from locations within Weeks Bay, AL taken at water surface level, reported by Monrreal (2007).

Site ID	Latitude	Longitude	pH	Conduct. (µS/cm)	ORP (mV)	DO (µg/L)	Temp (°C)
WB-1	30.4133	-87.8255	6.47	909	540	5950	30.93
WB-2	30.4095	-87.8266	6.41	942.6	609	5020	31.65
WB-3	30.3769	-87.8358	8.49	5700	533	6700	32.82
WB-4	30.3829	-87.8348	8.6	5522	467	7394	32.89
WB-5	30.3904	-87.8331	8.77	5174	493	8100	33.56
WB-6	30.3981	-87.8306	8.43	2715	384	6360	33.02
WB-7	30.4029	-87.8287	6.28	300	488	4455	31.5
WB-8	30.4008	-87.8296	6.6	1311	518	5498	32.16
WB-9	30.4072	-87.8274	6.38	204	502	6233	32.17
WB-10	30.3896	-87.8162	7	3000	457	5038	32
WB-11	30.3922	-87.8201	8.09	3975	432	6330	32.66
WB-12	30.3932	-87.8247	8.62	4002	381	7360	32.6
WB-13	30.3939	-87.8291	8.66	5136	365	6110	33.17
WB-14	30.3953	-87.8368	8.3	2340	356	6658	32.66
WB-15	30.3969	-87.8418	8.06	1865	361	7150	32.69
WB-16	30.3909	-87.8409	8.41	2880	344	6800	33.06
WB-17	30.3867	-87.8401	8.75	3350	327	7356	33.22
WB-18	30.383	-87.8389	8.79	3255	324	7746	33.22
WB-19	30.3784	-87.8371	8.8	3436	330	7815	33.25
WB-20	30.4012	-87.8374	8.19	2108	290	7255	33.63
WB-21	30.4067	-87.8342	6.69	560	386	5369	32.72
FISH-6	30.436	-87.8126	6.98	69.26	447	9500	31.83
FISH-7	30.4356	-87.8175	6.82	76.5	454	9540	31.65
FISH-8	30.4313	-87.8237	6.83	98.3	443	9140	32.17
FISH-9	30.4275	-87.8286	6.61	105.2	444	8600	31.97
FISH-10	30.4241	-87.8248	6.7	123.3	441	8659	32.5
WW-13,14	30.4047	-87.8484	N/A	N/A	N/A	N/A	N/A
WW-15,16	30.3987	-87.8455	N/A	N/A	N/A	N/A	N/A
WBSC	30.4125	-87.8307	8.3	>2000ppm	189	8000	22.8

Appendix 1b. Surface water chemistry from locations within Weeks Bay, AL taken at 1 meter depth, reported by Monrreal (2007).

Site ID	Latitude	Longitude	pH	Conduct. (µS/cm)	ORP (mV)	DO (µg/L)	Temp (°C)
WB-1	30.4133	-87.8255	6.3	950	632	7125	30.16
WB-2	30.4095	-87.8266	5.99	219	646	2930	27.8
WB-3	30.3769	-87.8358	8.45	5444	588	6900	32.76
WB-4	30.3829	-87.8348	8.5	5706	518	6790	32.36
WB-5	30.3904	-87.8331	8.58	5630	515	7080	32.13
WB-6	30.3981	-87.8306	8.29	5147	361	5879	31.89
WB-7	30.4029	-87.8287	7.19	2800	455	6031	31.24
WB-8	30.4008	-87.8296	8.45	4235	344	6220	31.81
WB-9	30.4072	-87.8274	6.06	217	541	3970	28.71
WB-10	30.3896	-87.8162	7.19	3254	455	3254	31.7
WB-11	30.3922	-87.8201	7.8	4296	437	5537	32.19
WB-12	30.3932	-87.8247	8.28	4616	414	5357	32.25
WB-13	30.3939	-87.8291	8.36	5442	370	5388	32.43
WB-14	30.3953	-87.8368	8.23	4860	404	5224	32.4
WB-15	30.3969	-87.8418	7.8	3985	422	5256	32.18
WB-16	30.3909	-87.8409	8.18	3981	397	6057	32.1
WB-17	30.3867	-87.8401	8.28	4980	400	5241	32.1
WB-18	30.3830	-87.8389	8.25	5056	387	5572	32.08
WB-19	30.3784	-87.8371	8.4	5636	394	5942	32.38
WB-20	30.4012	-87.8374	7.92	3676	346	5543	32.45
WB-21	30.4067	-87.8342	6.64	1180	402	4193	30.5
FISH-6	30.4360	-87.8126	6.27	64.15	530	7795	28.81
FISH-7	30.4356	-87.8175	6.65	72.27	489	9440	30.11
FISH-8	30.4313	-87.8237	6.6	102.5	477	9000	31.43
FISH-9	30.4275	-87.8286	6.36	88.22	521	8058	30.18
FISH-10	30.4241	-87.8248	6.6	123.3	496	8600	31.71
WW-13,14	30.4047	-87.8484	N/A	N/A	N/A	N/A	N/A
WW-15,16	30.3987	-87.8455	N/A	N/A	N/A	N/A	N/A
WBSC	30.4125	-87.8307	8.3	>2000ppm	189	8000	22.8

Appendix 1c. Surface water chemistry from locations within Wolf Bay, AL taken at water surface level, reported by Beasley (2010).

Site ID	Latitude	Longitude	pH	Conduct. (µS/cm)	ORP (mV)	DO (µg/L)	Temp. (°C)
Wolf-1	30.3018	-87.5750	7.92	36050	161	5692	31.72
Wolf-2	30.3016	-87.5850	7.93	35000	176	6644	31.2
Wolf-3	30.3015	-87.5891	7.9	34220	71	7130	30.15
Wolf-4	30.3019	-87.5995	7.8	32990	69	6972	30.27
Wolf-5	30.3049	-87.5992	7.8	34360	26	7090	30.6
Wolf-6	30.3054	-87.5940	7.79	34810	48	7149	31.65
Wolf-7	30.3058	-87.5872	7.81	35090	66	7151	29.86
Wolf-8	30.3057	-87.5824	7.74	34530	73	7568	29.05
Wolf-9	30.3102	-87.5824	7.8	34590	81	7095	30.75
Wolf-10	30.3102	-87.5863	7.75	35190	86	7122	30.88
Wolf-11	30.3098	-87.5923	7.82	35030	103	6730	30.64
Wolf-12	30.3097	-87.5950	7.75	34780	102	7025	30.21
Wolf-13	30.3147	-87.5927	7.62	34840	121	7023	28.36
Wolf-14	30.3156	-87.5892	7.65	34330	116	7110	29.54
Wolf-15	30.3166	-87.5841	7.66	34120	125	6791	28.92
Wolf-16	30.3238	-87.5858	7.5	34380	121	7228	27.27
Wolf-17	30.3239	-87.5895	7.67	32780	127	6329	30.43
Wolf-18	30.3233	-87.5939	7.74	32680	123	7160	28.35
Wolf-19	30.3277	-87.5983	7.73	32750	81	6977	29.67
Wolf-20	30.3295	-87.5908	7.78	32910	119	6937	29.58
Wolf-21	30.3342	-87.5818	7.76	34070	121	6203	29.73
Wolf-22	30.3345	-87.5787	7.79	34060	131	6362	27.59
Wolf-23	30.3412	-87.5810	7.75	33570	104	6928	27.41
Wolf-24	30.34	-87.5824	7.74	33800	112	7060	28.16
Wolf-25	30.3376	-87.5841	7.72	33790	-23	6766	29.44
Wolf-26	30.334	-87.5892	7.61	33580	60	5587	27.47
Wolf-27	30.3334	-87.5919	7.66	33080	94	6866	29.48
Wolf-28	30.3363	-87.5983	7.58	29420	97	7777	29.81
Wolf-29	30.3379	-87.5982	7.59	29200	106	6750	27.81
Wolf-30	30.3408	-87.6032	7.6	23660	97	6772	29.72
Wolf-31	30.3451	-87.6012	7.55	22980	114	7463	29.98
LBSC	30.308	-87.6230	7.03	>2000ppm	196	6980	25.3

Appendix 1d. Surface water chemistry from locations within Wolf Bay, AL taken at 1 meter depth, reported by Beasley (2010).

Site ID	Latitude	Longitude	pH	Conduct. (µS/cm)	ORP (mV)	DO (µg/L)	Temp. (°C)
Wolf-1	30.3018	-87.5750	8.3	37090	160	4973	31.43
Wolf-2	30.3016	-87.5850	8.31	37970	175	5431	30.76
Wolf-3	30.3015	-87.5891	8.42	34940	74	3704	30.32
Wolf-4	30.3019	-87.5995	8.05	34130	70	4550	31.17
Wolf-5	30.3049	-87.5992	8.85	34380	29	6453	30.18
Wolf-6	30.3054	-87.5940	8.79	35100	52	5458	30.12
Wolf-7	30.3058	-87.5872	8.08	35310	68	5101	30.71
Wolf-8	30.3057	-87.5824	7.87	34670	74	5594	30.23
Wolf-9	30.3102	-87.5824	7.91	35070	82	6040	30.88
Wolf-10	30.3102	-87.5863	7.74	35240	86	7208	30.33
Wolf-11	30.3098	-87.5923	7.9	35090	103	6484	30.58
Wolf-12	30.3097	-87.5950	7.85	34750	102	6568	29.97
Wolf-13	30.3147	-87.5927	7.52	34910	121	6724	30.03
Wolf-14	30.3156	-87.5892	7.44	34860	116	7700	29.98
Wolf-15	30.3166	-87.5841	7.64	35070	123	5791	29.93
Wolf-16	30.3238	-87.5858	7.64	34230	119	7054	30.36
Wolf-17	30.3239	-87.5895	7.55	33920	126	7324	30.07
Wolf-18	30.3233	-87.5939	7.4	33220	123	7305	29.88
Wolf-19	30.3277	-87.5983	7.42	33410	83	7314	29.79
Wolf-20	30.3295	-87.5908	7.92	34550	119	5872	29.83
Wolf-21	30.3342	-87.5818	7.05	33640	120	5784	29.71
Wolf-22	30.3345	-87.5787	7.91	33740	131	5852	29.82
Wolf-23	30.3412	-87.5810	7.61	33540	106	7129	29.86
Wolf-24	30.34	-87.5824	7.08	33740	113	6189	29.79
Wolf-25	30.3376	-87.5841	7.09	33740	-14	5163	29.78
Wolf-26	30.334	-87.5892	7.12	33790	62	4864	29.65
Wolf-27	30.3334	-87.5919	7.1	33820	94	7012	29.52
Wolf-28	30.3363	-87.5983	7.08	33640	101	9492	29.72
Wolf-29	30.3379	-87.5982	7.02	33080	109	8734	29.8
Wolf-30	30.3408	-87.6032	6.9	31800	104	11181	29.76
Wolf-31	30.3451	-87.6012	6.93	32800	122	11093	29.98
LBSC	30.308	-87.6230	7.03	>2000ppm	196	6980	25.3

APPENDIX 2

Appendix 2. Dissolved organic carbon, dissolved reduced Fe and sulfide contents of pore waters.

Sample ID	Sediment depth (cm)	Pore-water DOC (mg/kg)	Pore-water Fe (mg/kg)	Pore-water sulfide (mg/kg)
WB	0-3	38.19	-	-
WB	3-6	30.80	-	.002
WB	6-9	70.80	-	-
WB	9-12	64.88	0.09	.100
WB	12-15	46.77	-	-
WB	15-18	35.54	0.05	-
WB	18-21	38.80	0.07	-
WB	21-24	37.12	0.03	-
WB	24-27	32.62	-	-
WB	27-30	36.80	0.13	-
LB	0-3	19.88	-	-
LB	3-6	0.60	0.25	.080
LB	6-9	0.55	-	-
LB	9-12	26.30	0.36	.690
LB	12-15	12.90	-	-
LB	15-18	14.45	-	-
LB	18-21	1.92	-	-
LB	21-24	14.63	-	-
LB	24-27	0.16	-	-
LB	27-30	13.40	-	-
WI	0-3	0.21	-	-
WI	3-6	31.54	0.61	.003
WI	6-9	54.62	-	-
WI	9-12	25.83	0.62	.787
WI	12-15	26.91	-	-
WI	15-18	18.94	-	-
WI	18-21	-	-	-
WI	21-24	-	-	-
WI	24-27	-	-	-
WI	27-30	-	-	-
BH	0-3	16.19	0.03	-
BH	3-6	19.56	0.03	-
BH	6-9	12.06	0.01	-
BH	9-12	18.27	0.02	-
BH	12-15	13.08	0.01	-

BH	15-18	24.98	0.02	-
BH	18-21	19.65	0.01	-
BH	21-24	20.20	0.02	-
BH	24-27	22.86	0.01	-
BH	27-30	-	0.03	-
PACB	0-3	37.86	0.02	-
PACB	3-6	31.60	0.02	-
PACB	6-9	27.62	0.01	-
PACB	9-12	15.66	0.03	-
PACB	12-15	26.19	0.01	-
PACB	15-18	0.25	0.02	-
PACB	18-21	0.53	0.01	-
PACB	21-24	11.22	0.04	-
PACB	24-27	10.24	0.01	-
PACB	27-30	0.35	-	-
RG	0-3	35.74	-	.030
RG	3-6	48.67	0.01	-
RG	6-9	61.06	0.02	-
RG	9-12	56.56	0.02	-
RG	12-15	96.19	0.02	-
RG	15-18	112.60	-	-
RG	18-21	122.90	-	-
RG	21-24	142.90	-	-
RG	24-27	162.50	-	-
RG	27-30	173.00	0.01	8.86
BD	0-3	79.03	0.02	.003
BD	3-6	185.80	0.01	4.40
BD	6-9	234.00	0.01	-
BD	9-12	231.70	0.02	23.52
BD	12-15	224.40	0.01	28.96
BD	15-18	225.40	0.01	41.84
BD	18-21	229.80	0.02	58.68
BD	21-24	234.70	0.01	53.60
BD	24-27	227.30	0.01	46.00
BD	27-30	225.80	0.02	-
BB	0-3	69.40	0.03	41.50
BB	3-6	134.10	0.03	19.48
BB	6-9	148.40	0.01	26.92
BB	9-12	50.03	0.02	33.08
BB	12-15	213.80	0.01	32.96
BB	15-18	334.20	0.02	41.28
BB	18-21	361.10	0.01	44.64
BB	21-24	253.70	0.02	48.00
BB	24-27	226.00	0.01	49.20
BB	27-30	102.80	0.03	30.80
BJN	0-3	85.07	0.02	.270

BJN	3-6	182.40	0.01	4.82
BJN	6-9	239.50	0.01	20.12
BJN	9-12	137.90	0.02	35.34
BJN	12-15	234.40	0.01	54.24
BJN	15-18	269.40	0.01	50.80
BJN	18-21	108.20	0.02	69.10
BJN	21-24	75.42	0.01	65.10
BJN	24-27	308.00	0.01	70.40
BJN	27-30	391.10	0.02	82.80
BJS	0-3	69.63	0.03	.010
BJS	3-6	109.30	0.03	.240
BJS	6-9	142.20	0.01	4.62
BJS	9-12	188.70	0.02	6.32
BJS	12-15	231.40	0.01	9.12
BJS	15-18	274.00	0.02	7.52
BJS	18-21	308.40	0.01	8.32
BJS	21-24	334.20	0.02	6.64
BJS	24-27	279.90	0.01	4.06
BJS	27-30	346.90	0.03	2.78

APPENDIX 3

Appendix 3. Selected major ion and trace-metal concentrations in pore waters from WB and LB sites. Core sampling locations are shown in Figure 1**.**

Weeks Bay														
Depth cm	Tot-Hg ng/kg	Me-Hg ng/kg	Cl g/kg	SO_4^{2-} g/kg	NO_3^- mg/kg	NH_4 mg/kg	Na g/kg	K mg/kg	Mg mg/kg	Ca mg/kg	Mn µg/kg	Fe µg/kg	As µg/kg	Tot S mg/kg
0-3	8.30	-	6.70	0.54	-	-	2.98	95	354	92	2985	108	25.82	189
3-6	4.30	0.15	6.28	0.26	-	-	2.79	89	282	83	2244	70	9.58	110
6-9	0.49	-	5.18	0.15	-	-	2.40	74	231	69	1347	62	3.06	34
9-12	4.24	1.09	4.61	0.07	-	-	2.01	63	209	73	1441	384	8.46	48
12-15	2.80	-	4.81	0.08	-	28.90	2.03	61	227	39	1620	171	5.98	22
15-18	0.00	-	4.20	0.07	0.98	24.71	1.80	61	174	38	1534	236	8.03	19
18-21	2.48	-	6.62	0.18	-	32.79	2.84	95	325	124	1406	132	4.88	20
21-24	5.47	3.52	4.58	0.15	1.22	-	2.07	76	191	56	1308	29	4.95	48
24-27	1.93	-	4.08	0.13	-	-	1.84	62	155	356	1314	43	5.34	65
27-30	1.85	-	4.49	0.18	-	-	2.17	59	174	63	1275	38	6.28	89

Wolf Bay														
Depth cm	Tot-Hg ng/kg	Me-Hg ng/kg	Cl g/kg	SO_4^{2-} g/kg	NO_3^- mg/kg	NH_4 mg/kg	Na g/kg	K mg/kg	Mg mg/kg	Ca mg/kg	Mn µg/kg	Fe µg/kg	As µg/kg	Tot S mg/kg
0-3	2.50	1.03	-	-	-	-	-	-	-	-	-	-	-	-
3-6	2.03	-	14.81	1.83	-	-	6.68	224	837	262	524	100	2.95	573
6-9	1.08	<0.06	12.20	-	-	-	-	-	-	-	217	28	3.43	473
9-12	0.58	-	13.09	1.51	-	-	6.45	211	1025	254	180	75	4.49	283
12-15	0.55	-	15.45	1.85	-	-	7.17	240	886	278	148	27	9.91	143
15-18	2.42	-	15.32	1.83	-	-	7.44	246	905	285	142	64	5.33	235
18-21	2.43	-	14.83	1.70	-	-	6.81	233	829	260	96	46	13.04	427
21-24	2.84	-	-	-	-	-	-	-	-	-	23	206	1.28	-
24-27	1.88	-	-	-	-	-	-	-	-	-	21	206	2.35	-
27-30	2.34	-	-	-	-	-	-	-	-	-	32	117	2.08	-

APPENDIX 4

Appendix 4. Sediment total organic carbon contents (TOC) and carbon isotopic compositions of bulk sediments, marsh plants, oil scrapped off the oiled plants, and BP MC-252 oil.

Sample ID	Sample depth(cm)	TOC sed(%)	$\delta^{13}C$ $sed_{(PDB)}$	$\delta^{13}C$ $juncus_{(PDB)}$	$\delta^{13}C$ $spartina_{(PDB)}$	$\delta^{13}C$ $oil_{(PDB)}$
WB	plant	-	-	-27.6		
WB	0-3	2.230	-25.9			
WB	3-6	2.290	-25.5			
WB	6-9	1.830	-25.3			
WB	9-12	2.240	-25.4			
WB	12-15	2.190	-25.4			
WB	15-18	1.970	-25.3			
WB	18-21	1.770	-25.3			
WB	21-24	2.330	-25.2			
WB	24-27	1.770	-25.4			
WB	27-30	1.770	-25.4			
LB	plant	-	-	-24.1		
LB	0-3	1.980	-26.1			
LB	3-6	2.220	-26.3			
LB	6-9	2.060	-26.0			
LB	9-12	1.930	-25.9			
LB	12-15	1.850	-26.1			
LB	15-18	1.720	-25.8			
LB	18-21	1.100	-26.3			
LB	21-24	1.320	-26.0			
LB	24-27	1.390	-26.1			
LB	27-30	2.000	-26.1			
WI	plant	-	-		-15.0	
WI	0-3	2.720	-23.6			
WI	3-6	2.990	-22.6			
WI	6-9	3.030	-21.7			
WI	9-12	2.660	-21.9			
WI	12-15	1.910	-21.4			
WI	15-18	2.220	-21.6			
WI	18-21	1.390	-21.9			
WI	21-24	1.470	-22.7			
WI	24-27	1.760	-22.0			
WI	27-30	2.500	-23.4			
BH	plant	-	-	-25.2	-14.5	

BH	0-3	1.730	-24.0	
BH	3-6	2.040	-23.9	
BH	6-9	1.940	-23.5	
BH	9-12	2.120	-23.1	
BH	12-15	2.180	-23.9	
BH	15-18	1.710	-24.6	
BH	18-21	1.460	-25.0	
BH	21-24	1.490	-25.2	
BH	24-27	1.460	-25.8	
BH	27-30	1.420	-26.3	
PACB	plant	-	-	-14.1
PACB	0-3	0.323	-21.1	
PACB	3-6	0.697	-20.1	
PACB	6-9	0.598	-19.4	
PACB	9-12	0.811	-19.6	
PACB	12-15	0.909	-19.7	
PACB	15-18	0.985	-20.8	
PACB	18-21	0.835	-23.3	
PACB	21-24	1.120	-23.7	
PACB	24-27	0.831	-24.2	
PACB	27-30	0.818	-24.8	
RG	plant	-	-	-14.4
RG	0-3	1.010	-22.7	
RG	3-6	1.110	-23.1	
RG	6-9	1.200	-24.0	
RG	9-12	1.050	-23.6	
RG	12-15	1.940	-23.5	
RG	15-18	2.190	-20.2	
RG	18-21	1.690	-19.9	
RG	21-24	1.400	-18.5	
RG	24-27	1.580	-19.9	
RG	27-30	1.680	-19.9	
BD	plant	-	-	-15.1
BD	0-3	4.530	-19.4	
BD	3-6	21.500	-20.3	
BD	6-9	28.900	-21.1	
BD	9-12	19.800	-20.6	
BD	12-15	24.400	-19.7	
BD	15-18	19.200	-20.5	
BD	18-21	19.000	-19.6	
BD	21-24	18.600	-19.2	
BD	24-27	20.280	-18.6	
BD	27-30	22.350	-17.3	
BB	plant	-	-	-15.6
BB	0-3	6.790	-18.9	
BB	3-6	11.100	-20.3	
BB	6-9	10.700	-20.5	

BB	9-12	11.700	-19.8			
BB	12-15	13.600	-19.7			
BB	15-18	9.370	-18.2			
BB	18-21	4.270	-18.9			
BB	21-24	8.840	-17.4			
BB	24-27	9.160	-17.9			
BB	27-30	9.350	-17.8			
BJN	plant	-	-	-27.1	-14.7	-26.7
BJN	0-3	7.810	-18.2			
BJN	3-6	5.090	-18.0			
BJN	6-9	10.100	-18.1			
BJN	9-12	7.720	-18.7			
BJN	12-15	6.820	-18.2			
BJN	15-18	6.780	-18.3			
BJN	18-21	4.120	-18.4			
BJN	21-24	4.370	-18.8			
BJN	24-27	4.010	-17.6			
BJN	27-30	14.090	-18.3			
BJS	plant	-	-	-24.2	-14.3	-26.7
BJS	0-3	6.270	-22.2			
BJS	3-6	9.720	-22.6			
BJS	6-9	5.330	-22.1			
BJS	9-12	16.200	-21.2			
BJS	12-15	14.700	-20.7			
BJS	15-18	10.300	-20.0			
BJS	18-21	9.720	-19.3			
BJS	21-24	7.010	-19.7			
BJS	24-27	6.820	-18.7			
BJS	27-30	4.500	-18.9			
MC 252	Crude					27.1

APPENDIX 5

Appendix 5a. Grain-size distribution (weight percent) in 0-3 cm sediment samples.

Phi Size 0-3 cm	WB %	LB %	WI %	BH %	PACB %	RG %	BD %	BB %	BJN %	BJS %
<-1 phi	0.00	0.00	0.20	0.00	0.00	0.00	0.00	0.00	0.00	0.00
-1 to 0 phi	0.00	0.00	0.23	2.26	0.00	0.00	0.00	0.00	0.00	0.00
0 to 1 phi	0.00	0.15	4.96	0.55	0.05	0.00	0.00	0.00	0.00	0.00
1 to 2 phi	0.00	1.13	47.68	2.48	10.67	0.06	0.00	0.00	0.00	0.00
2 to 3 phi	0.00	23.41	29.06	14.75	33.60	23.51	0.00	0.00	0.00	0.00
3 to 4 phi	0.00	49.90	5.79	15.71	18.83	33.11	0.00	0.00	0.00	0.00
4 to 5 phi	3.32	5.95	1.14	9.56	8.32	22.44	7.29	19.77	22.56	30.81
5 to 6 phi	13.74	2.93	0.97	13.98	5.95	3.17	15.63	18.22	15.15	18.02
6 to 7 phi	22.75	3.21	2.11	8.22	4.50	6.05	30.21	21.71	13.47	13.95
7 to 8 phi	7.58	1.70	2.47	7.36	3.51	1.58	12.50	11.24	13.80	9.88
8 to 9 phi	6.64	2.08	1.23	6.01	1.60	1.58	4.69	5.04	2.36	4.65
9 to 10 phi	9.48	1.42	1.23	2.82	1.37	2.70	7.29	8.53	10.10	7.85
> 10 phi	36.49	7.46	2.38	16.19	11.06	5.77	22.40	15.50	22.56	14.83

Appendix 5b. Grain-size distribution (weight percent) in 12-15 cm sediment samples.

Phi Size 12-15 cm	WB %	LB %	WI %	BH %	PACB %	RG %	BD %	BB %	BJN %	BJS %
<-1 phi	0.00	0.00	0.00	0.00	0.00	0.00	0.00	0.00	0.00	0.00
-1 to 0 phi	0.00	0.02	0.09	0.00	0.00	0.00	0.00	0.00	0.00	0.00
0 to 1 phi	0.00	0.51	5.88	0.24	0.35	0.12	0.00	0.00	0.00	0.00
1 to 2 phi	0.00	1.11	56.28	3.30	11.76	0.41	0.00	0.00	0.00	0.00
2 to 3 phi	0.00	37.90	26.54	22.24	34.79	16.54	0.00	0.00	0.00	0.00
3 to 4 phi	0.00	43.63	3.92	21.89	9.02	30.46	0.00	0.00	0.00	0.00
4 to 5 phi	10.64	8.32	0.70	13.90	9.05	18.98	1.68	0.00	5.82	9.69
5 to 6 phi	14.01	1.00	0.70	10.25	8.28	9.24	7.56	3.79	9.84	23.35
6 to 7 phi	14.57	0.42	1.57	7.66	6.49	4.41	26.89	27.96	6.22	18.50
7 to 8 phi	11.48	1.16	0.52	4.54	3.93	3.25	20.17	23.22	12.45	13.22
8 to 9 phi	10.08	0.58	0.52	0.71	1.88	1.33	9.24	7.11	7.03	8.81
9 to 10 phi	4.76	0.83	1.30	1.96	3.59	4.08	9.24	9.00	11.65	7.05
> 10 phi	34.45	4.24	1.39	10.34	10.76	11.24	25.21	28.91	46.99	19.38

Appendix 5c. Grain-size distribution (weight percent) in 27-30 cm sediment samples.

Phi Size 27-30 cm	WB %	LB %	WI %	BH %	PACB %	RG %	BD %	BB %	BJN %	BJS %
<-1 phi	0.00	0.00	0.27	0.00	0.00	0.00	0.00	0.00	0.00	0.00
-1 to 0 phi	0.00	0.15	0.62	0.52	0.05	0.00	0.00	0.00	0.00	0.00
0 to 1 phi	0.00	0.76	6.92	1.08	0.66	0.00	0.00	0.00	0.00	0.00
1 to 2 phi	0.00	2.30	65.92	2.52	17.25	0.00	0.00	0.00	0.00	0.00
2 to 3 phi	0.00	34.56	16.30	11.49	45.64	0.00	0.00	0.00	0.00	0.00
3 to 4 phi	0.00	31.10	2.54	13.43	10.46	0.00	0.00	0.00	0.00	0.00
4 to 5 phi	3.91	4.88	2.87	19.19	6.91	3.75	4.51	1.64	4.05	21.86
5 to 6 phi	12.85	2.62	0.38	16.44	7.78	12.62	12.78	14.25	32.43	23.72
6 to 7 phi	15.92	4.25	0.38	10.46	4.07	24.46	11.65	16.71	45.27	13.26
7 to 8 phi	14.53	3.71	0.70	6.09	1.36	19.72	19.55	13.15	4.73	9.30
8 to 9 phi	14.53	2.35	0.32	7.31	1.73	7.50	9.02	10.96	0.68	5.35
9 to 10 phi	7.54	2.89	0.26	3.25	0.37	16.57	9.02	9.32	2.03	6.98
> 10 phi	30.73	10.22	2.43	8.22	3.70	15.38	33.46	33.97	10.81	19.53

APPENDIX 6

Appendix 6. Major ion compositions of coastal wetland sediments.

Sample ID	Sample depth (cm)	Fe %	K %	P %	Al %	S %	Ca %	Mg %	Na %
WB	0-3	3.400	0.25	0.043	2.090	1.670	0.160	0.450	0.791
WB	3-6	3.390	0.24	0.039	2.150	1.850	0.180	0.460	0.714
WB	6-9	3.270	0.26	0.034	2.170	1.860	0.180	0.530	1.007
WB	9-12	2.900	0.22	0.030	1.830	1.690	0.190	0.420	0.778
WB	12-15	2.930	0.20	0.027	1.970	1.860	0.200	0.400	0.502
WB	15-18	3.120	0.21	0.028	2.190	1.950	0.160	0.410	0.393
WB	18-21	2.940	0.19	0.024	1.930	1.870	0.140	0.370	0.275
WB	21-24	2.420	0.15	0.019	1.580	1.480	0.130	0.290	0.184
WB	24-27	2.570	0.17	0.020	1.600	1.440	0.130	0.340	0.190
WB	27-30	2.330	0.15	0.016	1.180	1.430	0.110	0.320	0.168
LB	0-3	0.250	0.04	0.003	0.310	0.290	0.600	0.100	0.428
LB	3-6	0.220	0.04	0.001	0.320	0.250	0.050	0.090	0.348
LB	6-9	0.240	0.03	0.002	0.300	0.300	0.050	0.070	0.247
LB	9-12	0.280	0.04	0.001	0.340	0.320	0.040	0.070	0.271
LB	12-15	0.430	0.04	0.001	0.370	0.510	0.040	0.080	0.283
LB	15-18	0.310	0.02	0.001	0.210	0.420	0.030	0.050	0.196
LB	18-21	0.460	0.04	0.001	0.370	0.590	0.040	0.080	0.212
LB	21-24	0.420	0.03	0.001	0.310	0.540	0.030	0.080	0.220
LB	24-27	0.430	0.03	0.001	0.250	0.550	0.030	0.060	0.187
LB	27-30	0.620	0.03	0.001	0.300	0.690	0.050	0.070	0.187
WI	0-3	0.450	0.09	0.019	0.360	0.500	0.130	0.260	0.917
WI	3-6	0.970	0.14	0.020	0.720	0.880	0.200	0.430	1.348
WI	6-9	1.260	0.16	0.022	1.010	1.080	0.230	0.560	1.337
WI	9-12	1.150	0.14	0.018	0.870	0.960	0.190	0.440	1.004
WI	12-15	1.030	0.13	0.014	0.740	0.870	0.340	0.400	1.006
WI	15-18	0.750	0.10	0.009	0.590	0.650	0.090	0.290	0.689
WI	18-21	0.750	0.11	0.008	0.630	0.650	0.100	0.310	0.847
WI	21-24	0.410	0.06	0.005	0.340	0.340	0.050	0.170	0.549
WI	24-27	0.370	0.06	0.004	0.340	0.330	0.060	0.160	0.500
WI	27-30	0.520	0.08	0.005	0.400	0.510	0.080	0.240	0.739
BH	0-3	0.700	0.12	0.004	0.550	0.640	0.180	0.190	0.745
BH	3-6	0.740	0.13	0.003	0.640	0.680	0.110	0.200	0.602

BH	6-9	0.890	0.14	0.002	0.640	0.870	0.110	0.200	0.496
BH	9-12	0.990	0.10	0.001	0.490	1.140	0.100	0.160	0.451
BH	12-15	1.120	0.06	0.001	0.330	1.320	0.060	0.110	0.320
BH	15-18	0.650	0.05	0.001	0.280	0.840	0.050	0.090	0.287
BH	18-21	0.310	0.05	0.001	0.220	0.430	0.050	0.080	0.266
BH	21-24	0.210	0.04	0.001	0.200	0.280	0.040	0.070	0.244
BH	24-27	0.190	0.04	0.001	0.200	0.270	0.040	0.070	0.252
BH	27-30	0.140	0.04	0.001	0.180	0.220	0.030	0.060	0.216
PACB	0-3	0.260	0.05	0.014	0.160	0.150	0.060	0.080	0.383
PACB	3-6	0.560	0.08	0.012	0.290	0.530	0.100	0.120	0.418
PACB	6-9	1.450	0.18	0.013	0.740	1.320	0.160	0.260	0.588
PACB	9-12	1.000	0.13	0.010	0.540	0.900	0.080	0.190	0.419
PACB	12-15	1.340	0.16	0.012	0.660	1.130	0.100	0.220	0.459
PACB	15-18	1.420	0.18	0.012	0.680	1.130	0.080	0.220	0.423
PACB	18-21	1.190	0.18	0.010	0.650	0.920	0.090	0.220	0.412
PACB	21-24	0.950	0.16	0.008	0.600	0.740	0.080	0.190	0.369
PACB	24-27	1.050	0.16	0.008	0.620	0.850	0.080	0.190	0.398
PACB	27-30	0.750	0.11	0.005	0.440	0.650	0.050	0.140	0.323
RG	0-3	1.010	0.15	0.050	0.580	0.340	0.200	0.300	0.512
RG	3-6	1.130	0.15	0.040	0.610	0.720	0.220	0.270	0.305
RG	6-9	1.400	0.16	0.038	0.680	0.960	0.140	0.300	0.296
RG	9-12	1.300	0.15	0.041	0.640	0.910	0.160	0.290	0.254
RG	12-15	1.420	0.17	0.040	0.730	0.960	0.180	0.340	0.258
RG	15-18	1.810	0.20	0.033	0.970	1.400	0.160	0.380	0.388
RG	18-21	1.460	0.24	0.031	1.190	0.940	0.160	0.450	0.494
RG	21-24	1.410	0.25	0.027	1.130	1.060	0.160	0.460	0.609
RG	24-27	1.140	0.25	0.027	1.110	0.640	0.150	0.440	0.507
RG	27-30	1.540	0.26	0.028	1.250	1.030	0.150	0.470	0.509
BD	0-3	1.390	0.33	0.043	1.010	1.320	0.530	0.620	1.336
BD	3-6	1.460	0.36	0.037	1.190	1.370	0.280	0.680	1.367
BD	6-9	1.680	0.38	0.031	1.190	1.570	0.270	0.680	1.256
BD	9-12	1.880	0.38	0.030	1.180	2.020	0.300	0.700	1.384
BD	12-15	1.810	0.33	0.035	1.020	2.440	0.370	0.700	1.617
BD	15-18	1.870	0.34	0.040	1.160	2.470	0.400	0.770	1.639
BD	18-21	1.480	0.26	0.042	0.760	2.890	0.500	0.790	2.159
BD	21-24	1.360	0.36	0.039	1.150	1.790	0.410	0.790	1.733
BD	24-27	1.150	0.31	0.036	1.000	1.570	0.410	0.740	1.617
BD	27-30	1.260	0.27	0.035	0.860	1.700	0.360	0.650	1.301
BB	0-3	1.760	0.30	0.049	0.860	1.780	0.510	0.590	1.402
BB	3-6	1.980	0.34	0.030	0.970	2.070	0.260	0.620	1.351
BB	6-9	1.430	0.36	0.028	1.060	1.310	0.240	0.640	1.180
BB	9-12	1.370	0.36	0.033	1.130	1.380	0.300	0.700	1.299
BB	12-15	1.900	0.28	0.047	0.930	2.990	0.490	0.740	1.946
BB	15-18	1.900	0.33	0.039	1.020	2.420	0.420	0.730	1.647
BB	18-21	1.410	0.25	0.031	0.790	1.300	0.210	0.470	0.744
BB	21-24	1.370	0.25	0.041	0.700	2.610	0.550	0.810	2.467

BB	24-27	1.600	0.36	0.030	1.250	1.110	0.230	0.660	0.850
BB	27-30	1.260	0.35	0.033	1.210	0.800	0.300	0.660	1.023
BJN	0-3	1.380	0.32	0.037	0.820	1.700	0.470	0.650	1.847
BJN	3-6	1.600	0.31	0.034	0.750	2.120	0.670	0.680	2.063
BJN	6-9	1.320	0.31	0.035	0.820	1.650	0.350	0.650	1.781
BJN	9-12	0.980	0.31	0.032	0.850	1.130	0.330	0.620	1.394
BJN	12-15	1.280	0.31	0.027	0.770	1.560	0.330	0.590	1.460
BJN	15-18	1.480	0.29	0.033	0.770	2.120	0.400	0.650	1.828
BJN	18-21	1.180	0.26	0.029	0.750	1.550	0.320	0.550	1.418
BJN	21-24	1.150	0.23	0.041	0.700	2.040	0.450	0.640	1.990
BJN	24-27	0.880	0.17	0.022	0.460	0.800	0.130	0.280	0.433
BJN	27-30	1.150	0.27	0.037	0.860	1.410	0.300	0.550	1.190
BJS	0-3	1.390	0.29	0.047	0.810	1.580	0.450	0.600	1.356
BJS	3-6	1.380	0.30	0.035	0.900	1.290	0.220	0.550	0.953
BJS	6-9	1.770	0.28	0.037	0.820	2.080	0.300	0.590	1.223
BJS	9-12	1.590	0.29	0.039	0.780	2.210	0.370	0.700	1.791
BJS	12-15	1.270	0.30	0.036	0.860	1.610	0.310	0.640	1.460
BJS	15-18	1.220	0.33	0.032	0.950	1.300	0.280	0.630	1.395
BJS	18-21	1.230	0.29	0.029	0.750	1.380	0.280	0.570	1.263
BJS	21-24	0.710	0.24	0.024	0.620	0.700	0.230	0.440	0.871
BJS	24-27	0.580	0.22	0.019	0.550	0.780	0.240	0.450	1.025
BJS	27-30	0.550	0.20	0.018	0.490	0.510	0.150	0.330	0.572

APPENDIX 7

Appendix 7. Trace metal compositions (in mg/kg) of coastal wetland sediments.

Sample ID	Sample depth (cm)	Cu mg/kg	Pb mg/kg	Zn mg/kg	Ni mg/kg	Co mg/kg	Mn mg/kg
WB	0-3	20.40	21.50	76.00	13.60	8.60	381.00
WB	3-6	21.00	20.80	78.00	13.30	8.40	384.00
WB	6-9	15.10	20.20	73.00	13.10	8.30	350.00
WB	9-12	13.30	16.90	63.00	11.20	7.00	308.00
WB	12-15	13.70	18.80	65.00	11.40	6.80	314.00
WB	15-18	14.80	21.20	68.00	12.70	7.40	296.00
WB	18-21	24.90	19.30	59.00	11.90	6.40	230.00
WB	21-24	10.80	15.90	46.00	8.80	5.20	167.00
WB	24-27	10.60	15.80	45.00	9.90	6.10	174.00
WB	27-30	8.70	13.90	39.00	8.20	5.80	149.00
LB	0-3	3.10	4.40	3.00	1.40	0.50	12.00
LB	3-6	2.30	4.90	3.00	1.30	0.60	7.00
LB	6-9	1.30	4.40	2.00	1.60	0.60	5.00
LB	9-12	2.90	4.50	2.00	1.20	0.70	5.00
LB	12-15	3.50	5.20	2.00	1.70	1.10	6.00
LB	15-18	3.20	3.50	2.00	0.90	0.60	4.00
LB	18-21	2.70	4.50	3.00	1.10	0.80	8.00
LB	21-24	2.30	3.90	3.00	1.40	0.70	8.00
LB	24-27	2.50	3.20	3.00	1.40	0.70	7.00
LB	27-30	3.60	3.90	4.00	1.70	1.20	8.00
WI	0-3	17.30	5.20	24.00	3.70	0.80	23.00
WI	3-6	21.20	10.00	33.00	7.90	1.90	53.00
WI	6-9	24.10	14.20	45.00	9.00	2.40	71.00
WI	9-12	21.00	12.60	50.00	7.90	2.20	61.00
WI	12-15	24.20	11.70	43.00	6.80	2.10	57.00
WI	15-18	14.80	8.30	23.00	4.20	1.40	39.00
WI	18-21	11.30	7.50	25.00	5.00	1.50	34.00
WI	21-24	15.50	4.00	14.00	3.20	0.80	17.00
WI	24-27	42.60	3.80	13.00	2.90	0.90	15.00
WI	27-30	13.00	4.40	10.00	4.20	1.60	17.00
BH	0-3	8.50	7.10	9.00	2.60	1.00	23.00
BH	3-6	3.00	8.10	7.00	3.00	1.00	18.00
BH	6-9	4.60	10.40	6.00	2.70	1.50	17.00
BH	9-12	6.90	9.70	5.00	2.60	1.40	15.00
BH	12-15	2.70	7.60	2.00	1.90	1.80	13.00

BH	15-18	2.20	5.60	1.00	0.80	0.50	10.00
BH	18-21	1.20	4.90	1.00	0.70	0.30	7.00
BH	21-24	2.10	4.40	1.00	0.60	0.30	6.00
BH	24-27	1.30	4.60	1.00	0.70	0.20	6.00
BH	27-30	4.50	4.30	1.00	0.40	0.10	5.00
PACB	0-3	3.40	3.20	6.00	1.00	0.80	52.00
PACB	3-6	4.60	4.20	11.00	2.10	1.30	71.00
PACB	6-9	7.00	8.50	22.00	5.10	3.30	240.00
PACB	9-12	5.60	6.40	17.00	4.10	2.40	156.00
PACB	12-15	10.80	8.10	19.00	4.80	2.80	205.00
PACB	15-18	4.30	8.20	18.00	4.40	3.00	224.00
PACB	18-21	5.70	7.60	13.00	4.60	2.70	141.00
PACB	21-24	2.90	6.50	12.00	4.00	2.10	78.00
PACB	24-27	3.40	7.10	11.00	4.10	2.30	61.00
PACB	27-30	2.70	5.60	7.00	3.00	2.30	32.00
RG	0-3	66.00	13.30	45.00	8.80	4.60	410.00
RG	3-6	22.80	10.90	39.00	9.50	5.50	176.00
RG	6-9	17.70	11.20	41.00	10.20	5.70	169.00
RG	9-12	28.40	10.40	43.00	9.90	5.40	164.00
RG	12-15	23.80	13.10	45.00	10.60	5.80	200.00
RG	15-18	19.80	17.70	48.00	12.10	5.80	236.00
RG	18-21	24.00	17.80	44.00	11.50	4.20	200.00
RG	21-24	45.10	17.10	46.00	10.60	4.30	205.00
RG	24-27	29.90	14.80	41.00	10.40	4.40	178.00
RG	27-30	25.30	17.30	51.00	14.50	7.30	180.00
BD	0-3	22.90	11.50	44.00	12.60	5.40	211.00
BD	3-6	28.20	11.40	61.00	14.80	5.20	206.00
BD	6-9	20.50	10.20	62.00	15.30	5.70	219.00
BD	9-12	21.20	11.10	41.00	12.30	5.40	258.00
BD	12-15	34.10	15.70	44.00	17.20	7.90	262.00
BD	15-18	30.70	14.00	61.00	19.40	6.80	264.00
BD	18-21	35.00	13.00	48.00	18.70	8.30	298.00
BD	21-24	36.30	12.50	73.00	17.80	7.30	247.00
BD	24-27	37.40	11.50	46.00	13.70	4.00	228.00
BD	27-30	25.40	10.70	53.00	13.50	5.70	217.00
BB	0-3	126.20	32.00	67.00	16.70	8.30	283.00
BB	3-6	40.80	11.00	62.00	16.50	7.80	229.00
BB	6-9	32.20	11.00	47.00	12.40	5.50	192.00
BB	9-12	25.70	14.50	47.00	14.20	5.30	198.00
BB	12-15	50.20	21.60	74.00	26.40	11.70	259.00
BB	15-18	36.40	14.70	60.00	20.10	8.00	252.00
BB	18-21	16.00	10.50	41.00	12.40	4.50	163.00
BB	21-24	42.50	12.70	51.00	17.30	6.40	251.00
BB	24-27	22.60	16.10	61.00	16.00	6.10	192.00
BB	27-30	35.10	17.00	50.00	14.60	4.60	198.00
BJN	0-3	24.70	13.20	52.00	15.40	4.40	173.00

BJN	3-6	28.10	12.60	50.00	14.90	6.10	195.00
BJN	6-9	25.00	11.80	40.00	13.30	4.40	170.00
BJN	9-12	27.10	11.00	42.00	11.70	5.30	160.00
BJN	12-15	20.60	10.30	39.00	10.60	6.40	191.00
BJN	15-18	26.70	12.80	35.00	11.30	5.20	220.00
BJN	18-21	23.90	10.20	30.00	11.50	3.80	127.00
BJN	21-24	25.70	13.80	27.00	12.60	3.90	151.00
BJN	24-27	9.00	5.60	19.00	6.60	3.00	72.00
BJN	27-30	18.00	9.80	31.00	12.50	3.70	119.00
BJS	0-3	31.80	12.80	43.00	13.40	5.60	219.00
BJS	3-6	45.60	12.40	48.00	14.40	5.60	241.00
BJS	6-9	26.00	12.40	46.00	14.60	6.20	271.00
BJS	9-12	27.30	12.60	42.00	14.00	5.30	279.00
BJS	12-15	38.00	11.80	44.00	13.60	4.90	204.00
BJS	15-18	22.70	10.80	37.00	11.20	3.50	181.00
BJS	18-21	21.90	9.90	32.00	10.30	3.20	172.00
BJS	21-24	20.00	7.20	24.00	8.00	1.90	123.00
BJS	24-27	15.80	8.00	21.00	6.80	1.80	111.00
BJS	27-30	12.50	6.20	18.00	6.30	2.20	79.00

Appendix 7 cont. Trace metal compositions (in mg/kg) of coastal wetland sediments.

Sample ID	Sample depth (cm)	As mg/kg	Th mg/kg	Sr mg/kg	V mg/kg	Ba mg/kg	Cr mg/kg	Hg mg/kg
WB	0-3	10.70	7.10	33.00	35.00	32.00	32.00	0.08
WB	3-6	10.50	7.20	32.00	35.00	32.00	31.00	0.08
WB	6-9	10.30	7.30	39.00	35.00	31.00	30.00	0.08
WB	9-12	9.60	6.30	33.00	29.00	25.00	26.00	0.07
WB	12-15	9.80	6.70	32.00	34.00	26.00	27.00	0.06
WB	15-18	10.90	7.20	29.00	38.00	28.00	29.00	0.07
WB	18-21	10.50	6.80	27.00	35.00	25.00	27.00	0.06
WB	21-24	8.30	5.70	21.00	29.00	20.00	21.00	0.05
WB	24-27	9.00	6.10	24.00	30.00	23.00	25.00	0.05
WB	27-30	9.30	5.40	22.00	25.00	19.00	19.00	0.04
LB	0-3	1.70	1.70	37.00	10.00	4.00	4.00	0.00
LB	3-6	1.50	1.90	8.00	11.00	3.00	4.00	0.00
LB	6-9	1.90	2.10	7.00	11.00	3.00	4.00	0.01
LB	9-12	2.10	2.10	7.00	10.00	5.00	3.00	0.00
LB	12-15	3.20	2.30	8.00	12.00	3.00	5.00	0.00
LB	15-18	1.90	1.50	5.00	8.00	2.00	3.00	0.00
LB	18-21	1.80	2.20	8.00	11.00	4.00	7.00	0.01
LB	21-24	1.30	1.80	7.00	8.00	4.00	6.00	0.00
LB	24-27	1.30	1.60	6.00	8.00	3.00	5.00	0.00
LB	27-30	1.80	1.80	8.00	10.00	4.00	6.00	0.02
WI	0-3	2.20	1.20	19.00	6.00	7.00	11.00	0.05
WI	3-6	4.80	2.20	28.00	19.00	9.00	22.00	0.05
WI	6-9	5.20	2.70	32.00	26.00	13.00	28.00	0.06
WI	9-12	4.50	2.40	26.00	22.00	10.00	12.00	0.07
WI	12-15	4.10	2.00	26.00	18.00	8.00	20.00	0.06
WI	15-18	2.80	1.90	15.00	13.00	7.00	15.00	0.04
WI	18-21	3.50	1.90	17.00	14.00	7.00	15.00	0.04
WI	21-24	2.40	1.00	10.00	9.00	5.00	9.00	0.04
WI	24-27	2.10	1.20	10.00	8.00	5.00	10.00	0.03
WI	27-30	3.70	1.70	14.00	13.00	5.00	12.00	0.01
BH	0-3	2.40	2.70	21.00	13.00	9.00	7.00	0.00
BH	3-6	1.90	3.20	18.00	14.00	8.00	7.00	0.00
BH	6-9	2.00	3.10	19.00	13.00	7.00	7.00	0.01
BH	9-12	2.70	2.70	17.00	10.00	6.00	5.00	0.01
BH	12-15	2.20	1.80	12.00	6.00	4.00	3.00	0.01
BH	15-18	0.70	1.70	10.00	4.00	3.00	2.00	0.00
BH	18-21	0.50	1.50	9.00	3.00	3.00	2.00	0.01
BH	21-24	0.50	1.40	7.00	3.00	3.00	2.00	0.00
BH	24-27	0.50	1.40	8.00	3.00	6.00	2.00	0.00
BH	27-30	0.50	1.40	7.00	2.00	4.00	2.00	0.00
PACB	0-3	1.70	0.90	7.00	9.00	4.00	2.00	0.00
PACB	3-6	3.10	1.50	10.00	12.00	5.00	5.00	0.00

PACB	6-9	6.50	3.40	19.00	20.00	9.00	12.00	0.02
PACB	9-12	4.20	2.60	13.00	14.00	7.00	1.00	0.00
PACB	12-15	6.10	3.20	15.00	18.00	9.00	11.00	0.00
PACB	15-18	6.30	3.40	15.00	18.00	9.00	11.00	0.00
PACB	18-21	6.10	3.50	15.00	17.00	9.00	10.00	0.00
PACB	21-24	4.90	3.20	13.00	16.00	8.00	9.00	0.02
PACB	24-27	5.30	3.40	14.00	17.00	8.00	9.00	0.00
PACB	27-30	3.80	2.40	10.00	12.00	6.00	6.00	0.01
RG	0-3	4.30	3.80	26.00	14.00	123.00	11.00	0.02
RG	3-6	4.60	4.00	26.00	15.00	71.00	11.00	0.03
RG	6-9	5.60	4.50	20.00	16.00	52.00	11.00	0.03
RG	9-12	6.60	4.20	21.00	15.00	105.00	11.00	0.03
RG	12-15	6.50	4.70	24.00	18.00	134.00	12.00	0.05
RG	15-18	8.00	5.20	33.00	23.00	82.00	15.00	0.06
RG	18-21	5.30	5.90	37.00	27.00	72.00	17.00	0.06
RG	21-24	6.90	5.50	41.00	29.00	65.00	17.00	0.06
RG	24-27	4.70	5.80	40.00	26.00	60.00	17.00	0.06
RG	27-30	7.70	6.40	36.00	29.00	52.00	18.00	0.07
BD	0-3	3.00	3.80	65.00	23.00	97.00	16.00	0.02
BD	3-6	2.60	4.20	58.00	22.00	58.00	17.00	0.02
BD	6-9	3.30	5.00	55.00	23.00	62.00	18.00	0.03
BD	9-12	5.20	5.00	59.00	25.00	63.00	18.00	0.04
BD	12-15	10.40	3.90	69.00	24.00	61.00	16.00	0.05
BD	15-18	5.00	3.80	71.00	22.00	66.00	16.00	0.04
BD	18-21	6.00	2.20	81.00	21.00	54.00	12.00	0.05
BD	21-24	3.60	3.70	71.00	26.00	71.00	17.00	0.04
BD	24-27	2.70	3.20	73.00	24.00	72.00	15.00	0.02
BD	27-30	2.70	3.30	63.00	21.00	60.00	14.00	0.03
BB	0-3	5.40	3.70	64.00	21.00	78.00	14.00	0.05
BB	3-6	4.80	4.50	56.00	21.00	57.00	16.00	0.04
BB	6-9	3.10	4.50	57.00	23.00	63.00	17.00	0.04
BB	9-12	3.20	4.20	60.00	25.00	65.00	18.00	0.04
BB	12-15	7.10	2.10	85.00	22.00	58.00	14.00	0.05
BB	15-18	4.50	3.40	73.00	23.00	72.00	16.00	0.05
BB	18-21	2.70	3.70	42.00	16.00	62.00	12.00	0.02
BB	21-24	4.80	2.30	94.00	24.00	65.00	13.00	0.06
BB	24-27	2.80	6.00	49.00	24.00	77.00	19.00	0.04
BB	27-30	2.20	5.30	59.00	27.00	86.00	19.00	0.04
BJN	0-3	4.60	3.60	63.00	21.00	67.00	13.00	0.05
BJN	3-6	4.60	3.40	86.00	20.00	71.00	12.00	0.07
BJN	6-9	3.00	3.30	64.00	20.00	65.00	13.00	0.05
BJN	9-12	2.50	3.40	59.00	21.00	64.00	14.00	0.05
BJN	12-15	3.50	3.90	59.00	23.00	59.00	13.00	0.06
BJN	15-18	4.20	3.70	69.00	24.00	56.00	7.00	0.07
BJN	18-21	2.70	3.50	59.00	20.00	55.00	12.00	0.04
BJN	21-24	3.30	2.60	78.00	21.00	59.00	12.00	0.03
BJN	24-27	1.60	2.60	28.00	12.00	41.00	7.00	0.02

BJN	27-30	2.30	3.30	55.00	20.00	66.00	13.00	0.02
BJS	0-3	6.70	3.50	60.00	21.00	69.00	14.00	0.05
BJS	3-6	6.70	4.30	42.00	20.00	50.00	14.00	0.05
BJS	6-9	9.40	3.60	52.00	20.00	52.00	13.00	0.06
BJS	9-12	9.00	3.10	64.00	20.00	54.00	5.00	0.06
BJS	12-15	4.60	3.60	58.00	21.00	56.00	14.00	0.05
BJS	15-18	3.10	4.10	55.00	22.00	62.00	15.00	0.02
BJS	18-21	3.20	4.10	49.00	20.00	56.00	13.00	0.04
BJS	21-24	1.70	3.70	41.00	16.00	51.00	10.00	0.03
BJS	24-27	1.70	3.50	45.00	18.00	49.00	10.00	0.03
BJS	27-30	1.40	3.30	30.00	14.00	41.00	9.00	0.02

APPENDIX 8

Appendix 8a. Summary of number of positive tubes in the SRB MPN cultures inoculated with sediment core samples from heavily contaminated sites (Bennidict Okeke, personal communication, 2011).

Sample	Depth (cm)	10 fold	100 fold	1000 fold	MPN
Bay Jimmy South (BJ) 1	0 - 3	5	2	0	150
Bay Jimmy South (BJ) 2	0 - 3	5	2	0	150
Bay Jimmy South (BJ) 1	12 - 15	5	3	1	79
Bay Jimmy South (BJ) 2	12 - 15	5	3	0	110
Bay Jimmy South (BJ) 1	27 - 30	5	2	0	150
Bay Jimmy South (BJ) 2	27 - 30	5	0	1	31
Bay Jimmy North (BN) 1	0 - 3	5	2	0	150
Bay Jimmy North (BN) 2	0 - 3	5	5	2	540
Bay Jimmy North (BN) 1	12 - 15	5	5	1	350
Bay Jimmy North (BN) 2	12 - 15	5	4	3	280
Bay Jimmy North (BN) 1	27 - 30	5	3	0	79
Bay Jimmy North (BN) 2	27 - 30	5	4	0	130
Bayou Batiste Core C (BB) 1	0 - 3	5	4	5	1600
Bayou Batiste Core C (BB) 2	0 - 3	5	5	5	1600
Bayou Batiste Core C (BB) 1	12 - 15	5	5	3	920
Bayou Batiste Core C (BB) 2	12 - 15	5	5	3	920
Bayou Batiste Core C (BB) 1	27 - 30	5	1	5	220
Bayou Batiste Core C (BB) 2	27 - 30	5	5	0	240
Bayou Dulac Core C (BD) 1	0 - 3	5	5	3	920
Bayou Dulac Core C (BD) 2	0 - 3	5	5	3	920
Bayou Dulac Core C (BD) 1	12 - 15	5	5	0	240
Bayou Dulac Core C (BD) 2	12 - 15	5	4	0	130
Bayou Dulac Core C (BD) 1	27 - 30	5	1	0	33
Bayou Dulac Core C (BD) 2	27 - 30	5	1	0	33

Appendix 8b. Summary of number of positive tubes in the SRB MPN cultures inoculated with sediment core samples from intermediate contaminated sites (Bennidict Okeke, personal communication, 2011)

Sample	Depth (cm)	10 fold	100 fold	1000 fold	MPN
Rigolets (RG) 1	0 - 3	5	5	4	1600
Rigolets (RG) 2	0 - 3	5	5	5	1600
Rigolets (RG) 1	12 - 15	5	5	5	1600
Rigolets (RG) 2	12 - 15	5	5	5	1600
Rigolets (RG) 1	27 - 30	5	5	5	1600
Rigolets (RG) 2	27 - 30	5	5	5	1600
Point Aux Chenes Bay (PA) 1	0 - 3	5	5	1	350
Point Aux Chenes Bay (PA) 2	0 - 3	5	5	1	350
Point Aux Chenes Bay (PA) 1	12 - 15	3	2	0	14
Point Aux Chenes Bay (PA) 2	12 - 15	5	5	1	350
Point Aux Chenes Bay (PA) 1	27 - 30	5	2	1	70
Point Aux Chenes Bay (PA) 2	27 - 30	3	2	0	14
Walker Island (W) 1	0 - 3	5	5	1	350
Walker Island (W) 2	0 - 3	5	5	1	350
Walker Island (W) 1	9-12	5	1	0	33
Walker Island (W) 2	9-12	5	0	0	23
Walker Island (W) 1	15-18	5	1	0	33
Walker Island (W) 2	15-18	5	2	1	70

Appendix 8c. Summary of number of positive tubes in the SRB MPN cultures inoculated with sediment core samples from pristine sites (Bennidict Okeke, personal communication, 2011).

Sample	Depth (cm)	10 fold	100 fold	1000 fold	MPN
Long's Bayou (LB) 1	0 - 3	5	5	3	920
Long's Bayou (LB) 2	0 - 3	5	5	2	540
Long's Bayou (LB) 1	12 - 15	5	1	0	33
Long's Bayou (LB) 2	12 - 15	5	0	0	23
Long's Bayou (LB) 1	27 - 30	0	1	1	1.8
Long's Bayou (LB) 2	27 - 30	1	1	0	1.9
Weeks Bay Force F Core (WF) 1	0 - 3	5	5	1	350
Weeks Bay Force F Core (WF) 2	0 - 3	5	5	2	540
Weeks Bay Force F Core (WF) 1	12 - 15	5	4	1	170
Weeks Bay Force F Core (WF) 2	12 - 15	5	5	2	540
Weeks Bay Force F Core (WF) 1	27 - 30	5	5	2	540
Weeks Bay Force F Core (WF) 2	27 - 30	5	5	3	920
Weeks Bay Force E Core (WE) 1	0 - 3	5	5	3	920
Weeks Bay Force E Core (WE) 2	0 - 3	5	5	1	350
Weeks Bay Force E Core (WE) 1	15-18	5	4	0	130
Weeks Bay Force E Core (WE) 2	15-18	5	4	0	130
Weeks Bay Force E Core (WE) 1	27 - 30	5	5	4	1600
Weeks Bay Force E Core (WE) 2	27 - 30	5	5	1	350
Bayou Heron (BH) 1	0 - 3	5	5	2	540
Bayou Heron (BH) 2	0 - 3	5	5	3	920
Bayou Heron (BH) 1	12 - 15	5	2	0	49
Bayou Heron (BH) 2	12 - 15	5	0	0	23
Bayou Heron (BH) 1	27 - 30	3	1	0	11
Bayou Heron (BH) 2	27 - 30	2	0	0	4.5

APPENDIX 9

Appendix 9a. Summary of number of positive tubes in the IRB MPN cultures inoculated with sediment core samples from heavily contaminated sites (Bennidict Okeke, personal communication, 2011).

Sample	Depth	10 fold	100 fold	1000 fold	MPN
Bay Jimmy South (BJ) 1	0 - 3	5	5	5	>1600
Bay Jimmy South (BJ) 2	0 - 3	5	5	5	>1600
Bay Jimmy South (BJ) 1	12 - 15	5	5	5	>1600
Bay Jimmy South (BJ) 2	12 - 15	5	5	5	>1600
Bay Jimmy South (BJ) 1	27 - 30	5	5	5	>1600
Bay Jimmy South (BJ) 2	27 - 30	5	5	5	>1600
Bay Jimmy North (BN) 1	0 - 3	5	5	5	>1600
Bay Jimmy North (BN) 2	0 - 3	5	5	5	>1600
Bay Jimmy North (BN) 1	12 - 15	5	5	5	>1600
Bay Jimmy North (BN) 2	12 - 15	5	5	5	>1600
Bay Jimmy North (BN) 1	27 - 30	5	5	5	>1600
Bay Jimmy North (BN) 2	27 - 30	5	5	5	>1600
Bayou Batiste Core C (BB) 1	0 - 3	5	5	5	>1600
Bayou Batiste Core C (BB) 2	0 - 3	5	5	5	>1600
Bayou Batiste Core C (BB) 1	12 - 15	5	5	5	>1600
Bayou Batiste Core C (BB) 2	12 - 15	5	5	5	>1600
Bayou Batiste Core C (BB) 1	27 - 30	5	5	5	>1600
Bayou Batiste Core C (BB) 2	27 - 30	5	5	5	>1600
Bayou Dulac Core C (BD) 1	0 - 3	5	5	5	>1600
Bayou Dulac Core C (BD) 2	0 - 3	5	5	5	>1600
Bayou Dulac Core C (BD) 1	12 - 15	5	5	5	>1600
Bayou Dulac Core C (BD) 2	12 - 15	5	5	5	>1600
Bayou Dulac Core C (BD) 1	27 - 30	5	5	5	>1600
Bayou Dulac Core C (BD) 2	27 - 30	5	5	5	>1600

Appendix 9b. Summary of number of positive tubes in the IRB MPN cultures inoculated with sediment core samples from pristine sites (Bennidict Okeke, personal communication, 2011).

Sample	Depth (cm)	10 fold	100 fold	1000 fold	MPN
Long's Bayou (LB) 1	0 - 3	5	5	5	>1600
Long's Bayou (LB) 2	0 - 3	5	5	5	>1600
Long's Bayou (LB) 1	12 - 15	5	5	5	>1600
Long's Bayou (LB) 2	12 - 15	5	5	5	>1600
Long's Bayou (LB) 1	27 - 30	5	5	5	>1600
Long's Bayou (LB) 2	27 - 30	5	5	5	>1600
Weeks Bay Force F Core (WF) 1	0 - 3	5	5	5	>1600
Weeks Bay Force F Core (WF) 2	0 - 3	5	5	5	>1600
Weeks Bay Force F Core (WF) 1	12 - 15	5	5	5	>1600
Weeks Bay Force F Core (WF) 2	12 - 15	5	5	5	>1600
Weeks Bay Force F Core (WF) 1	27 - 30	5	5	5	>1600
Weeks Bay Force F Core (WF) 2	27 - 30	5	5	5	>1600
Weeks Bay Force E Core (WE) 1	0 - 3	5	5	5	>1600
Weeks Bay Force E Core (WE) 2	0 - 3	5	5	5	>1600
Weeks Bay Force E Core (WE) 1	15-18	5	5	5	>1600
Weeks Bay Force E Core (WE) 2	15-18	5	5	5	>1600
Weeks Bay Force E Core (WE) 1	27 - 30	5	5	5	>1600
Weeks Bay Force E Core (WE) 2	27 - 30	5	5	5	>1600
Bayou Heron (BH) 1	0 - 3	5	5	5	>1600
Bayou Heron (BH) 2	0 - 3	5	5	5	>1600
Bayou Heron (BH) 1	12 - 15	5	5	5	>1600
Bayou Heron (BH) 2	12 - 15	5	5	5	>1600
Bayou Heron (BH) 1	27 - 30	5	5	5	>1600
Bayou Heron (BH) 2	27 - 30	5	5	5	>1600

APPENDIX 10

Appendix 10a. Plots showing LA-ICP/MS spectra of pyrites from Bayou Dulac, LA.

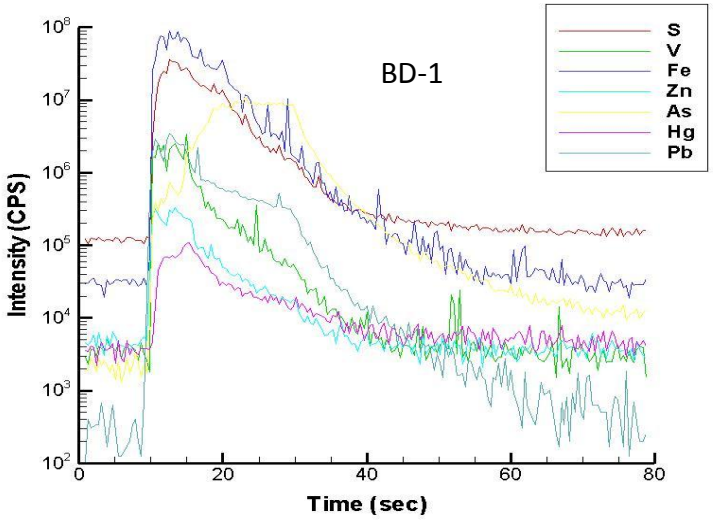

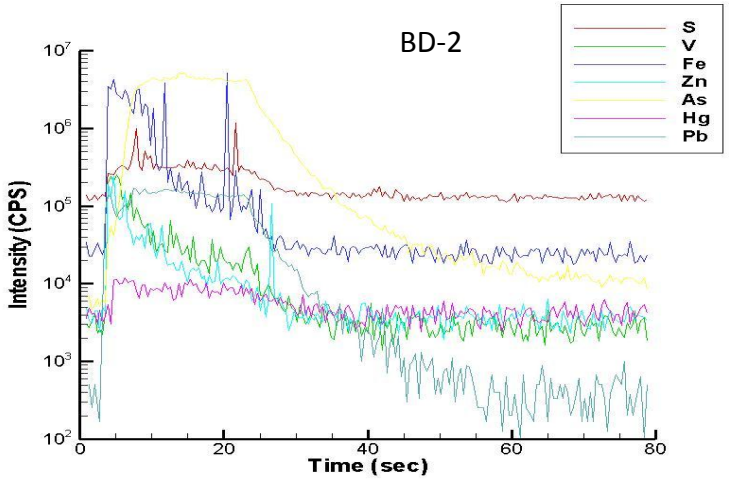

Appendix 10a. Plots showing LA-ICP/MS spectra of pyrites from Bayou Dulac, LA.

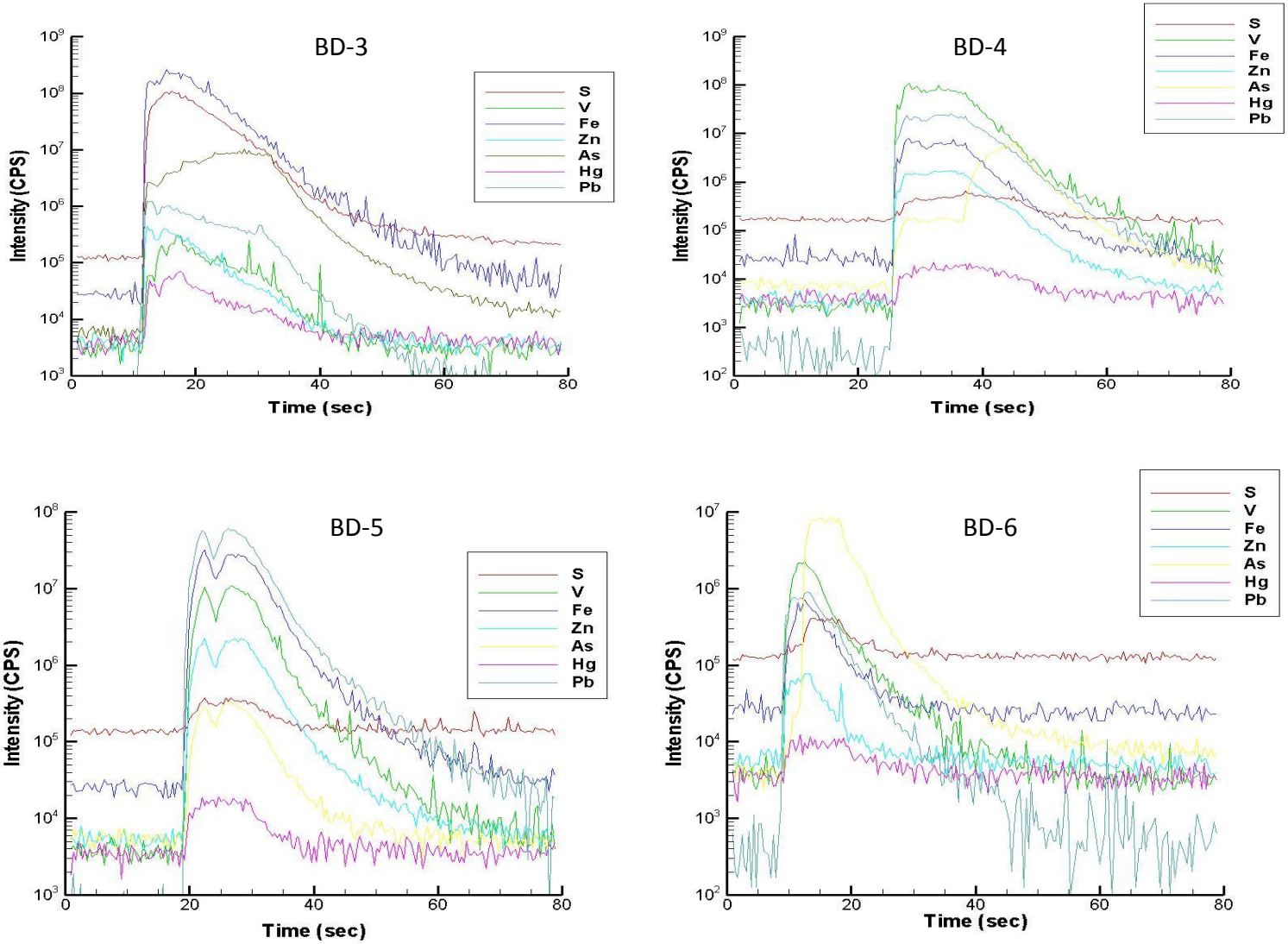

Appendix 10a. Plots showing LA-ICP/MS spectra of pyrites from Bayou Dulac, LA

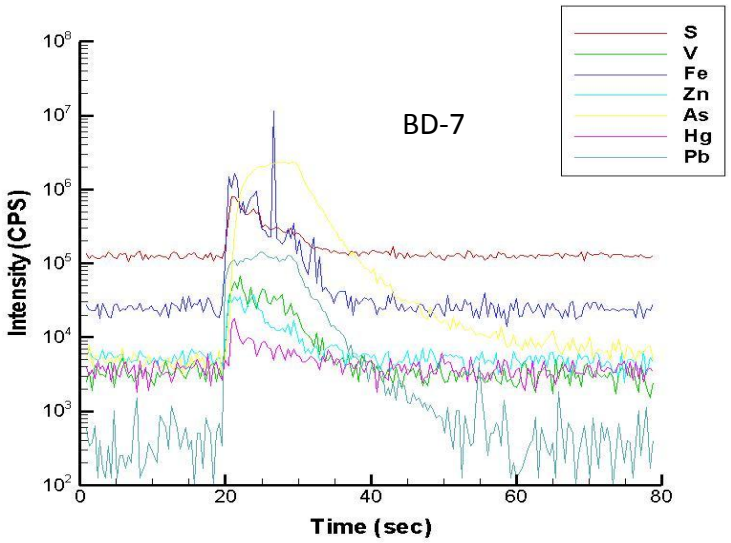

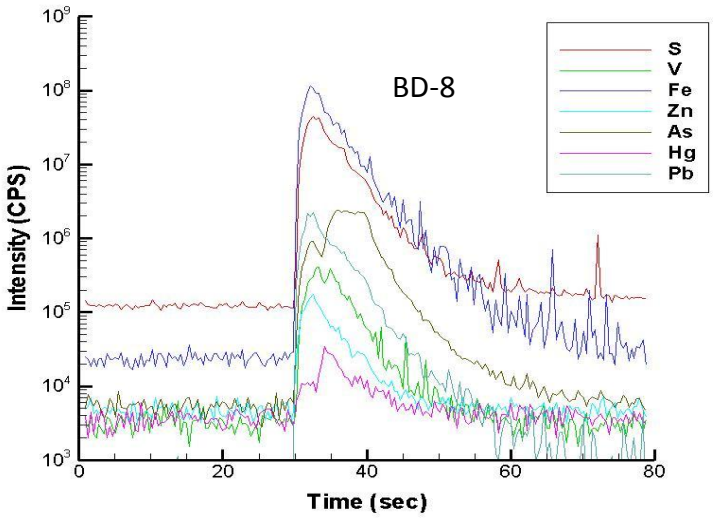

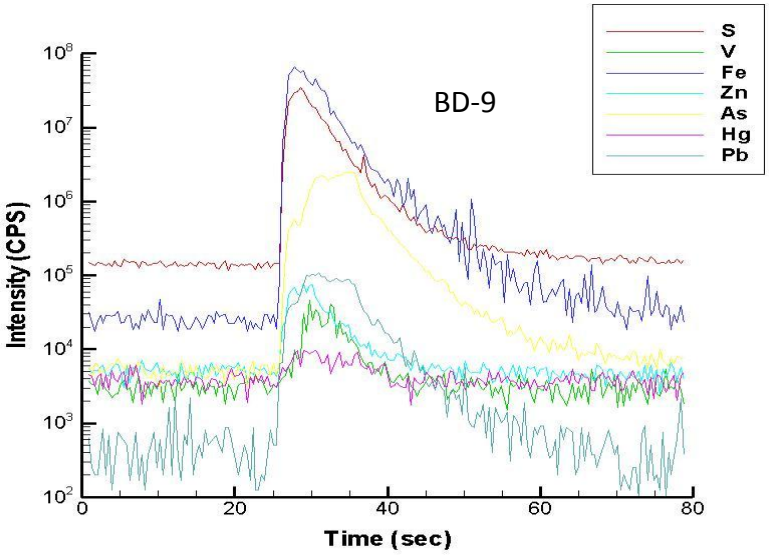

.

Appendix 10b. Average elemental concentrations measured from LA-ICP/MS analysis of pyrites from Bayou Dulac, LA. Results are normalized to Fe.

Metals	Conc.	BD 1	BD 2	BD 3	BD 4	BD 5
S	**wt. %**	**47.9**	**31.3**	**49.6**	**14.2**	**2.5**
V	ppm	208	477	10	134332	5202
Mn	ppm	738	4131	1312	14768	13968
Fe	**wt. %**	**51.2**	**54.1**	**50.0**	**62.8**	**91.9**
Co	ppm	29	87	209	235	739
Ni	ppm	51	0	449	240	1030
Cu	ppm	130	1071	38	1191	642
Zn	ppm	192	1872	83	18006	7765
As	ppm	7591	137509	2238	24137	679
Se	ppm	6	7	5	68	27
Mo	ppm	16	32	48	1096	274
Cd	ppm	3	9	4	394	32
Te125(LR)	ppm	0	0	0	0	0
Hg202(LR)	ppm	0	0	0	0	0
Pb	ppm	280	1128	43	36000	26024

Metal	Conc.	BD 6	BD 7	BD 8	BD 9
S	**wt. %**	**43.4**	**40.7**	**50.7**	**52.5**
V	ppm	14569	312	39	4
Mn	ppm	6824	4718	1216	72
Fe	**wt. %**	**25.6**	**51.6**	**48.9**	**47.3**
Co	ppm	74	59	137	27
Ni	ppm	0	0	237	0
Cu	ppm	1814	1402	230	98
Zn	ppm	3859	1127	84	65
As	ppm	285240	75952	1295	2033
Se	ppm	0	0	3	0
Mo	ppm	14	243	44	2
Cd	ppm	138	50	6	4
Te125(LR)	ppm	0	0	0	0
Hg202(LR)	ppm	0	0	0	0
Pb	ppm	6367	1063	149	20

Appendix 10c. LA-ICP/MS spectra of pyrites from Bay Jimmy North, LA.

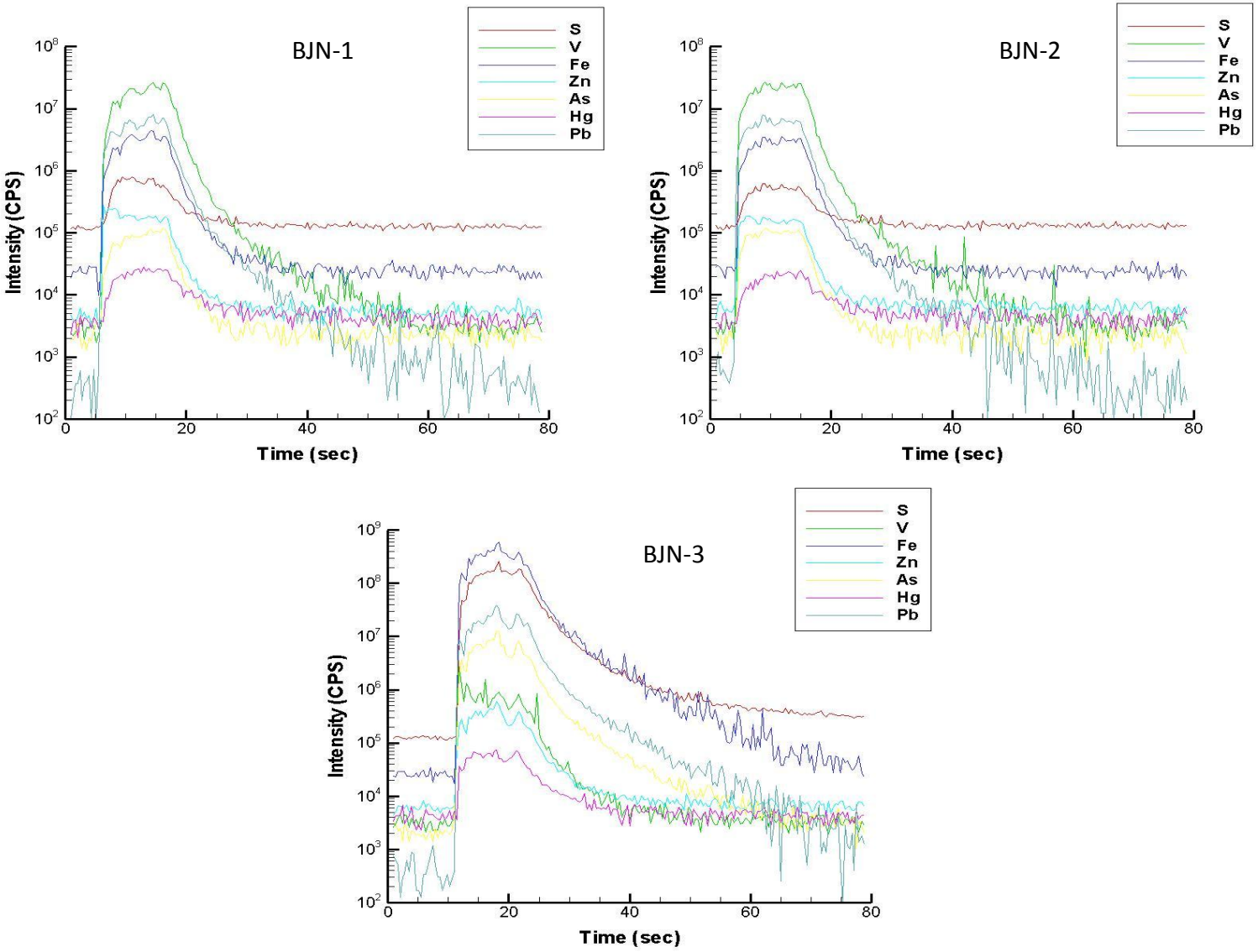

Appendix 10d. Averaged elemental concentrations measured from LA-ICP/MS analysis of pyrites from Bay Jimmy North, L.A.. Results are normalized to Fe.

Metal	Conc.	BJN 1	BJN 2	BJN 3
S	**wt. %**	**26.2**	**23.8**	**51.0**
V	ppm	65984	83702	21
Mn	ppm	1901	1994	1068
Fe	**wt. %**	**64.5**	**65.0**	**48.4**
Co	ppm	135	130	1484
Ni	ppm	0	0	1671
Cu	ppm	1558	1390	312
Zn	ppm	4543	4211	56
As	ppm	1200	1500	652
Se	ppm	141	191	18
Mo	ppm	748	773	74
Cd	ppm	532	497	10
Te125(LR)	ppm	0	0	0
Hg202(LR)	ppm	0	0	0
Pb	ppm	17011	20068	445